Fisheries and Oceans Canada | Pêches et Océans Canada
Ecosystems and Oceans Science | Sciences des écosystèmes et des océans

Canadian Science Advisory Secretariat (CSAS)

Research Document 2023/016

Maritimes Region

Optical, Chemical, and Biological Oceanographic Conditions on the Scotian Shelf and in the eastern Gulf of Maine during 2021

B. Casault, C. Johnson, E. Devred, E. Head, and L. Beazley.

Fisheries and Oceans Canada
Bedford Institute of Oceanography
1 Challenger Drive, PO Box 1006
Dartmouth, Nova Scotia B2Y 4A2

April 2023

Canada

Foreword

This series documents the scientific basis for the evaluation of aquatic resources and ecosystems in Canada. As such, it addresses the issues of the day in the time frames required and the documents it contains are not intended as definitive statements on the subjects addressed but rather as progress reports on ongoing investigations.

Published by:

Fisheries and Oceans Canada
Canadian Science Advisory Secretariat
200 Kent Street
Ottawa ON K1A 0E6

http://www.dfo-mpo.gc.ca/csas-sccs/
csas-sccs@dfo-mpo.gc.ca

ISSN 1919-5044
ISBN 978-0-660-47389-5 Cat. No. Fs70-5/2023-016E-PDF

Correct citation for this publication:

Casault, B., Johnson, C., Devred, E., Head, E., and Beazley, L. 2023. Optical, Chemical, and Biological Oceanographic Conditions on the Scotian Shelf and in the eastern Gulf of Maine during 2021. DFO Can. Sci. Advis. Sec. Res. Doc. 2023/016. v + 74 p.

Aussi disponible en français :

Casault, B., Johnson, C., Devred, E., Head, E., et Beazley, L. 2023. Conditions océanographiques optiques, chimiques et biologiques sur le plateau néo-écossais et dans l'est du golfe du Maine en 2021. Secr. can. des avis sci. du MPO. Doc. de rech. 2023/016. vi + 79 p.

TABLE OF CONTENTS

ABSTRACT

Ocean physical conditions in the Maritimes Region in 2021 were characterized by generally warm water with sea-surface temperatures approaching the record-high levels reached in 2012. Annual inventories of surface and deep nitrate and silicate were mainly above normal across the region with the exception of Prince-5 (P5). Annual inventories of surface and deep phosphate were also higher than in previous years although they remained near or below the long-term averages. Annual inventories of *in situ* chlorophyll-*a* over the 0–100 m layer were mainly near or below normal across the region in 2021, while annual mean surface concentrations of chlorophyll-*a* measured by satellite were mainly above normal. The spring phytoplankton bloom was mainly earlier than normal across the region, with variable duration, and consistently higher-than-normal amplitude and magnitude. Relatively intense fall bloom conditions were evident across the region. Phytoplankton composition at Halifax-2 (HL2) indicated near-normal abundance of diatoms and dinoflagellates in 2021 in contrast with recent years, while ciliate and flagellate abundances continued to be higher than normal. At P5, lower abundance of diatoms and higher abundance of ciliates and flagellates continued the long-term pattern. The abundance of *C. finmarchicus* was mainly lower than normal, particularly at HL2 and in the western area (Browns Bank and P5). *Pseudocalanus* spp. and non-copepod abundances were mainly higher than normal across the region, while total copepod abundance and mesozooplankton biomass were variable across the region. The abundances of Arctic *Calanus* and warm-shelf copepod species were mainly lower and mainly higher than normal across the region in 2021, respectively. Apart from *Pseudocalanus* spp. which were mainly more abundant than normal across the region in 2021, the copepod community indicated near- or lower-than-normal abundances of the small copepods *O. similis*, *O. atlantica* (HL2), and *Microcalanus* spp. and *Paracalanus* spp. (HL2 and P5).

Average surface and bottom temperatures in Bedford Basin were above normal in 2021, consistent with the general pattern observed across the broader Scotian Shelf. Surface nutrients were near or slightly below normal, while bottom nitrate, phosphate, and silicate were above normal in 2021, with bottom nitrate showing its highest values during the month of June since the start of the Bedford Basin time series in 1994. In contrast to 2020, no intrusions of shelf water into the deeper layers of Bedford Basin occurred during 2021. Dissolved oxygen concentrations revealed hypoxic conditions in the bottom 30–40 m of Bedford Basin, possibly as a result of the lack of replenishment through shelf-water intrusion.

The 2020 Continuous Plankton Recorder data indicated near-normal values for the phytoplankton colour index, a proxy for the phytoplankton biomass, and annual abundances of diatoms on the Eastern Scotian Shelf (ESS) and Western Scotian Shelf (WSS), while dinoflagellate annual abundance was above (ESS) or near (WSS) normal. Annual abundances of *Calanus* CI–IV were above normal in both regions, while those of *C. finmarchicus* CV–VI were above (ESS) or near normal (WSS). Annual abundances of *C. glacialis* CIV–VI were higher than normal in both regions, while annual abundances of *C. hyperboreus* CIII–VI, *Para/Pseudocalanus*, euphausiids and hyperiid amphipods were higher than normal on the ESS but normal on the WSS.

INTRODUCTION

The Atlantic Zone Monitoring Program (AZMP) was implemented in 1998 to enhance Fisheries and Oceans Canada's (DFO's) capacity to describe, understand, and forecast the state of the marine ecosystem (Therriault et al. 1998). The AZMP derives its information on the marine environment and ecosystem from data collected at a network of sampling locations (high-frequency sampling stations, cross-shelf sections, and ecosystem trawl surveys) in four DFO regions (Québec, Gulf, Maritimes, and Newfoundland), sampled at a frequency of twice-monthly to once-annually. The sampling design provides fundamental information on the variability in physical, chemical, and biological properties of the Northwest Atlantic continental shelf and slope on seasonal and inter-annual scales. Ecosystem trawl surveys and cross-shelf sections provide information about broad-scale environmental variability (Harrison et al. 2005) but are limited in their seasonal coverage. High-frequency sampling stations complement the broad-scale sampling by providing detailed information on seasonal changes in ocean properties. In recent years, data collected from buoys and gliders, although not presented in this report, also complement the core observations with high-resolution temporal and/or spatial observations. In addition, the North Atlantic Continuous Plankton Recorder (CPR) survey provides monthly sampling along commercial shipping routes between Reykjavik and the New England coast, via the Scotian Shelf (SS). The CPR sampling extends a dataset started in 1960, allowing present-day plankton observations to be set within a longer time frame than the AZMP core sampling. *In situ* sampling is also complemented by remote-sensing ocean colour measurements providing additional information on the distribution of phytoplankton in the surface layer on a broad scale. This report provides an assessment of the distribution and variability of nutrients and plankton on the SS and in the eastern Gulf of Maine (GoM), and focuses on conditions observed during 2021 (2020 for the CPR data) in the context of warmer conditions in the marine environment observed in recent years. It complements assessments for the physical environment of the Maritimes Region (Hebert et al. In preparation)[1] and for the state of the Canadian Northwest Atlantic shelf system as a whole (DFO 2022). Although not considered a core AZMP station, the Compass Buoy station located in the Bedford Basin has been sampled weekly since 1992 and a summary of the observed environmental and phytoplankton conditions is also presented in this report.

The SS is located in a transition zone influenced by both sub-polar waters, mainly flowing into the region from the Gulf of St. Lawrence and the Newfoundland Shelf, and warmer offshore waters of Gulf Stream origin. The deep-water properties of the western SS exhibit significant shifts in temperature, reflecting changes in the source of deep slope water to the shelf between cold, low-nutrient Labrador Slope Water, and warm, nutrient-rich Atlantic slope water, that can be driven by changes in large-scale atmospheric pressure patterns (Petrie 2007). Temperature and salinity on the SS are also influenced by heat transfer between the atmosphere and ocean, local mixing, precipitation, and, to some extent, runoff from land. Physical changes in the

[1] Hebert, D., Layton, C., Brickman, D., and Galbraith, P.S. In preparation. Physical Oceanographic Conditions on the Scotian Shelf and in the Gulf of Maine during 2021. DFO Can. Sci. Advis. Sec. Res. Doc. Presented at the March 21, 2022, Twenty-fourth Annual Meeting of the Atlantic Zone Monitoring Program.

pelagic environment influence both plankton community composition and annual biological production cycles, with implications for energy transfer to higher trophic-level production.

METHODS

Sample collection and processing conform to established standard protocols to the best extent possible (Mitchell et al. 2002). Non-standard measurements or derived variables are described below.

MISSIONS

AZMP-DFO Maritimes Region sea-going personnel participated in several broad-scale missions (ecosystem trawl surveys and seasonal cross-shelf oceanographic surveys) during the 2021 calendar year, in addition to day trips to the two high-frequency sampling stations (Table 1). A total of 182 hydrographic station occupations were completed with plankton net samples collected at 154 of these stations (Table 1). Table 1 includes hydrographic and zooplankton net samples collected on Browns Bank and Halifax sections as part of sea trials performed during spring on the newly acquired research vessel CCGS *Capt. Jacques Cartier*. Table 1 also includes samples collected during spring on the Cabot Strait and the Louisbourg sections as part of the Labrador Sea mission which was later cancelled due to vessel issues. For these two missions, occupation of the sections occurred considerably later than normal and, therefore, data derived from those samples are not directly comparable to the rest of the time series and are not included in this report.

High-Frequency Sampling Stations

The Halifax-2 (HL2) and Prince-5 (P5) high-frequency sampling stations (Figure 1) were sampled 18 and 8 times, respectively, in 2021. For P5, the lower-than-usual sampling frequency compared to previous years was due to wharf accessibility issues. As a result, there was no sampling at P5 from February to May inclusively.

The standard sampling suite for the high-frequency stations includes the following:

- Conductivity, Temperature, Depth (CTD; measured using a Sea-Bird instrument) profiles with dissolved oxygen, fluorescence, and Photosynthetically Active Radiation (PAR).
- Niskin water bottles sampled at standard depths (see Gear Deployment) for nutrient, salinity and oxygen (for calibration of the CTD), and chlorophyll-*a* analyses. Accessory phytoplankton pigments are also measured near the surface only, but are not reported in this document.
- Niskin water bottles sampled for phytoplankton enumeration.
- Vertical ring net tows (202-µm mesh net) for zooplankton biomass (wet and dry weights), abundance, and community composition.
- Secchi depth measurement for light attenuation when possible.

Shelf Sections

During the spring and fall seasonal surveys, samples are collected on the four primary sections (Cabot Strait [CSL]; Louisbourg [LL]; Halifax [HL]; Browns Bank [BBL]; Figure 1) and at a number of ancillary sections/stations (gray markers in Figure 2). However, results from the ancillary sections/stations are not reported in this document. In 2021, due to the cancellation of the spring mission, only samples collected during the fall mission on the shelf sections were used to calculate the annual estimates of the key indices for the sections. Therefore, the estimated annual anomalies for the sections should be interpreted with caution.

The standard sampling suite for the cross-shelf section stations is the same as for the high-frequency sampling stations as listed above, except for phytoplankton enumeration. In addition to the standard suite of analyses performed on water samples, particulate organic carbon is measured at standard depths but not reported in this document.

Ecosystem Trawl Surveys

AZMP-DFO Maritimes Region participated in one primary ecosystem trawl survey in 2021. The March winter survey on Georges Bank (GB) took place during the second half of March (Table 1). The summer survey on the SS and in the eastern GoM, which typically takes place from early July to mid-August, was cancelled due to vessel availability issues.

The sampling suite for the ecosystem trawl survey stations includes the measurements listed above for the high-frequency sampling stations, but the standard set of water bottle sampling depths is reduced to four depths, and vertical ring net tows (202-µm mesh) are only collected at a subset of stations (Table 1 and Figure 3).

GEAR DEPLOYMENT

Conductivity, Temperature, Depth

The CTD is lowered to a target depth within 2 m of the bottom.

Standard depths for water samples include:

- High-frequency sampling stations:
    1. HL2: 1 m, 5 m, 10 m, 20 m, 30 m, 40 m, 50 m, 75 m, 100 m, 140 m
    2. P5: 1 m, 10 m, 25 m, 50 m, 95 m
- Seasonal sections: near-surface, 10 m, 20 m, 30 m, 40 m, 50 m, 60 m, 80 m, 100 m, 250 m, 500 m, 1000 m, 1500 m, 2000 m, near-bottom (depths sampled are limited by bottom depth)
- Ecosystem trawl surveys: 5 m, 25 m, 50 m, and near bottom when possible

Net Tows

Ring nets of a standard 202-µm mesh are towed vertically from near bottom to surface at approximately 1 $m \cdot s^{-1}$. In deep offshore waters, the maximum tow depth is 1000 m. Samples are preserved in a 4% solution of buffered formaldehyde and analyzed according to the protocol outlined in Mitchell et al. (2002).

DERIVED METRICS

Mixed Layer and Stratification Indices

Two simple indices of the vertical physical structure of the water column are computed and reported here:

1. The mixed layer depth is determined from CTD observations as the minimum depth where the density gradient is equal to or exceeds 0.01 $kg \cdot m^{-4}$.

2. The stratification index is calculated as:

$$\text{Stratification Index } (kg \cdot m^{-4}) = (\sigma_{t\text{-}50} - \sigma_{t\text{-}zmin})/(50 - z_{min})$$

   where $\sigma_{t\text{-}50}$ and $\sigma_{t\text{-}zmin}$ are measured or interpolated values of density (σ_t) at 50 m and z_{min}, the minimum depth of reliable CTD data, which is typically around 1 m or 2 m and always less than approximately 5 m.

Optical Properties

The optical properties of seawater (attenuation coefficient [K_d], euphotic depth [Z_{eu}]) are derived from *in situ* light attenuation measurements using a rosette-mounted PAR meter and from Secchi disk, according to the following procedures:

1. The downward vertical attenuation coefficient for PAR ($K_{d\text{-}PAR}$) is estimated as the slope of the linear regression of $\ln(E_d(z))$ as a function of depth z (where $E_d(z)$ is the value of downward irradiance at depth z) in the depth interval from minimum depth to around 50 m. The minimum depth is typically around 2 m although the calculation is sometimes forced below that target when near-surface PAR measurements appear unreliable.

2. The value of the light attenuation coefficient $K_{d\text{-}Secchi}$ from Secchi disc observations is found using:

$$K_{d\_secchi} \ (m^{-1}) = 1.44 \ / \ Z_{sd}$$

   where Z_{sd} is the depth (in m) at which the Secchi disc disappears from view (Holmes 1970).

Estimates of the euphotic depth (Z_{eu}), defined as the depth where PAR is 1% of the surface value, are obtained using the following expression (Churilova et al. 2017):

$$Z_{eu} \ (m) = 4.6 \ / \ K_d$$

Vertically Integrated Variables

Integrated chlorophyll-*a* and nutrient inventories are calculated over various depth intervals (e.g., 0–100 m for chlorophyll-*a*, and 0–50 m and 50–150 m for nutrients) using trapezoidal numerical integration. When the maximum depth at a given station is shallower than the lower depth limits noted above, the inventories are calculated by setting the lower integration limit to the maximum depth at that station (e.g., 95 m for P5). Data at the surface (0 m) is taken as the closest near-surface sampled value. Data at the lower depth is taken as:

1. the interpolated value when sampling is below the lower integration limit; or

2. the closest deep-water sampled value when sampling is shallower than the lower integration limit.

Phytoplankton Taxonomic Groups

Phytoplankton abundance and taxonomic composition at the high-frequency sampling stations are estimated from pooled aliquots of water collected in the upper 100 m of the water column using the Utermöhl technique (Utermöhl 1931).

SATELLITE REMOTE SENSING OF OCEAN COLOUR

Near-surface chlorophyll-*a* concentrations derived from ocean colour data collected by the Moderate Resolution Imaging Spectroradiometer (MODIS) "Aqua" sensor are used for the purpose of constructing composite time series for different sub-regions. The MODIS time series extends from July 2002 to present for the selected stations (HL2 and P5) and sub-regions of the Maritimes Region (Cabot Strait [CS], Eastern Scotian Shelf [ESS], Central Scotian Shelf [CSS], Western Scotian Shelf [WSS], Lurcher Shoal [LS], Georges Bank [GB]; Figure 4). The POLY4 band-ratio algorithm (Clay et al. 2019) was used to derive the chlorophyll-*a* concentrations from remote sensing reflectance data which were downloaded from NASA's Ocean Color website (accessed on October 11, 2022). This algorithm is based on the O'Reilly et al. (1998) algorithm but with coefficients that were regionally tuned using the AZMP chlorophyll-*a* database (i.e., high performance liquid chromatography [HPLC] inferred chlorophyll-*a* concentrations). The R Shiny app PhytoFit (accessed on October 11, 2022) was used to download and visualize data as well as compute statistics and bloom metrics (Clay et al. 2021). Basic statistics (mean and standard deviation) are extracted from the weekly MODIS data for the purpose of visualizing the annual cycle and the inter-annual variability of surface chlorophyll-*a* concentrations for the sub-regions (see Figure 14 and Figure 19). Characteristics of the spring bloom are estimated from the daily MODIS data using the shifted-Gaussian function of time model (Zhai et al. 2011). Four metrics are computed to describe the spring bloom characteristics: start date (day of year), cycle duration (days), magnitude (the integral of chlorophyll-*a* concentration under the Gaussian curve), and amplitude (maximum minus the background chlorophyll-*a* concentration).

ANNUAL ANOMALIES SCORECARDS

Scorecards of key indices, based on normalized, seasonally-adjusted annual anomalies, represent physical, chemical, and biological observations in a compact format. Annual estimates of water column inventories of nutrients, chlorophyll-*a,* and the mean abundance of key zooplankton species or groups, at both the high-frequency sampling stations and as an overall average along each of the four standard sections, are based on general linear models of the form:

$$Density = \alpha + \beta_{YEAR} + \delta_{MONTH} + \varepsilon$$ for the high-frequency sampling stations, and

$$Density = \alpha + \beta_{YEAR} + \delta_{STATION} + \gamma_{SEASON} + \varepsilon$$ for the sections.

Density is in units of m^{-2} (or L^{-1} for microplankton abundance), α is the intercept and ε is the error. For the high-frequency sampling stations, β and δ are categorical effects for year and month, respectively. For the sections, β, δ *and* γ take into account the effect of year, station and season, respectively.

This approach is also used to calculate the seasonal estimates of zooplankton indices (i.e., zooplankton biomass and *Calanus finmarchicus* abundance) for the individual sections. In this case, a reduced model including the year and station effects is fitted to the seasonal data subsets. Note that for 2021, seasonal estimates were only calculated for the fall due to the absence of a spring mission.

The general linear model approach is also applied to the weekly remote sensing data to calculate annual estimates of near-surface chlorophyll-*a*. In this case, the model is fitted for each selected sub-region (i.e., HL2, P5, CS, ESS, CSS, WSS, LS and GB) using year and day-of-year as categorical variables.

Density in terms of surface chlorophyll-*a* concentration and *in situ* chlorophyll-*a* inventory is log-transformed [$log_{10}(n)$] to normalize the skewed distribution of the observations. For zooplankton and phytoplankton abundance, one is added to the log-transformed *Density* term [$log_{10}(n+1)$] to include observations for which the value equals zero. Integrated inventories of nutrients and zooplankton biomass are not log-transformed. An estimate of the least-squares means based on Type III Sums of Squares (Lenth et al. 2022) is used as the measure of the overall year effect.

For the ecosystem trawl surveys, seasonal mean indices are calculated as the arithmetic mean of the zooplankton biomass or the log-transformed *C. finmarchicus* abundance data collected within each season/year and each Northwest Atlantic Fisheries Organization (NAFO) area. The reporting of the zooplankton indices based on the NAFO areas for the ecosystem trawl surveys conforms with similar reporting for the physical indices (e.g., DFO 2022) and with most fisheries stock assessment reports.

Annual anomalies are calculated as the deviation of an individual year from the mean of the annual estimates over the period 1999–2020. For the remote sensing surface chlorophyll-*a* and bloom metrics, a reference period of 2003–2020 is used due to missing data prior to 2003. The annual anomalies are expressed either in absolute units or as normalized quantities (i.e., by dividing by the standard deviation [sd] of the annual estimates over the same period). For the purpose of data interpretation, normalized anomalies are considered near normal when within ±0.5 sd, slightly above/below normal when between ±0.5 sd and ±1 sd, and above/below normal otherwise (i.e., larger/smaller than ±1 sd).

A standard set of indices representing anomalies of nutrient availability, phytoplankton biomass, and the abundance of dominant zooplankton species and groups (*C. finmarchicus*, *Pseudocalanus* spp., total copepods, and total non-copepods) are produced in each of the AZMP regions, including the Maritimes. To visualize Northwest Atlantic shelf scale patterns of variability, a zonal scorecard including observations from all of the AZMP regions is presented in DFO's Science Advisory Report (DFO 2022).

ACCESS TO DATA PRODUCTS

Data products presented in Figures 6, 8, 10, 11, 13, 16–18, and 21–32 are published on the Government of Canada's Open government website; a link to the data is available upon request to the corresponding author. Remote sensing data used to calculate the chlorophyll-*a* estimates presented in Figure 14 and Figure 19, and the bloom metrics presented in Figure 15 and Figure 20 can be retrieved from the PhytoFit (accessed on October 11, 2022) open repository.

BEDFORD BASIN MONITORING PROGRAM

The Compass Buoy station (44.69° N, 63.64° W) has been occupied weekly as part of the Bedford Basin Monitoring Program since 1992 (Li 2014). Regular occupations consist of a CTD equipped with a standard suite of sensors (accessed on October 11, 2022) and a vertical net tow for zooplankton identification and enumeration using AZMP protocols. Water samples are collected with Niskin bottles for a variety of analyses (accessed on October 11, 2022) at 2 m, 5 m, 10 m, and 60 m depths. Only zooplankton samples from 1999–2002 and 2012–2020 have been analyzed and archived in a local database; thus, only the CTD sensor and bottle observations are reported in this summary of 2021 conditions.

For ease of interpretation, surface conditions are expressed as the mean conditions across 2 m, 5 m, and 10 m. There is strong seasonal agreement among these depths for the physical and chemical conditions being measured and generally a minor difference in magnitude.

CONTINUOUS PLANKTON RECORDER

The Continuous Plankton Recorder (CPR) is an instrument towed by commercial ships that collects plankton at a depth of approximately 7 m, on a long continuous ribbon of silk (approximately 260-µm mesh). The position on the silk corresponds to the location of the different sampling stations. CPR data are analyzed to detect differences in the surface indices of phytoplankton (colour and relative numerical abundance of large taxa) and zooplankton (relative abundance) for different months, years, or decades in the Northwest Atlantic. Abundance data are expressed in numbers per sample and each sample represents approximately 3 m^3 of filtered seawater. The indices are used to indicate relative changes in concentration over time (Richardson et al. 2006). The sampling methods from the first surveys in the Northwest Atlantic (1960 for the continental shelf) to the present ones have been exactly the same so that valid comparisons can be made between years and decades.

The tow routes between Reykjavik and the GoM are divided into eight regions: WSS, ESS, the southern Newfoundland Shelf, the Newfoundland Shelf, and four regions in the Northwest Atlantic sub-polar gyre, divided into 5 degrees of longitude bins (Figure 5). Only CPR data collected on the SS since 1992 are reported here, since these are comparable, to some extent, to AZMP survey results which date back to 1999 (Head et al. 2022). CPR data collected in all regions and all decades (i.e., including the four regions in the sub-polar gyre east of 45° W) are presented in annual Atlantic Zone Offshore Monitoring Program reports (e.g., Ringuette et al. 2022). In 2020, there was CPR sampling during 10 months on the WSS and 8 months on the ESS.

Monthly log-transformed abundances [$log_{10}(n+1)$] of 14 taxa and the Phytoplankton Colour Index (PCI), a semi-quantitative measure of total phytoplankton abundance, are calculated by averaging values for all individual samples collected within either the WSS or ESS region for each month and year sampled. The examined taxa include: the PCI, diatoms and dinoflagellates (phytoplankton), four groups of *Calanus* species/stages, three representative small copepod taxa, two macrozooplankton taxa, and three acid-sensitive taxa.

Climatological seasonal cycles are obtained by averaging monthly averages for 1992–2020 for three indices of phytoplankton abundance and for the *Calanus* I–IV and *C. finmarchicus* V–VI taxa, and these are compared with values in the months sampled in 2020. Annual abundances

and their anomalies are calculated for all 14 examined taxa for years during which there are 8 or more months of sampling, with no gaps of 3 or more consecutive months, conditions that were met in both regions in 2020.

OBSERVATIONS

MIXING AND OPTICAL PROPERTIES

At HL2, the mixed layer is deepest and the stratification index lowest during the winter months when surface heating is weak and wind-driven mixing is strong (Figure 6). The mixed layer shoals in the spring to minimum depth values from June to August and deepens in the last four months of the year. Similarly, the stratification index increases in the spring to maximum values in August and September and then declines during the fall months. Since the stratification index is calculated using a reference depth of 50 m, low values of the stratification index typically coincide with mixed layer depths deeper than 50 m. Conversely, shallow mixed layer depths (< 50 m) correspond to higher stratification index values that are determined by the strength of the pycnocline below the mixed layer.

In 2021, mixed layer depths at HL2 were near normal and stratification slightly lower than normal during the late-winter and early-spring months (Figure 6). During that period, the mixed layer depth remained near or deeper than 50 m and, therefore, corresponded to low stratification index values. Higher-than-normal wind gusts registered in March at Halifax airport (Figure 7) might have contributed to the deep mixed layer depths observed at that time (Figure 6) and a delay in the onset of stratification. During summer, higher-than-normal water temperatures near the surface (Figure A.1) contributed to slightly shallower-than-normal mixed layer depths and near- or above-normal stratification index values (Figure 6). The mixed layer remained near or shallower than normal during the early fall with mainly above-normal stratification index values (Figure 6). In December, the mixed layer depth was again deeper than normal and the stratification index weaker than normal (Figure 6).

At P5, the mixed layer is typically deeper and more variable, and stratification weaker, than at HL2 due to strong tidal mixing. The stratification index normally remains low (below 0.01 $kg \cdot m^{-4}$) for most of the year and mixed layer depths vary from nearly full depth (90 m) in winter to approximately 40 m in summer (Figure 6).

In 2021, with the exception of the January sampling, mixing parameters could not be calculated for the winter and spring months due to the unavailability of CTD profiles during that period. The mixed layer was markedly deeper than normal during the summer months, except for the July sampling (Figure 6). For June, August and September, the CTD profiles indicated weak warming and freshening in the first few meters of the water column without, however, exceeding the 0.01 $kg \cdot m^{-4}$ density gradient criterion set for determining the depth of the mixed layer. The mixed layer was near normal during the fall but shallower than normal in December (Figure 6). The stratification index values were near normal for most months where sampling occurred with the exception of July where it was slightly above normal and coinciding with the shallowest mixed layer (Figure 6). Wind conditions at Grand Manan were unavailable for a major part of 2021 (Figure 7) but were near normal for the months where CTD profiles were collected, which suggests that the mainly deep mixed layer observed in 2021 likely occurred when tidal mixing was particularly strong.

Euphotic depths (Z_{eu}) in Case 1 waters (e.g., HL2) are generally deepest during the winter months and after the decline of the spring phytoplankton bloom, and shallowest during the period of the bloom when light attenuation in the water column is maximal (Figure 8). In 2021 at HL2, Z_{eu} estimates based on PAR measurements were variable in winter and fall, and near or slightly shallower than normal during summer. Secchi depths were only measured for 6 occupations at HL2 in 2021. Secchi-based euphotic depths were mainly near or slightly deeper than normal, and mostly followed the pattern of seasonal variability (Figure 8).

At P5, which is characterized by Case 2 waters, euphotic depths are relatively constant year-round since the primary attenuator is non-living suspended matter due to tidal action and continental freshwater input (Figure 8). In 2021, the PAR-based euphotic depths were mainly near normal at P5, with the exception of deeper-than-normal values in June and December (Figure 8). Secchi-based euphotic depths were also near normal, with the exception of January and November where the estimated Z_{eu} depth was slightly shallower than normal.

NUTRIENTS

The primary dissolved inorganic nutrients (nitrate, silicate, and phosphate) measured by the AZMP strongly co-vary in space and time (Petrie et al. 1999). For this reason, and because the availability of nitrogen is most often associated with phytoplankton growth limitation in coastal waters of the Maritimes Region (DFO 2000), this report focuses mainly on variability patterns for nitrate, with information on silicate and phosphate concentrations presented mainly to help interpret phytoplankton taxonomic group succession at HL2 and P5.

High-frequency Sampling Stations

At HL2, the highest surface nitrate concentrations are observed in the winter when the water column is well mixed and primary production is low (Figure 9). Surface nitrate declines with the onset of the spring phytoplankton bloom, and the lowest surface nitrate concentrations are observed in spring through early fall. Deep-water nitrate concentrations are lowest in the late fall and early winter, and they increase from February to August, perhaps reflecting sinking and decomposition of the spring phytoplankton bloom (Petrie and Yeats 2000).

The surface and deep nitrate inventories were both lower than normal at HL2 in January 2021 (Figure 10). For surface nitrate, this was consistent with the lower-than-normal levels observed in the fall of 2020 while for deep nitrate, this represented a sharp decrease of around 50% of the value observed in December 2020 (Casault et al. 2022). The deep mixed layers observed in March (Figure 6) appear to have contributed to the upward flux of nitrate resulting in higher-than-normal surface inventories measured in mid- to late-March (Figure 10). Surface nitrate concentrations quickly declined in early April likely in response to the onset of the phytoplankton bloom. Higher-than-normal nitrate concentrations reaching the 50 m depth were observed in July and September (Figure 9) such that the surface nitrate inventory was higher than normal later during those two months (Figure 10). Surface nitrate depletion appear to have persisted until November (Figure 9) resulting in the surface inventory being considerably lower than normal (Figure 10). The late December sampling indicated slightly higher-than-normal surface nitrate inventory and slightly lower-than normal deep nitrate inventory (Figure 10), which were likely associated with the deeper-than-normal mixed layer observed at that time (Figure 6). Overall, the deep and surface nitrate annual inventories at HL2 were respectively above and slightly above average in 2021, ending the trend of lower than average nitrate that has been

observed since 2016 (Figure 11). In parallel with the nitrate conditions, the surface and deep annual inventories of silicate were also above normal at HL2 in 2021, while surface and deep phosphate inventories remained below normal (Figure 11).

The nitrate dynamics at P5 differ considerably from those at HL2 because of nutrient input from the effluent of the nearby Saint John River, combined with the strong tidal mixing which contributes to a lower nitrate accumulation in the deep water while maintaining a higher overall surface inventory. The highest nitrate concentrations are observed in the winter and late fall, when the water column is well mixed from surface to bottom and phytoplankton growth is minimal due to light limitation (Figure 9). Nitrate concentrations start to decline in the upper water column when the spring phytoplankton bloom starts in April or May, and the lowest surface nitrate concentrations are typically observed from June to September.

At P5, the sampling gap that extended from February to May prevented a comprehensive evaluation of the nutrient status for 2021 (Figure 9 and Figure 10). Lower-than-normal nitrate concentrations were observed near the surface in June and July, and low concentrations extended deeper than normal in the water column in August (Figure 9). Sampling in summer and fall indicated mainly near- or below-normal levels for both the surface and deep nitrate inventories in 2021 (Figure 10). Perhaps indicative of deep mixing conditions at P5, there was strong similarity in the pattern of variability between the surface and the deep nitrate inventories (Figure 10). Overall, both the surface and deep nitrate annual inventories at P5 were slightly below average in 2021 for a seventh consecutive year (Figure 11). In parallel with the nitrate conditions, the surface and deep annual inventories of silicate and phosphate were also lower than normal at P5 in 2021 (Figure 11). Inventories of surface and deep silicate and phosphate at P5 have remained mainly below normal levels for the past nine years (Figure 11).

Broad-scale Surveys

There was no seasonal survey in the spring of 2021 and, therefore, the analysis of the broad-scale nutrients on the core sections is limited to the fall observations, which indicated nitrate depletion in the upper 50 m at all stations of all sections (Figure 12). Nonetheless, the annual anomaly estimates of surface nitrate were positive on all sections in 2021 with record-high value for BBL, in sharp contrast with 2020 for that section (Figure 11). For CSL, negative anomalies in surface nitrate in the fall were particularly evident at the easternmost station (CSL6) perhaps indicative of nutrient-poor water associated with the northward inflow to Cabot Strait (Figure 12). For the 50–150 m layer, the anomalies of the annual nitrate estimates were positive on the eastern (CSL and LL) and central (HL) sections and slightly negative for the western (BBL) section, suggesting an east-west along-shelf pattern in nitrate availability. Surface silicate was mainly higher than normal in 2021 with the strongest positive anomalies observed on CSL and BBL (Figure 11). On the other hand, surface phosphate continued the trend of near- or below-normal levels of the last 8 years with the exception of BBL where it was slightly above normal in 2021 (Figure 11). With the exception of BBL, deep silicate was mainly higher than normal in 2021 in sharp contrast with the previous 4 years (Figure 11). Similarly, with the exception of BBL, near- or slightly-above-normal levels of deep phosphate were observed in 2021 in contrast with the previous 5 to 7 years (Figure 11).

PHYTOPLANKTON

Although phytoplankton temporal and spatial variability is high in coastal and shelf waters, a recurrent annual pattern, including a pronounced spring diatom-dominated phytoplankton bloom, is observed across the SS, followed by small secondary summer-fall blooms. A bloom develops as phytoplankton growth outpaces losses such as grazing and sinking (Behrenfeld and Boss 2014). Spring bloom initiation is thought to be regulated by the light environment as well as temperature, starting when the water column stabilizes in late winter and early spring (Sverdrup 1953). Bloom magnitude is thought to be regulated largely by nutrient supply, while bloom duration is regulated by both nutrient supply and, to a lesser extent, by loss processes such as aggregation-sinking, grazing by zooplankton (Johnson et al. 2012), and lysis (Mojica et al. 2016). Phytoplankton biomass is assessed in terms of the integrated chlorophyll-*a* inventory derived from *in situ* measurements and the surface chlorophyll-*a* concentration derived from remote sensing observations. The two indices are complementary and often present divergent patterns due to differences in the spatial and temporal extent of the signal they capture.

High-frequency Sampling Stations

In 2021, *in situ* sampling of chlorophyll-*a* at HL2 suggested that the spring phytoplankton bloom started slightly later than normal with a fast increase and also a rapid decline of biomass such that the bloom duration was seemingly shorter than usual (Figure 13). However, metrics derived from the shifted-Gaussian model using higher temporal resolution chlorophyll-*a* data suggested an earlier-than-normal bloom initiation and a near-normal duration (Figure 14 and Figure 15). Both *in situ* and remotely-sensed data indicated a higher-than normal bloom amplitude with the chlorophyll-*a* inventory or the surface chlorophyll-*a* concentration reaching nearly three to four times their normal levels at the peak of the bloom (Figure 13 and Figure 14). The spring bloom was as usual dominated by diatoms, which accounted for approximately 95% of the total phytoplankton abundance (Figure 16). Following the spring bloom, the chlorophyll-*a* inventory remained slightly below normal until early fall (Figure 13) while surface chlorophyll-*a* concentrations were mainly near or above normal in mid-summer and fall (Figure 14). Flagellates dominated the phytoplankton assemblage from late-spring until early-fall with a higher-than-normal relative abundance (Figure 16). Sub-surface chlorophyll-*a* accumulation appeared in July, August and September, followed by a seemingly intense fall bloom that started in early November (Figure 13). The intense fall bloom in late November was also detected from the surface chlorophyll-*a* concentrations measured by remote sensing (Figure 14). The relative abundance of diatoms in late December was considerably larger than normal (Figure 16). Overall at HL2, the annual estimate of the *in situ* 0–100 m chlorophyll-*a* inventory was lower than normal in 2021 continuing the trend of the previous five years (Figure 17). On the other hand, the annual mean surface chlorophyll-*a* concentration measured by remote sensing reached a record-high value in 2021 and continuing higher-than-normal levels observed in the previous two years (Figure 17). The estimated annual abundance of diatoms was normal in 2021 and contrasting with the lower-than-normal levels observed since 2016. Flagellate and ciliate abundances remained slightly higher than average in 2021, continuing the trend of the last 5 to 7 years (Figure 17).

At P5 in 2021, there was no sampling in February, March, April and May, which prevented any description of the onset of the spring bloom based on *in situ* data (Figure 13). Although the surface chlorophyll-*a* concentrations measured by remote sensing were quite variable during

the spring period (Figure 14), the fitted metrics of the spring bloom suggested a later-than-normal initiation with a shorter-than-normal duration (Figure 15). Except for January, the *in situ* chlorophyll-*a* inventory was lower than normal in all months where sufficient data were available (Figure 13). Relatively high chlorophyll-*a* concentrations were observed *in situ* near the surface in June (Figure 13) but were not detected by remote sensing (Figure 14). The summer phytoplankton bloom which typically develops in August–September indicated lower-than-normal chlorophyll-*a* concentration throughout the upper part of the water column (Figure 13). The phytoplankton community during the August–September bloom was completely dominated by diatoms (Figure 16). Overall at P5, the *in situ* chlorophyll-*a* inventory was below normal in 2021 for a fourth consecutive year and the annual mean surface chlorophyll-*a* concentration measured by remote sensing was also slightly below normal (Figure 17) due mostly to lower-than-normal concentrations observed during summer and early fall (Figure 14). The abundance of dinoflagellates and ciliates was higher than normal while the abundance of diatoms remained lower than normal in 2021, continuing the trend of the last 11 to 13 years, respectively (Figure 17). Flagellate abundance was slightly higher than normal in 2021 and has shown considerable inter-annual variability during the last decade (Figure 17). For P5, the annual estimates of the *in situ* chlorophyll-*a* inventory and the abundance of diatoms could be negatively biased due to the absence of sampling during the critical spring period when phytoplankton biomass increases considerably.

Broad-scale Surveys

Annual estimates of the integrated *in situ* chlorophyll-*a* inventories indicated near or slightly lower-than-normal levels on CSL, LL and HL, and slightly above-normal level on BBL in 2021 (Figure 18). The time series of the *in situ* chlorophyll-*a* inventory annual anomalies indicates considerable short-term variability (approximately 1 to 3 years) within each section, as well as important spatial variability within specific years (Figure 18). For 2021, the annual estimates of the *in situ* chlorophyll-*a* inventory could again be biased negatively due to the absence of spring sampling. In contrast, near-surface chlorophyll-*a* concentrations derived from satellite remote sensing reached record-high levels across most of the region in 2021 (Figure 18). With the exception of GB, surface chlorophyll-*a* levels have remained mainly above normal for the last 3 to 6 years (Figure 18).

Contradictory patterns between the *in situ* integrated chlorophyll-*a* inventory and the remotely sensed surface chlorophyll-*a* concentrations are noticeable for different periods of the time series. For example in 2016 and 2017, the *in situ* integrated chlorophyll-*a* inventory showed predominantly negative anomalies across the region while the surface chlorophyll-*a* concentration from remote sensing showed predominantly positive anomalies (Figure 18). Similar contradictory patterns are also evident in previous years (e.g., 2003–2006, 2010). These apparent inconsistencies could be attributed in part to the inherent differences between the two indices, such as the vertical extent of the signal they capture (i.e., surface vs. water column integrated), the temporal resolution of the observations (i.e., weekly vs. semi-annual), and the spatial extent they represent (i.e., averaging over boxes vs. section means).

The remote-sensing weekly surface chlorophyll-*a* concentrations for 2021 indicated well-defined spring bloom conditions for most sub-areas of the region with the exception of GB (Figure 19a and Figure 19b). Peak surface concentrations reaching two to four times their corresponding climatological values were observed during spring which translated into positive anomalies of

the bloom amplitude and magnitude for all sub-regions with the exception of GB (Figure 20). Following the spring bloom, surface chlorophyll-*a* concentrations remained mainly above normal from late-spring and into the summer in the eastern part of the region (CS, ESS and CSS) (Figure 19a) and mainly near- or below-normal levels in the western part of the region (WSS, LS and GB) (Figure 19b). During fall, surface chlorophyll-*a* concentrations were higher than normal in most sub-regions and indicative of fall bloom conditions across the region. CSS and GB displayed the largest amplitude of the fall bloom (Figure 19a and Figure 19b). Apart from GB, bloom metrics derived from the remote sensing chlorophyll-*a* observations indicated near or slightly earlier-than-normal bloom initiation and variable bloom duration across the region in 2021, with the strongest negative (initiation) and positive (duration) anomalies observed for WSS (Figure 20).

For GB in 2021, surface chlorophyll-*a* concentrations during spring did not clearly indicate the development of spring bloom conditions (Figure 19b) and, therefore, the anomalies of the bloom initiation and duration estimated from the shifted-Gaussian model (Figure 20) are questionable. For the tidally mixed LS sub-region, bloom conditions were evident in 2021, contrasting with the typically low annual variability in the surface chlorophyll-*a* (Figure 19b). Apart from the amplitude, the spring bloom metrics shown in Figure 20 are highly subject to the ability of the shifted-Gaussian model to accurately detect the start and the end of the spring bloom. Inaccurate predictions of the timing of the bloom in one or multiple years can introduce important biases in the resulting anomalies for a given sub-region.

ZOOPLANKTON

High-frequency Sampling Stations

At HL2, the total abundance of zooplankton is lowest in January and February, and increases to maximum values in April, similar to the spring phytoplankton bloom peak timing, before declining to low levels again in the fall (Figure 21). In 2021, the total zooplankton abundance was mainly lower-than-normal from January through September, with the exception of the mid-July sampling, and slightly higher than normal throughout the fall (Figure 21). The total zooplankton abundance was particularly low in early and late spring, and late summer (Figure 21). As expected, the zooplankton community at HL2 was dominated by copepods, representing roughly 80% or more of the total zooplankton abundance throughout the year (Figure 21). Sampling in mid-April and late May indicated a higher-than-normal proportion of euphausiids and decapods in the zooplankton assemblage, which in late May, coincided with zooplankton abundance being considerably lower than climatological levels (Figure 21). Overall at HL2, the annual mean abundance of copepods and non-copepods in 2021 were slightly below and near normal, respectively (Figure 22).

At P5, the total abundance of zooplankton is lowest from January through May and increases to maximum values in July–October, lagging the increase in phytoplankton by about a month, before declining to low levels again in the late fall (Figure 21). In 2021, zooplankton abundance was near normal in January but unavailable from February through May due to the absence of sampling (Figure 21). Total zooplankton abundance was higher than normal during summer but variable from late summer through fall (Figure 21). Exceptionally high counts of bivalve larvae were measured in July which represented nearly 40% of the total abundance and which contributed to the considerably larger-than-normal total zooplankton abundance at that time

(Figure 21). Overall at P5, the annual mean abundance of copepods and non-copepods were both higher than normal in 2021 (Figure 22).

Because copepods generally dominate the local zooplankton community at both stations, their seasonal abundance pattern closely follows that of total zooplankton abundance (Figure 21, Figure 23a and Figure 23b). Therefore, total copepod abundance at HL2 in 2021 was mainly near or below normal from January through September, and near or slightly higher than normal during the fall (Figure 23a). The dominant copepods *Oithona similis* and *Pseudocalanus* spp. represented a combined proportion of roughly 60 to 70% of the total copepod abundance in 2021 while the relative contribution of *Calanus finmarchicus* was slightly higher than normal during spring and early summer (Figure 23a). During the fall, the relative abundance of *Pseudocalanus* spp. and *Centropages* spp. were both higher than normal while that of *Paracalanus* spp. was considerably lower than normal (Figure 23a). Overall at HL2 in 2021, the mean annual abundance of *Pseudocalanus* spp. was higher than normal, and the abundance of *C. finmarchicus* was below normal, continuing a 7-year sequence of mainly below-normal abundances (Figure 22 and Figure 24). Also, *Metridia lucens* and *O. atlantica* were both less abundant in 2021 following periods of 7 to 9 years of mainly higher-than-normal abundances (Figure 24).

At P5, the total copepod abundance in 2021 was normal in January, higher than normal during summer, and variable during late summer and fall (Figure 23b). The relative abundance of the dominant *Pseudocalanus* spp. was below normal during the early summer (Figure 23b) but its overall abundance was above normal in 2021 (Figure 22 and Figure 24). On the other hand, the relative abundance of *C. finmarchicus* was lower than normal for each individual sample (Figure 23b), and it had an overall below-normal annual abundance (Figure 22 and Figure 24). The sub-dominant copepods *Acartia* spp., *Temora longicornis*, and *Eurytemora* spp. had the strongest positive anomalies in 2021 on the basis of their estimated annual means (Figure 24).

The abundance of *C. finmarchicus* at HL2 in 2021 was mainly lower than normal throughout the year with abundance levels particularly low during winter and early spring, and from mid-summer until late fall (Figure 25). The predominance of stages CV and CVI, although at low absolute abundance, persisted slightly longer than usual during early spring (Figure 25). The first generation, characterized by a higher abundance of early stages, peaked at the normal time in mid-April, and a second generation developed later in mid-July (Figure 25). The *C. finmarchicus* population during fall was typically dominated by stage CV with the absence of early stages (CI–CIII) from October until December (Figure 25). Overall at HL2, the abundance of *C. finmarchicus* was considerably lower than normal in 2021 (Figure 22 and Figure 24).

At P5, the abundance of *C. finmarchicus* in 2021 was also mainly lower than normal during each of the months when sampling occurred (Figure 25). Although the initiation of first generation production was not observed due to the absence of sampling in winter and spring, the peak *C. finmarchicus* abundance seemingly occurred at the normal time in June. The *C. finmarchicus* population during summer (June–August) was dominated by the early stages CI–CIII, and in late summer and early fall by stage CV (Figure 25). The absence or exceptionally low abundance (approximately 45 individuals·m^{-2}) of *C. finmarchicus* in November and December, respectively, were atypical, but exceptionally low abundances were confirmed with independent, non-standard net tows performed concomitantly at P5 (J. Fife, DFO, *personal communication*). Overall at P5, the abundance of *C. finmarchicus* was below normal in 2021 (Figure 22 and Figure 24).

Zooplankton biomass is presented in terms of the total wet biomass for zooplankton larger than 0.202 mm and the dry biomass for zooplankton in the size range of 0.202 mm to 10 mm. Consequently, the dry biomass estimates are a close representation of the mesozooplankton size class while the wet biomass estimates can represent both mesozooplankton and macrozooplankton, including gelatinous plankton. However, as Figure 26 suggests, there is strong similarity in the annual variability pattern of dry and wet biomass at both the HL2 and P5 stations. In 2021, mesozooplankton biomass at HL2 was near normal in winter and lower than normal in early spring when it typically increases (Figure 26). Peak biomass was observed in mid-May when it reached a slightly higher-than-normal level. Zooplankton biomass declined rapidly following the peak and remained lower than normal for the rest of the year (Figure 26). Overall, zooplankton biomass was below normal at HL2 in 2021 (Figure 22). At P5 in 2021, mesozooplankton biomass peaked in July with levels nearly four times the climatological value. Otherwise, zooplankton biomass remained mainly near or slightly above normal during the summer and early fall, and near or slightly below normal in late fall (Figure 26). Overall, the annual mean mesozooplankton biomass was above normal in 2021 owing in large part to the large biomass measured in July (Figure 22).

Broad-scale Surveys

The abundance of *C. finmarchicus* during the 2021 winter ecosystem trawl survey on area 5Ze was above average (Figure 27) and the mesozooplankton biomass was near normal (Figure 28). However, those averages were based on only four samples which were all collected in the northeast part of area 5Ze (Figure 27 and Figure 28). Apart from a single sampling event that occurred at HL2, the summer ecosystem trawl survey was cancelled and, therefore, the corresponding seasonal estimates of *C. finmarchicus* abundance and mesozooplankton biomass were unavailable for 2021 (Figure 27 and Figure 28).

The abundance of *C. finmarchicus* during the 2021 fall survey on the main sections was near normal on CSL, LL, and HL, and slightly below normal on BBL (Figure 29). The same spatial pattern was also observed in the annual anomalies of the *C. finmarchicus* abundance estimated from the statistical model (Figure 22). On the other hand, mesozooplankton biomass was normal on LL, below normal on CSL and HL, and slightly above normal on BBL (Figure 30). Again, the annual anomalies of mesozooplankton biomass estimated from the statistical model followed sensibly the same spatial pattern observed for the fall anomalies (Figure 22). For the SS sections (LL, HL, and BBL), stations at the shelf-break generally indicated slightly larger biomass than the on-shelf stations during fall (Figure 30).

The annual abundance of *Pseudocalanus* spp. in 2021, a dominant small copepod taxa on the SS, was below normal for LL, near normal for HL, and slightly above normal for CSL and BBL (Figure 22). For BBL, this represents a 4-year sequence of near- or above-normal abundances, unlike other sections where more inter-annual variability has been observed. Total copepod abundance was slightly below or near normal for CSL and LL, and slightly above normal for HL and BBL in 2021 (Figure 22). For CSL, this represents a 7-year sequence of near- or below-normal abundances whereas other sections have shown more inter-annual variability over the same period.

The abundance of non-copepods in 2021 was higher than normal for CSL, HL, and BBL, and slightly below normal for LL (Figure 22). The strongest positive anomaly in 2021 was observed for euphausiids which was in sharp contrast with 2020 (Figure 31). Euphausiids were

particularly abundant at BBL5 and BBL6 during the fall mission. The strongest negative anomaly in 2021 was observed for chaetognaths which again was in contrast with 2020 (Figure 31). The abundance of chaetognaths during the fall mission was highest at CSL1, HL7, BBL3, and BBL7, but otherwise low at all other stations. Apart from ostracods, which have been nearly absent since 2016, there is considerable inter-annual variability during recent years within the other non-copepod groups such that trends in their abundance are hardly discernible (Figure 31).

Indicator Species

Indicator species provide insights into the response of the copepod community to changes in water mass properties. Arctic *Calanus* species (*Calanus hyperboreus* and *Calanus glacialis*) were less abundant than normal across most of the region in 2021, consistent with the main trend observed since 2012 (Figure 32). The annual anomalies of Arctic *Calanus* species in 2021 are possibly negatively biased due to the absence of sampling during spring, a period when cold water species are typically more abundant. Consequently, the strong negative anomaly for BBL in 2021 was likely driven by the fall sampling during which both *C. hyperboreus* and *C. glacialis* were absent for all BBL occupations. Warm offshore species (*Clausocalanus* spp., *Mecynocera clausi*, and *Pleuromamma borealis*) have been generally more abundant than normal across the region since 2012. In 2021, abundance anomalies were mainly near normal or slightly negative, except at P5 where a strong positive anomaly was recorded (Figure 32) as a result of higher-than-normal abundances of *Clausocalanus* spp. in late summer and fall. The abundance of warm-shelf copepod species (the summer-fall copepods *Paracalanus* spp. and *Centropages typicus*) was near or above normal across the region in 2021, contrasting with the rather variable pattern observed in recent years. The strongest positive abundance anomaly for 2021 was observed at P5 (Figure 32) as a result of higher-than-normal abundances of *C. typicus* in August, and *Paracalanus* spp. in October and November.

DISCUSSION

In the Maritimes Region, the SS is characterized by a strong annual cycle of temperature and stratification, and spatial variability in the form of longitudinal and cross-shelf gradients. While the temperature annual cycle and its perturbations are mostly driven by meteorological forcing, spatial variability is mostly the result of interacting water inputs with the advection of cold fresh waters onto the inshore ESS from the Gulf of St. Lawrence in the northeast and the intrusion of warm and salty slope waters onto the WSS and CSS in the southwest. In addition, the complex bathymetry of the SS contributes to local circulation patterns, which combined with the temporal and spatial hydrographic patterns, have direct and indirect influences on the distribution and dynamics of plankton and nutrients in the region.

Ocean temperatures on the SS and in the GoM have exhibited strong inter-decadal variability since the 1950s, with recent years (2010 and onward) being generally warmer than the long-term averages. A composite index of several *in situ* ocean temperature time series from surface to bottom indicated warmer-than-normal conditions across most of the region in 2021, with record-high temperatures observed near the surface in the central SS (Emerald Basin) and in the Bay of Fundy (BoF) (i.e., at P5) (Hebert et al. In preparation[1]). Sea surface temperatures measured by remote sensing indicated warmer-than-normal conditions across the Maritimes region in 2021, approaching the record-high values observed in 2012 with the strongest annual anomalies observed in the central and western SS, and in the eastern GoM and the BoF.

Stratification on the SS was consistent with the general increasing trend resulting from the combined warming and freshening of surface waters (Hebert et al. In preparation)[1]. The winter North Atlantic Oscillation index dropped from a +1.20 value in 2020 to a −0.14 value in 2021, the largest inter-annual change since 2012–2013. Warmer ocean temperatures observed in 2021 may be directly or indirectly linked to changes observed in the nutrient conditions and the two trophic levels (phytoplankton and zooplankton) surveyed in this report.

The nutrient environment on the SS is influenced directly or indirectly by water inputs from upstream, for example, the Labrador Current and the outflow from the Gulf of St. Lawrence, as well as by intrusions of slope water and Gulf Stream meanders (Pepin et al. 2013). Surface nutrients display strong seasonality linked to phytoplankton production, with surface nutrient depletion typically associated with high production during spring and summer, followed by surface nutrient replenishment during late fall and winter when phytoplankton production is low and vertical mixing is high. On the other hand, deep nutrients, especially nitrate, provide a better representation of the nutrient pool available for new primary production. In addition to changes in shelf circulation, deep nitrate concentrations are also dependent on changes in the export of surface particulate nitrogen and its remineralisation at depth, and on the vertical transport toward the surface via mixing and/or upwelling. Deep nutrient concentrations have been mainly lower than normal since 2013 for silicate and phosphate, and since 2016 for nitrate. Conditions in 2021 suggest a bimodal spatial pattern with deep nutrients being higher (nitrate and silicate) or slightly higher (phosphate) than normal in the eastern and central parts of the region, and slightly lower than normal in the western part of the region (BBL and Prince-5). As mentioned above, the temperature regime in 2021 was comparable to some extent to 2012 when deep nutrients were also observed to be mainly higher than normal across most of the region. Warming events such as observed in 2012 appear to originate from the interaction between the Gulf Stream and the Labrador Current at the tail of the Grand Banks, resulting in the creation of anomalous warm/salty (or cold/fresh) eddies that travel east-to-west along the shelf-break and penetrate onto the shelf via deep channels (Brickman et al. 2018), with possible impacts on the distribution of nutrients in the region. However, the absence of sampling due to the cancellation of the spring survey, and especially the summer ecosystem survey, in 2021 negatively impacts the ability to thoroughly assess the possible mechanisms driving the warm water conditions and the increased nutrient inventories observed in 2021. Although the deep nutrient inventories were near or above normal in 2021, the general trend of lower-than-normal levels observed in recent years coupled with the increase in stratification observed on the SS (Hebert et al. In preparation)[1] could imply lower primary productivity, with potential impacts on the structure and functioning of the food web.

In ocean regions where annual-scale environmental variability is a dominant frequency, plankton life history, behavior, and physiology provide adaptations that focus reproductive effort on favorable times of year and minimize exposure to risk at unfavorable times of year. However, unpredictable perturbations in the range of environmental seasonality and in seasonal timing can disrupt these adaptations (Greenan et al. 2008, Mackas et al. 2012). Large-scale shifts in water mass boundaries also influence local plankton community composition (e.g., Keister et al. 2011). The main recurring feature of the phytoplankton dynamics on the SS and in the GoM is the spring bloom, which develops under favourable conditions of increased insolation, warming water temperatures, and water column stratification. However, Ross et al. (2017) observed spring blooms on the SS when stratification was at its lowest, water temperature at its coldest, and when the surface mixed layer was still much deeper than the euphotic depth, in apparent

contradiction with the critical-depth hypothesis. Phytoplankton biomass declines after the bloom peak as grazing increases or growth becomes nutrient limited. In summer, sporadic occurrences of sub-surface chlorophyll peaks reflect primary production fuelled by regenerated nutrients within the stratified upper water column. Sub-surface summer production makes a significant contribution to the annual primary production on the SS (Ross et al. 2017).

The characteristics of the spring phytoplankton bloom, as inferred from remote-sensing ocean color observations, indicated an earlier-than-normal initiation, longer-than-normal duration, and larger-than-normal magnitude at HL2, and an opposite pattern characterized by a delayed initiation, shorter-than-normal duration, and lower-than-normal magnitude at P5 in 2021. Both cases indicate inverse relationships between start day and duration, and between start day and magnitude, which patterns have been reported previously by Friedland et al. (2018). This pattern of earlier (later) initiation, longer (shorter) and larger (smaller) magnitude also mostly prevailed at the broader scale of the SS in 2021. *In situ* observations at HL2 indicated that the spring bloom occurred during the period when the mixed layer was deepest, and stratification and temperature were lowest, in agreement with the statement by Ross et al. (2017) cited above. Weekly images (not shown) of surface chlorophyll-*a* concentrations indicated that spring bloom conditions in 2021 first developed in the central and western SS prior to the eastern SS, which is inconsistent with the general pattern of westward progression suggested by Song et al. (2010). Weekly satellite composite images also showed relatively high surface chlorophyll-*a* concentrations around Sable Island in mid-April likely due in part to the injection of nutrients by the island's grey seal colony thus supporting enhanced phytoplankton growth (Devred et al. 2021). The PhytoFit application used to derive metrics of the spring phytoplankton bloom from satellite surface chlorophyll-*a* concentrations currently uses a set of generic parameters of the shifted-Gaussian model, which are applied universally to each sub-region of the Maritimes Region. As a result, the application possibly fails to accurately predict some metrics of the bloom as was the case for the bloom initiation for GB in 2021, which suggested a record-high 52-day delay. Future development in the use of the application will require manual fine-tuning of the parameters of the shifted-Gaussian model specific to each sub-region.

Observations at HL2 have indicated the recent period (2015 to present) to be characterised by mainly lower-than-normal abundances of diatoms (also observed at P5) and dinoflagellates, and higher-than-normal abundances of ciliates and flagellates. The CPR observations in recent years also provide evidence of changes toward lower abundances of diatoms and dinoflagellates on the central and western parts of the SS (Casault et al. 2022). Diatoms at HL2 in 2021 were near normal levels due mainly to a higher-than-normal abundance observed in December, which could possibly be linked to the higher-than-normal levels of silicate observed at HL2 in 2021. While the fall period, and especially the fall bloom (Song et al. 2010), is typically dominated by small phytoplankton, Eggy and Aksnes (1992) suggest that flagellate dominance can change to diatom dominance under sufficient silicate availability. Although the minor increase in diatom abundance observed at HL2 in 2021 may be transient, the mainly lower abundance of diatoms observed in recent years could possibly affect the ecosystem at several levels. On the SS, diatoms typically dominate the phytoplankton biomass during the spring bloom, and a decrease in their abundance is likely to result in lower overall annual primary production. Diatom abundance can also be linked to secondary production since large copepods preferentially feed on larger cells. Diatoms also contribute to the deep nitrate pool through remineralisation of particulate nitrate in the deep water resulting from the sedimentation of senescent cells and copepod faecal pellets. An apparent shift toward smaller phytoplankton

taxa could be driven by the warmer ocean conditions on the SS, as has been observed in other areas of the ocean (Doney et al. 2012).

Zooplankton biomass on the SS and in the eastern GoM is normally dominated by large, energy-rich copepods, mainly *C. finmarchicus*, which are important prey for planktivorous consumers such as herring and mackerel, North Atlantic right whales, and other pelagic species. The population responses of *C. finmarchicus* to environmental changes are complex due to interactions among several processes, such as transport by ocean circulation, annual primary production cycles, and *Calanus* life history. The latter focuses reproductive effort on spring bloom production of diatoms and includes a period of late-juvenile-stage dormancy in deep water during less productive seasons. The winter abundance level of *C. finmarchicus* is an indicator of initial conditions for production, while the late-fall abundance level is an indicator of the overwintering stock for production in the following year. *Pseudocalanus* spp. are smaller than *Calanus* spp. and less energy-rich, but they are also important prey for small fish due to their high abundance and wide spatial distribution.

A persistent change in the zooplankton assemblage on the SS has been evident since 2011, marked most notably by the decline in the abundance of *C. finmarchicus*, and a similar decline in mesozooplankton biomass over that same period as *C. finmarchicus* is a biomass-dominant member of zooplankton assemblage. The year 2011 marked a regime shift to lower biomass of *Calanus* spp. on the SS which also coincided with a shift to warmer temperatures (Sorochan et al. 2019). The trend of mainly lower-than-normal abundance of *C. finmarchicus* persisted in 2021, particularly at HL2 and in the western area (BBL and P5). For HL2 and P5, warmer-than-normal water throughout the year was likely linked to low abundance of *C. finmarchicus* during late summer and fall, concurring with observations in the GoM where warming has been linked to a decline in the summer and fall abundance of *C. finmarchicus* since 2010 (Pershing and Stamieszkin 2020, Record et al. 2019).

At the seasonal scale, data collected at HL2 indicated an increase of about 50% of the total *C. finmarchicus* abundance over a one-month period (between December 14, 2020 and January 14, 2021) which could be indicative of advective transport. During the same period, the proportion of stage CV decreased from about 90% of the total *C. finmarchicus* abundance in mid-December 2020 to about 50% in mid-January 2021 as a result of molting to adult stage, thus suggesting early emergence from diapause. The maximum abundance of stages CI–III occurred within a short period following the spring bloom chlorophyll maximum, in agreement with Melle et al.'s (2014) synthesis of HL2 data. Moreover, the presence of warm water (anomalies of +2 to +5°C) throughout the water column (Figure A.1) during the spring period appear to have promoted faster developmental rates and recruitment to stages CI–III.

Along with the overall decline in the abundance of *C. finmarchicus* and zooplankton biomass, observations at HL2 and P5 have indicated consistent changes in the copepod community with generally higher-than-normal abundances of small copepods since around 2012–2014, especially *Centropages* spp., *Temora longicornis*, *Oithona atlantica* (HL2), and *O. similis* (P5). On the other hand, the abundance of *Pseudocalanus* spp. has been generally more variable over the same period. At HL2, *Pseudocalanus* spp. are typically more abundant from spring until mid-summer; however, in 2021, high abundance levels were recorded in fall nearly coinciding with the important fall phytoplankton bloom that developed in November. Small copepods are preferred prey for larval stages of many fish stocks due to their high abundance, appropriate size, and good nutritional value, which promotes larval fish survival and subsequent recruitment

(Shi et al. 2020). The concurrent lower-than-normal abundance of Arctic *Calanus* species and higher-than-normal abundance of warm shelf species is perhaps the most evident manifestation of the warm temperatures observed on the SS in 2021.

In recent years, sampling at the high-frequency sampling stations, cross-shelf sections, and during ecosystem trawl surveys has been compromised as a result of ship unavailability and/or pandemic conditions limiting at-sea activities. A sensitivity analysis was previously implemented (Casault et al. 2022) to address the impact of missed seasonal missions on the annual estimates of the different metrics reported in this document. In summary, the analysis revealed that: i) the uncertainty in the annual anomalies resulting from missing spring sampling is highly variable and typically in the range of ±2 standard deviations; and ii) for several indices, it was possible to infer qualitatively the annual anomaly with respect to the fall anomaly due to strong correlation between the two values. The sensitivity analysis was repeated this year in the context of the missing 2021 spring survey. The results (Figure A.2) indicated that for most metrics, the estimated annual anomalies for 2021 agreed with the measured fall anomalies on the basis of their overall correlations, thus providing reassurance about the qualitative assessment of the 2021 annual anomalies.

The relationships among environmental and plankton conditions are complex and their interpretation from a deterministic perspective requires a comprehensive analysis that is beyond the scope of this report. However, observations in recent years provide increasing evidence of warmer ocean conditions and changes in deep-nutrient availability, coupled with a shift in both phytoplankton and zooplankton communities away from the dominance of large phytoplankton cells and large, energy-rich copepods like *C. finmarchicus* toward smaller phytoplankton and copepod species. Since “classical” food webs, dominated by diatoms and *C. finmarchicus,* are associated with more efficient transfer of energy to higher trophic level pelagic animals than are food webs dominated by small phytoplankton cells and small zooplankton taxa, this shift may indicate a change to less-productive conditions for planktivorous fish, North Atlantic Right Whales, and planktivorous or piscivorous seabirds in the Maritimes Region.

BEDFORD BASIN MONITORING PROGRAM

IMPACTS TO PROGRAM ACTIVITIES

A total of 43 sampling events at the Compass Buoy station in Bedford Basin were conducted in 2021 as part of DFO’s Bedford Basin Monitoring Program (BBMP). Station sampling and subsequent laboratory analyses conducted during 2021 were both impacted by COVID-19 and a series of technical equipment issues. The SBE 25 CTD used failed on sampling event 005 (February 10, 2021), resulting in a total of 42 CTD casts for assessment in this report. On April 26, 2021, BBMP sampling was paused due to the rise in local COVID-19 cases. The program was granted permission to re-commence on June 16, 2021. This resulted in the loss of approximately two months of data and the majority of the spring season from the calculation of annual anomalies of bottom and surface conditions. Oxygen data were not available for the March 4 and March 9 occupations due to sensor unavailability. Moreover, the oxygen values from the March 17 occupation were erroneous and were, therefore, not included for assessment in this report. Finally, the chlorophyll-*a* measured by fluorometer were lost in December 2021 due to sensor failure.

PHYSICAL CONDITIONS

Annual sea surface temperature from the CTD profile data collected in 2021 was above normal (+1.37 sd; Figure 33) compared to the 1999–2020 reference period. Monthly anomalies in surface temperature (Figure 34) in 2021 mostly showed the same above-normal pattern with the exception of the months of August and September, when sea surface temperatures were near normal (+0.03 sd) and slightly above (+0.53 sd) normal, respectively.

Annual average bottom temperature (60 m) was also above normal in 2021 (+1.01 sd; Figure 35). Bottom temperatures were at, slightly above, or above normal across all months of the year, with the highest anomalies occurring during the spring and summer months (Figure 36). Monthly bottom salinities were above or slightly above normal from January to April, near normal from June to August, and below or slightly below normal in September, November and December (but normal in October; Figure 37). The above-normal bottom salinities observed at the beginning of 2021 marks a continuation of the warmer and more saline conditions observed in the bottom waters of Bedford Basin at the end of 2020, when an intrusion of shelf water occurred (Casault et al. 2022). No such intrusion events were evident from evaluation of section plots of temperature, salinity, and density for 2021 (Figure 38), and the bottom waters of the basin remained relatively warm throughout the majority of the year. These intrusion events are an important mechanism for the ventilation of the bottom waters of Bedford Basin (Burt et al. 2013) as they bring oxygen-rich surface waters to the deeper layers of the basin, preventing anoxic conditions from occurring (Hargrave et al. 1976). While the temporally-limited time series of dissolved oxygen samples collected at the Compass Buoy station prevents the calculation of a climatology and anomalies, dissolved oxygen conditions from 39 occupations were at hypoxic levels (1–2 $ml \cdot L^{-1}$; Tyson and Pearson 1991) in the bottom 30–40 m of the basin for the majority of 2021 (Figure 39).

NUTRIENTS AND PLANKTON CONDITIONS

Annual anomalies in all five inorganic nutrients at the surface were near or slightly below normal in 2021 (Figure 33). In contrast, bottom nitrate, phosphate, and silicate were all above normal, while bottom nitrite and ammonium were slightly below or below normal (Figure 35), similar to the pattern in nutrient inventories observed across the broader SS. Bottom nitrate was anomalously high from January until October and subsequently declined to near-normal (but negative) conditions in November and December (Figure 40). The highest concentration of bottom nitrate observed since the start of the time series in 1994 occurred during the month of June (+4.40 sd).

Annual anomalies in surface chlorophyll-*a* (Turner), particulate organic carbon (POC) and nitrogen (PON) were near or slightly above normal in 2021 (Figure 33), similar to the pattern observed in 2020. In contrast, metrics describing the phytoplankton community (e.g., HPLC and plankton pigments) were mostly slightly below normal in 2021, opposite to the conditions observed in 2020. While POC and PON at the bottom (60 m) showed normal conditions, the anomalies for chlorophyll, HPLC and plankton pigments were all below normal in 2021 (Figure 35). With the exception of 2016, this marks a continuation of near- or lower-than-normal metrics of bottom phytoplankton biomass observed in Bedford Basin since 2010.

CONTINUOUS PLANKTON RECORDER

Observations of the abundances of a variety of planktonic taxa are made at monthly intervals in the near surface layer (0–10 m) on the SS by means of the Continuous Plankton Recorder (CPR). However, data are only available with a year's lag compared with AZMP observations so that reporting in this section is for 2020.

PHYTOPLANKTON

Average monthly values of the phytoplankton colour index (PCI) and diatom abundances (1992–2020) on the ESS and WSS show the spring bloom occurring in March–April, with low values in summer (Figure 41). In fall and winter, the PCI is low, but diatom abundance increases over the fall, remaining relatively high in winter. Dinoflagellate abundance shows no clear seasonal cycle. In 2020, PCI values were generally close to normal, although lower than normal in February (ESS) and March (WSS, ESS). Monthly diatom abundances were generally close to normal in both regions, but below normal in March and December (WSS) and February and October (ESS). Monthly dinoflagellate abundances were below normal in March, October and December on the WSS, but otherwise close to normal in both regions. Annual anomalies were mainly neutral or slightly below normal for all three phytoplankton metrics in both regions, but positive for dinoflagellates on the ESS (Figure 42). Diatom abundance has remained mainly below normal on the WSS and ESS since 1999, while the PCI and dinoflagellate abundance have shown no clear trends. These observations are consistent with regional phytoplankton trends reported by AZMP (Casault et al. 2022) and support the idea that the phytoplankton community is changing to one composed of smaller taxa.

ZOOPLANKTON

CPR-derived climatological (1992–2020) seasonal cycles for *Calanus* I–IV (mostly *C. finmarchicus*) and *C. finmarchicus* CV–VI have broad spring–summer (April–July) peaks in abundance on the WSS (Figure 43). On the ESS, *Calanus* CI–IV abundance has a similar, lower-magnitude peak, but *C. finmarchicus* CV–VI does not. On the WSS in 2020, monthly abundances for *Calanus* I–IV were close to normal, but slightly above normal in July, while those for *C. finmarchicus* V–VI were close to normal, but slightly below normal in February. On the ESS, *Calanus* I–IV and *C. finmarchicus* V–VI abundances were higher or slightly higher than normal in May, July and September, lower than normal in August, and near normal February–April and in October. Annual abundances were above normal for both taxa on the ESS and for *Calanus* I–IV on the WSS, where *C. finmarchicus* V–VI abundance was normal (Figure 42). Vertical net tow sampling at HL2 has indicated relatively low annual abundances for *C. finmarchicus* since 2011 (Casault et al. 2022). Consistent with this, the CPR abundance of *C. finmarchicus* V–VI on the WSS has shown a downward trend since 2009 (Figure 42). Annual abundances of the Arctic *Calanus* taxa (*C. glacialis*, *C. hyperboreus*) were above normal in both SS sub-regions in 2020, while those of three small copepod taxa (copepod nauplii, *Para/Pseudocalanus*, *Oithona*) were normal. Annual abundances of two large taxa (euphausiids, hyperiid amphipods) were above (ESS) or near (WSS) the 1992–2020 averages (Figure 42). Since 1992 hyperiid amphipods abundances have shown upward trends in both SS sub-regions and euphausiid abundance has shown a downward trend on the WSS.

ACID SENSITIVE ORGANISMS

In 2020, annual abundances of all three acid-sensitive taxa (coccolithophores, foraminifera, *Limacina* spp.) were near or slightly below normal on the WSS, and near or slightly above normal on the ESS (Figure 42).

SUMMARY

- In 2021, the sampling protocol for the high-frequency sampling stations, seasonal surveys, ecosystem trawl surveys, and Bedford Basin monitoring program, was negatively impacted by ship availability issues and the on-going COVID-19 pandemic restricting at-sea activities. Consequently, there is increased uncertainty in the annual means and anomalies of key indices reported in this document due to gaps in the input data used for their estimation.
- In 2021, surface and deep inventories of nitrate and silicate were higher than average across most of the region while surface and deep phosphate remained mainly near or below normal. Surface and deep inventories of the three nutrients mainly remained near or below normal at P5. For nitrate and silicate, this is the first time in the last 6 to 8 years that the inventories have been consistently higher than normal across most of the region.
- The inventory of chlorophyll-*a* over the 0–100 m layer was mainly lower than normal across the region in 2021. For HL2 and P5, this is continuing the trend of the last 3 to 6 years. On the other hand, surface chlorophyll-*a* as measured by satellite remote sensing remained mainly higher than normal across the region as observed during the last 3 to 6 years.
- With the exception of GB, where the fitted parameters of the shifted-Gaussian model appear inaccurate, the phytoplankton spring bloom, as derived from satellite remote sensing chlorophyll-*a* observations, was mainly earlier than normal across the region with an amplitude and magnitude both higher than normal. However, bloom duration was variable across the region. At HL2, the spring bloom observed by *in situ* measurements showed a rapid onset and decline, a large amplitude, and deep penetration (approximately 60 m) within the water column. Fall blooms were observed in most sub-regions except LS.
- Observations at HL2 indicated near-normal levels of diatoms and dinoflagellates in 2021 in contrast with recent years. Ciliates and flagellates at HL2 continued to be more abundant than normal. At P5, the pattern of lower abundance of diatoms and higher abundance of dinoflagellates and ciliates continued as in the last 11–13 years. Flagellate abundance at P5, which has been variable over that same period, was near normal in 2021.
- In 2021, the abundance of *C. finmarchicus* was mainly lower than normal, particularly at HL2 and in the western area (BBL and P5). *Pseudocalanus* spp. and non-copepod abundances were mainly higher than normal across the region, except for lower-than-normal levels on LL, while total copepod abundance was variable across the region. Mesozooplankton biomass was mainly lower than normal in the eastern and central (CSL to HL2) areas but higher than normal in the west (BBL and P5).
- The abundance of Arctic *Calanus* and warm-shelf copepod species were, respectively, mainly lower and mainly higher than normal across the region in 2021, perhaps in response to overall warm water conditions. Apart from *Pseudocalanus* spp. which were more

abundant than normal at both HL2 and P5 in 2021, near- or lower-than-normal abundances were observed for the small copepods *O. similis*, *O. atlantica* (HL2), and *Microcalanus* spp. and *Paracalanus* spp. (HL2 and P5).

- Average surface and bottom temperatures in Bedford Basin were above normal in 2021. Nutrient inventories at the surface were near or slightly below normal, while nitrate, phosphate, and silicate in the bottom layers of Bedford Basin (60 m) were all above normal. These results are consistent with the general trends in temperatures and nutrients observed across the broader SS in 2021.
- There was no evidence to suggest that an intrusion event, which is an important mechanism for deep water ventilation, occurred in Bedford Basin during 2021. Evaluation of dissolved oxygen concentrations indicated hypoxic conditions in the bottom layers of the basin throughout most of 2021.
- CPR observations indicated that in 2020 annual average PCI values and diatoms abundances were close to normal in both SS regions, while dinoflagellate abundance was close to (WSS) or above (ESS) normal.
- CPR observations indicated that in 2020 annual abundances of the *Calanus* I– IV taxon (mostly *C. finmarchicus* CI–IV) were above normal in both SS regions, while those for *C. finmarchicus* CV–VI were above (ESS) or near (WSS) normal. Average annual abundances for two arctic *Calanus* species, the small copepods (*Para/Pseudocalanus*) and two macrozooplankton (euphausiids, hyperiids) taxa were above normal on the ESS. Of these, only *C. glacialis* was more abundant than normal on the WSS, where the other four were at normal levels.

ACKNOWLEDGEMENTS

The authors thank the personnel at the Bedford Institute of Oceanography and St. Andrews Biological Station who contributed to sample collection, sample analysis, data analysis, data management, and data sharing. We also thank the officers and crews of the Canadian Coast Guard Ships *Capt. Jacques Cartier, Hudson, Teleost, Sigma-T*, and *Viola M. Davidson* for their assistance in the collection of oceanographic data during 2021. Reviews by David Bélanger and Marjolaine Blais improved the manuscript.

REFERENCES CITED

Behrenfeld, M.J., and Boss, E.S. 2014. Resurrecting the Ecological Underpinnings of Ocean Plankton Blooms. Annu. Rev. Mar. Sci. 6: 167–194.

Brickman, D., Hebert, D., and Wang, Z. 2018. Mechanism for the recent ocean warming events on the Scotian Shelf of eastern Canada. Cont. Shelf Res. 156: 11–22.

Burt, W.J., Thomas, H., Fennel, K., and Horne, E. 2013. Sediment-water column fluxes of carbon, oxygen and nutrients in Bedford Basin, Nova Scotia, inferred from ^{224}Ra measurements. Biogeosciences. 10: 53–66.

Casault, B., Johnson, C., Devred, E., Head, E., Beazley, L., and Spry, J. 2022. Optical, Chemical, and Biological Oceanographic Conditions on the Scotian Shelf and in the eastern Gulf of Maine during 2020. DFO Can. Sci. Advis. Sec. Res. Doc. 2022/018. v + 82 p.

Churilova, T., Suslin, V., Krivenko, O., Efimova, T., Moiseeva, N., Mukhanov, V., and Smirnova L. 2017. Light Absorption by Phytoplankton in the Upper Mixed Layer of the Black Sea: Seasonality and Parametrization. Frontiers in Mar. Sci. 4: 90.

Clay, S., Peña, A., DeTracey, B., and Devred, E. 2019. Evaluation of Satellite-Based Algorithms to Retrieve Chlorophyll-a Concentration in the Canadian Atlantic and Pacific Oceans. Remote Sens. 11(22): 2609.

Clay, S., and Layton, C. 2021. BIO-RSG/PhytoFit: First release (Version v1.0.0). Zenodo.

Devred, E., Hilborn, A., and den Heyer, C. E. 2021. Enhanced chlorophyll-*a* concentration in the wake of Sable Island, eastern Canada, revealed by two decades of satellite observations: a response to grey seal population dynamics? Biogeosciences. 18: 6115–6132.

DFO. 2000. Chemical and Biological Oceanographic Conditions in 1998 and 1999 – Maritimes Region. DFO Sci. Stock Status Rep. G3-03 (2000).

DFO. 2022. Oceanographic Conditions in the Atlantic Zone in 2021. DFO Can. Sci. Advis. Sec. Sci. Advis. Rep. 2022/025.

Doney, S.C., Ruckelshaus, M., Duffy, J.E., Barry, J.P., Chan, F., English, C.A., Galindo, H.M., Grebmeier, J.M., Hollowed, A.B., Knowlton, N., Polovina, J., Rabalais, N.N., Sydeman, W.J., and Talley, L.D. 2012. Climate change impacts on marine ecosystems. Annu. Rev. Mar. Sci. 4: 11–37.

Eggy, J.K., and Aksnes, D.L. 1992. Silicate as regulating nutrient in phytoplankton competition. Mar. Ecol. Prog. Ser. 83: 281–289.

Friedland, K.D., Mouw, C.B., Asch, R.G., Ferreira, A.S.A, Henson, S., Hyde, K.J.W., Morse, R.E., Thomas, A.C., and Brady, D.C. 2018. Phenology and time series trends of the dominant seasonal phytoplankton bloom across global scales. Glob. Ecology Biogeography. 27(5): 551–569.

Greenan B.J.W., Petrie B.D., Harrison W.G., Strain P.M. 2008. The onset and evolution of a spring bloom on the Scotian Shelf. Limnol. Oceanogr. 53(5): 1759-1775.

Hargrave, B.T., Phillips, G.A., and Taguchi, S. 1976. Sedimentation Measurements in Bedford Basin, 1973–1974. Tech. Rep. Fish. Mar. Serv. Envir. 608, xv + 129 p.

Harrison, G., Colbourne, E., Gilbert, D., and Petrie, B. 2005. Oceanographic Observations and Data Products Derived from Large-scale Fisheries Resource Assessment and Environmental Surveys in the Atlantic Zone. AZMP/PMZA Bull. 4: 17–23.

Head, E.J.H., Johnson, C.L., and Pepin, P. 2022. Plankton monitoring in the Northwest Atlantic: a comparison of zooplankton abundance estimates from vertical net tows and Continuous Plankton Recorder sampling on the Scotian and Newfoundland shelves, 1999–2015. ICES J. Mar. Sci. 79(3): 901-916.

Holmes, R.W. 1970. The Secchi Disk in Turbid Coastal Waters. Limnol. Oceanogr. 15(5): 688–694.

Johnson, C., Harrison, G., Head, E., Casault, B., Spry, J., Porter, C., and Yashayaev, I. 2012. Optical, Chemical, and Biological Oceanographic Conditions in the Maritimes Region in 2011. DFO Can. Sci. Advis. Sec. Res. Doc. 2012/071.

Keister, J.E., Di Lorenzo, E., Morgan, C.A., Combes, V., and Peterson, W.T. 2011. Zooplankton species composition is linked to ocean transport in the Northern California Current. Global Change Biol. 17: 2498–2511.

Lenth, R., Singmann, H., Love, J., Buerkner, P., and Herve, M. 2022. emmeans: Estimated Marginal Means, aka Least-Squares Means. R package version 1.7.5.

Li, W.K.W. 2014. The state of phytoplankton and bacterioplankton at the Compass Buoy Station: Bedford Basin Monitoring Program 1992–2013. Can. Tech. Rep. Hydrogr. Ocean Sci. 304.

Mackas, D.L., Greve, W., Edwards, M., Chiba, S., Tadokoro, K., Eloire, D., Mazzocchi, M.G., Batten, S., Richardson, A.J., Johnson, C., Head, E., Conversi, A., and Pelosi, T. 2012. Changing zooplankton seasonality in a changing ocean: Comparing time series of zooplankton phenology. Progr. Oceanogr. 97–100: 31–62.

Melle, W., Runge, J., Head, E., Plourde, S., Castellani, C., Licandro, P., Pierson, J., Jonasdottir, S., Johnson, C., Broms, C., Debes, H., Falkenhaug, T., Gaard, E., Gislason, A., Heath, M., Niehoff, B., Nielsen, T. G., Pepin, P., Stenevik, E. K., and Chust, G. 2014. The North Atlantic Ocean as habitat for *Calanus finmarchicus*: Environmental factors and life history traits. Prog. Ocean. 129: 244–284.

Mitchell, M., Harrison, G., Pauley, K., Gagné, A., Maillet, G., and Strain, P. 2002. Atlantic zonal monitoring program sampling protocol. Can. Tech. Rep. Hydrogr. Ocean Sci. 223.

Mojica, K.D.A., Huisman, J., Wilhelm, S.W., and C.P.D. Brussaard. 2016. Latitudinal variation in virus-induced mortality of phytoplankton across the North Atlantic Ocean. ISME J. 10: 500–513.

O'Reilly, J.E., Maritorena, S., Mitchell, B. G., Siegel, D. A., Carder, K. L., Garver, S. A., Kahru, M., and McClain, C. R. 1998. Ocean color chlorophyll algorithms for SeaWiFS. J. Geophys. Res. 103: 24937–24953.

Pepin, P., Maillet, G.L., Lavoie, D., and Johnson, C. 2013. Temporal trends in nutrient concentrations in the Northwest Atlantic basin. Ch. 10 (pp. 127–150) In: Aspects of climate change in the Northwest Atlantic off Canada [Loder, J.W., G. Han, P.S. Galbraith, J. Chassé and A. van der Baaren (Eds.)]. Can. Tech. Rep. Fish. Aquat. Sci. 3045: x + 190 p.

Pershing, A.J. and Stamieszkin, K. 2020. The North Atlantic Ecosystem, from Plankton to Whales. Annu. Rev. Mar. Sci. 12(1): 339–359.

Petrie, B. 2007. Does the north Atlantic oscillation affect hydrographic properties on the Canadian Atlantic continental shelf? Atmos. Ocean 45(3): 141–151.

Petrie, B., and Yeats, P. 2000. Annual and interannual variability of nutrients and their estimated fluxes in the Scotian Shelf - Gulf of Maine region. Can. J. Fish. Aquat. Sci. 57: 2536–2546.

Petrie, B., Yeats, P., and Strain, P. 1999. Nitrate, Silicate and Phosphate Atlas for the Scotian Shelf and the Gulf of Maine. Can. Tech. Rep. Hydrogr. Ocean Sci. 203.

Record, N.R., et al. 2019. Rapid Climate-Driven Circulation Changes Threaten Conservation of Endangered North Atlantic Right Whales. Oceanography. 32(2): 162–169.

Richardson, A.J., Walne, A.W., John, A.W.G., Jonas, T.D., Lindley, J.A., Sims, D.W., Stevens, D., and Witt, M. 2006. Using continuous plankton recorder data. Progr. Oceanogr. 68: 27–74.

Ringuette, M., Devred, E., Azetsu-Scott, K., Head, E., Punshon, S., Casault, B., and Clay, S. 2022. Optical, Chemical, and Biological Oceanographic Conditions in the Labrador Sea between 2014 and 2018. DFO Can. Sci. Advis. Sec. Res. Doc. 2022/021. v + 38 p.

Ross, T., Craig, S.E., Comeau, A., Davis, R., Dever, M., and Beck, M. 2017. Blooms and subsurface phytoplankton layers on the Scotian Shelf: Insights from profiling gliders. J Marine Syst. 172: 118–127.

Shi, Y., Wang, J., Zuo, T., Shan, X., Jin, X., Sun, J., Yuan, W., and Pakhomov, E.A. 2020. Seasonal Changes in Zooplankton Community Structure and Distribution Pattern in the Yellow Sea, China. Frontiers in Mar. Sci. 7: 391.

Song, H., Ji, R., Stock, C., and Wang, Z. 2010. Phenology of phytoplankton blooms in the Nova Scotian Shelf–Gulf of Maine region: remote sensing and modeling analysis. J. Plankton Res. 32(11): 1485–1499.

Sorochan, K.A., Plourde, S., Morse, R., Pepin, P., Runge, J., Thompson, C., and Johnson, C.L. 2019. North Atlantic right whale (*Eubalaena glacialis*) and its food: (II) interannual variations in biomass of *Calanus* spp. on western North Atlantic shelves. J. Plankton Res. 41(5): 687–708.

Sverdrup, H.U. 1953. On Conditions for the Vernal Blooming of Phytoplankton. J. Cons. Perm. Int. Explor. Mer. 18: 287–295.

Therriault, J.-C., Petrie, B., Pepin, P., Gagnon, J., Gregory, D., Helbig, J., Herman, A., Lefaivre, D., Mitchell, M., Pelchat, B., Runge, J., and Sameoto, D. 1998. Proposal for a Northwest Atlantic Zonal Monitoring Program. Can. Tech. Rep. Hydrogr. Ocean Sci. 194.

Tyson, R.V., and Pearson, T.H. 1991. Modern and Ancient Continental Shelf Anoxia. Geological Society Special Publications. No 58. pp 1–24.

Utermöhl, von H. 1931. Neue Wege in der quantitativen Erfassung des Plankton.(Mit besonderer Berücksichtigung des Ultraplanktons.). Verh. Int. Verein. Theor. Angew. Limnol. 5**:** 567–595.

Zhai, L., Platt, T., Tang, C., Sathyendranath, S., and Hernández Walls, R. 2011. Phytoplankton Phenology on the Scotian Shelf. ICES J. Mar. Sci. 68: 781–791.

TABLES

Table 1. Atlantic Zone Monitoring Program sampling missions in the Maritimes Region in 2021.

Group	Location	Mission ID	Dates	# Hydro Stations	# Net Stations
Ecosystem Trawl Survey	Georges Bank	TEL2021-002	Mar 17–Apr 1	29	5
Labrador Sea Mission	Cabot Strait & Louisbourg sections	HUD2021-127	May 20–Jun 1	14	13
Sea Trials	Browns Bank & Halifax sections	CAR2021-102	Jun 4–6 Jun 20–22	14	14
Seasonal Sections	Scotian Shelf	HUD2021-185	Sep 16–Oct 4	100	96
High-frequency Stations	Halifax-2	BCD2021-666	Jan 01–Dec 31	18(10)*	18(10)*
High-frequency Stations	Prince-5	BCD2021-669	Jan 01–Dec 31	8	8
			Total:	*182*	*154*

* Total station occupations, including occupations during trawl surveys and seasonal sections (dedicated occupations with mission ID as listed at left are in parentheses).

FIGURES

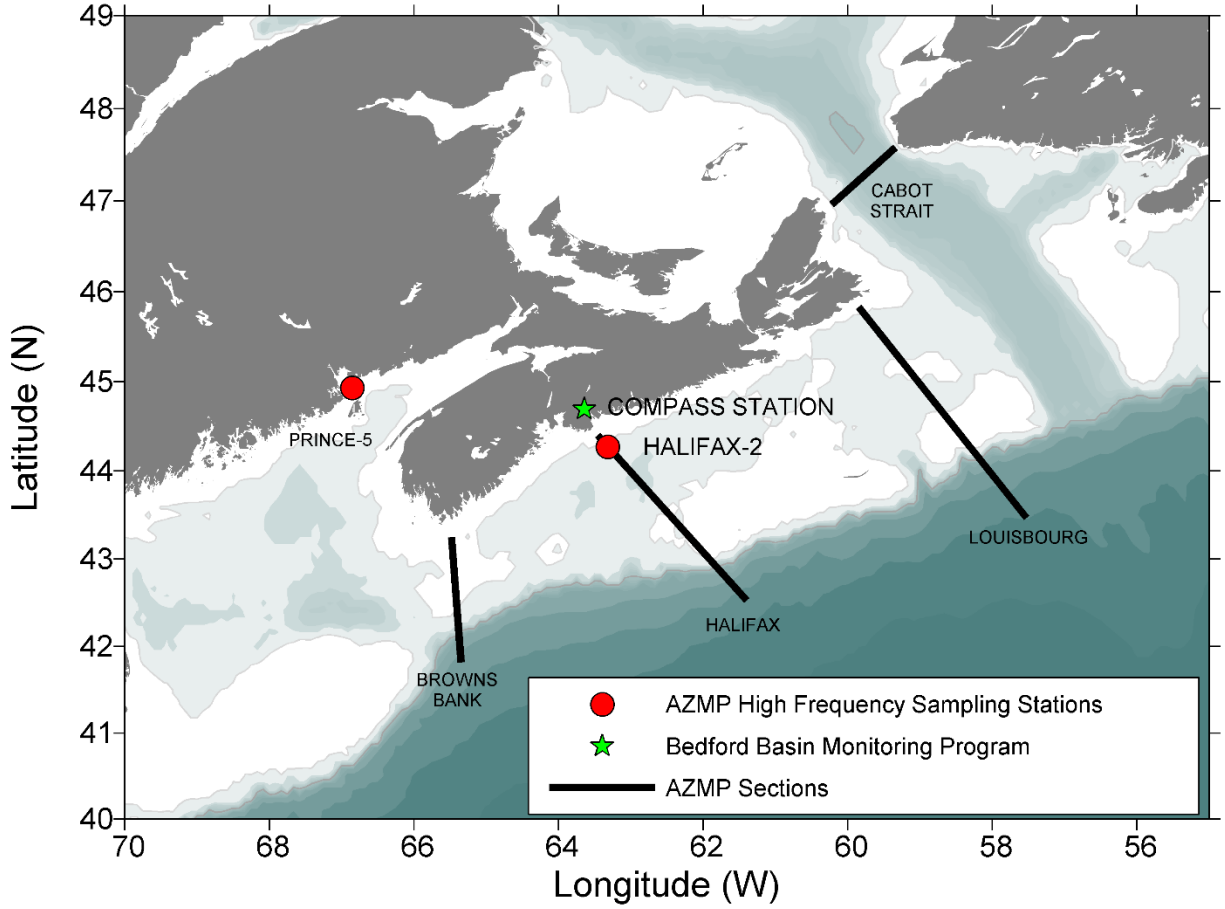

Figure 1. Map of primary sections (Cabot Strait [CSL]; Louisbourg [LL]; Halifax [HL]; Browns Bank [BBL]) and high-frequency sampling stations (Halifax-2 [HL2]; Prince-5 [P5]) sampled in the DFO Maritimes Region. The Compass Buoy station is sampled as part of the Bedford Basin Monitoring Program.

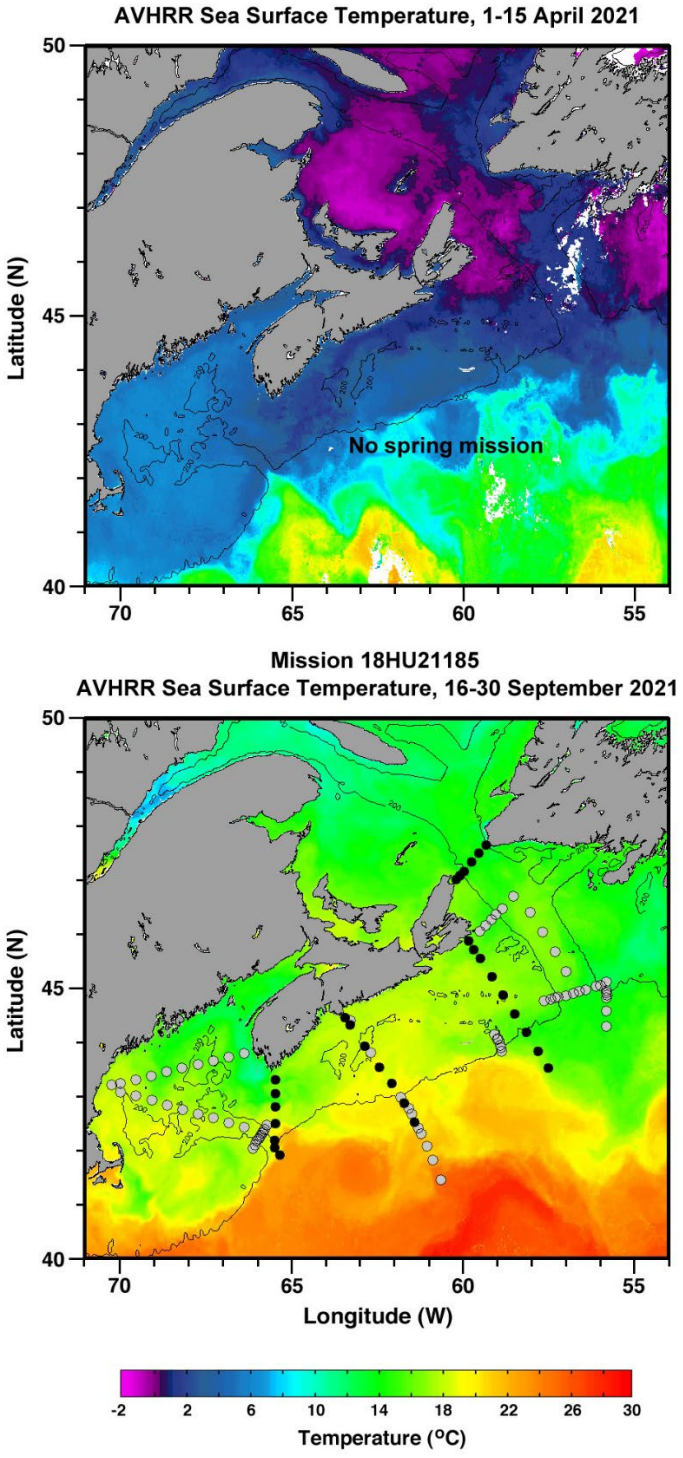

Figure 2. Stations sampled during the 2021 fall survey (lower panel). Station locations are superimposed on sea-surface-temperature composite images for dates close to the 2021 mission dates (fall mission only). Black markers indicate core stations, and gray markers indicate stations sampled for ancillary programs.

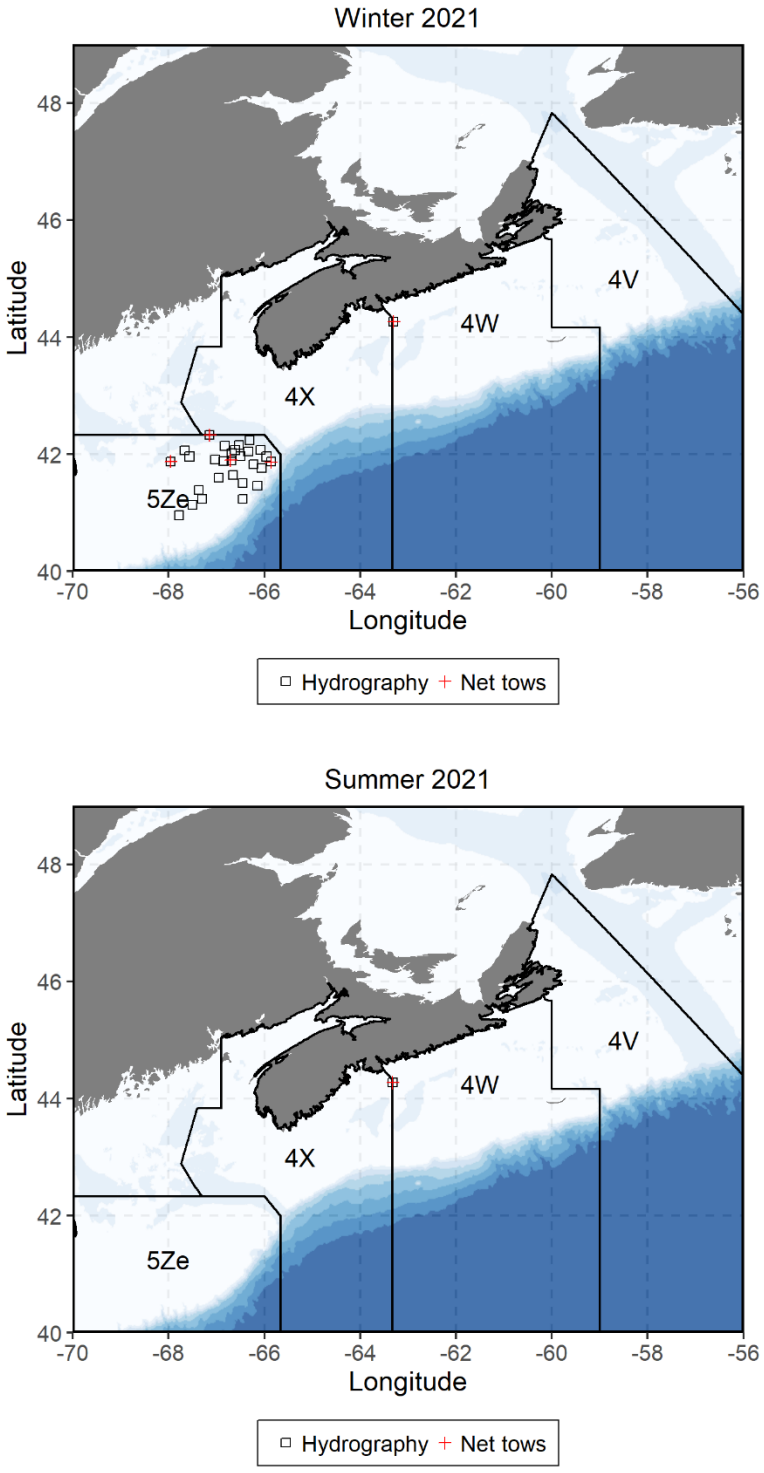

Figure 3. Stations sampled during Maritimes Region ecosystem trawl surveys in 2021. Station locations are superimposed on NAFO areas.

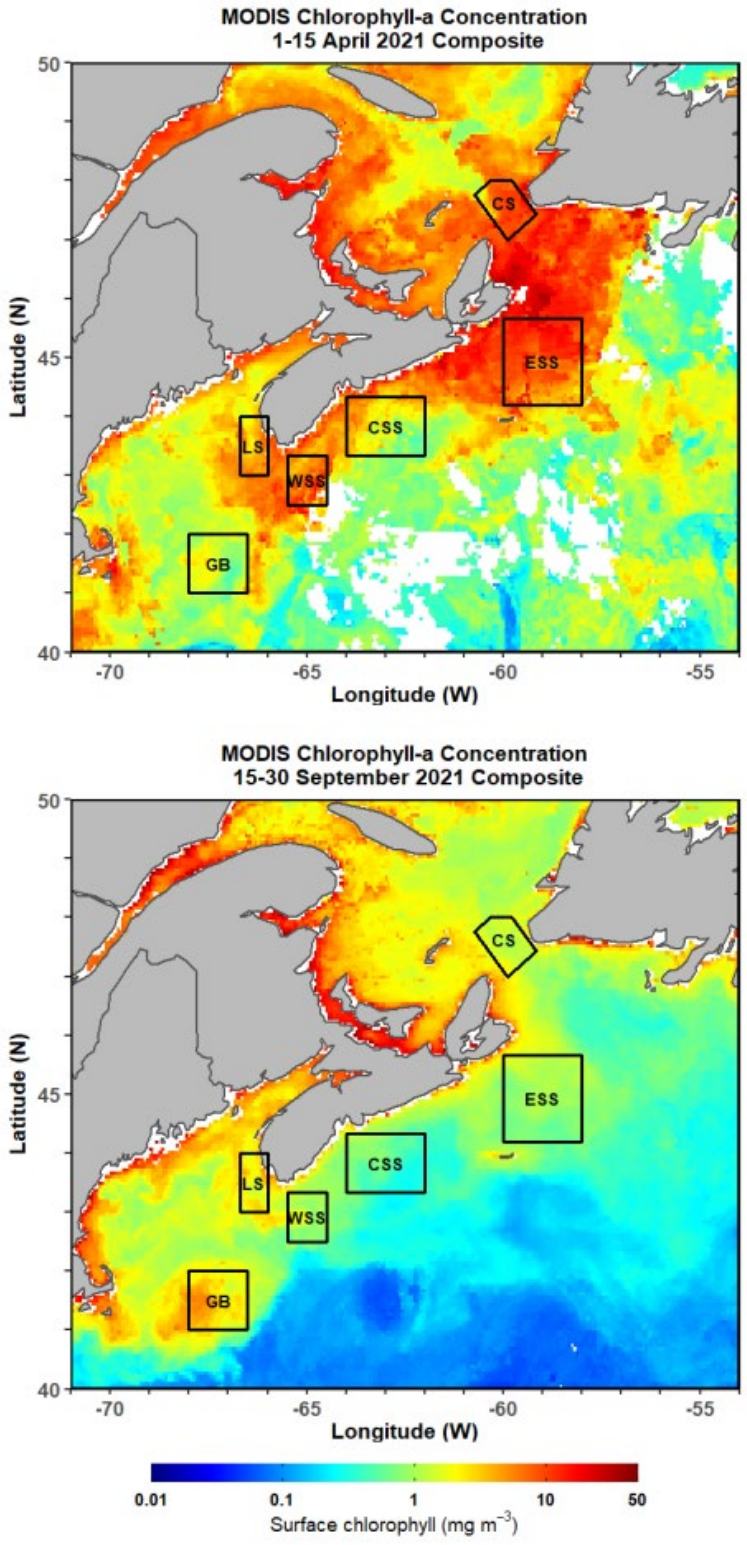

Figure 4. Sub-regions in the Maritimes Region identified for spatial/temporal analysis of satellite ocean colour data. Sub-regions are superimposed on surface chlorophyll-a composite images for dates close to the 2021 mission dates (fall mission only). Cabot Strait [CS]; Eastern Scotian Shelf [ESS]; Central Scotian Shelf [CSS]; Western Scotian Shelf [WSS]; Lurcher Shoal [LS]; Georges Bank [GB].

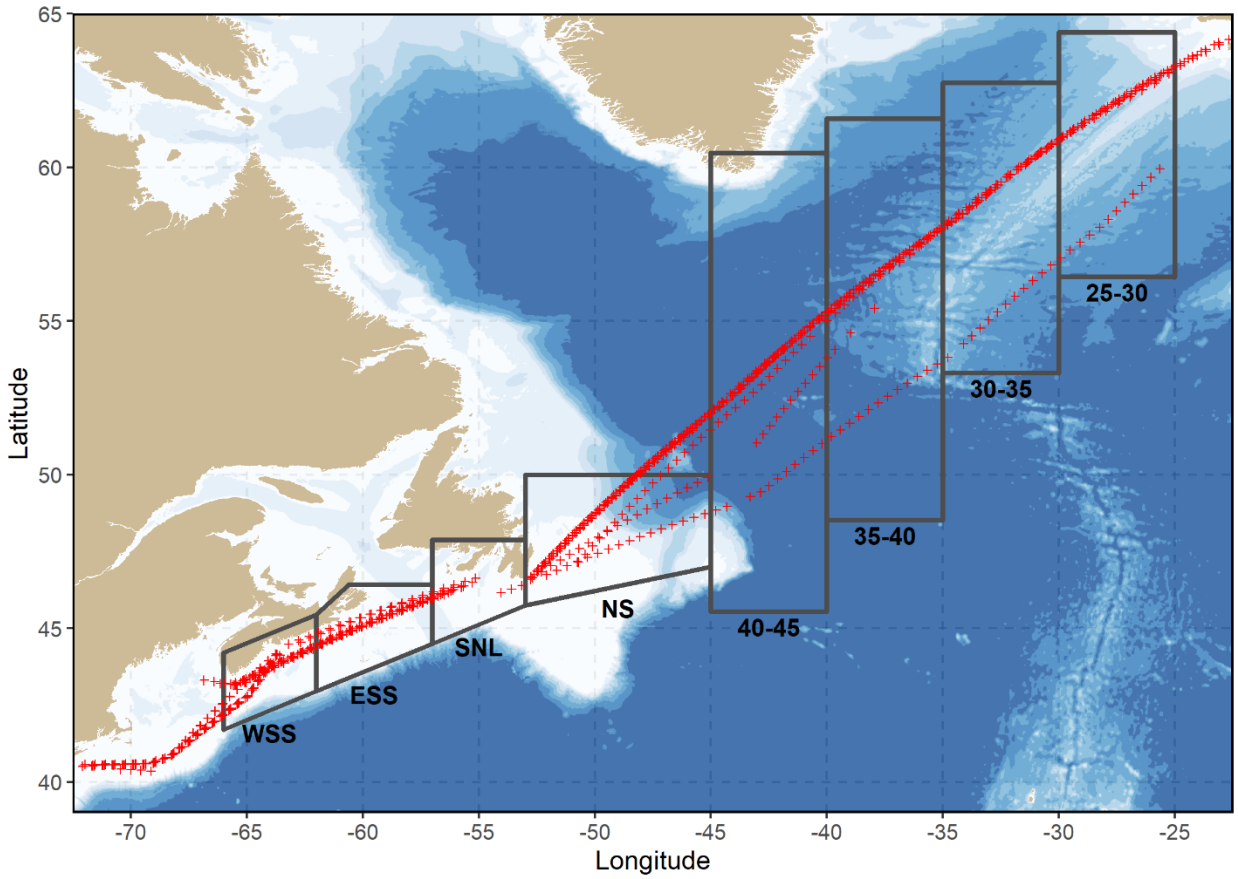

Figure 5. Continuous Plankton Recorder (CPR) lines and stations sampled in 2020 (red markers). Data are analysed by region. Regions are: Western Scotian Shelf (WSS), Eastern Scotian Shelf (ESS), South Newfoundland Shelf (SNL), Newfoundland Shelf (NS), and between longitudes 40–45°W, 35–40°W, 30–35°W, 25–30°W.

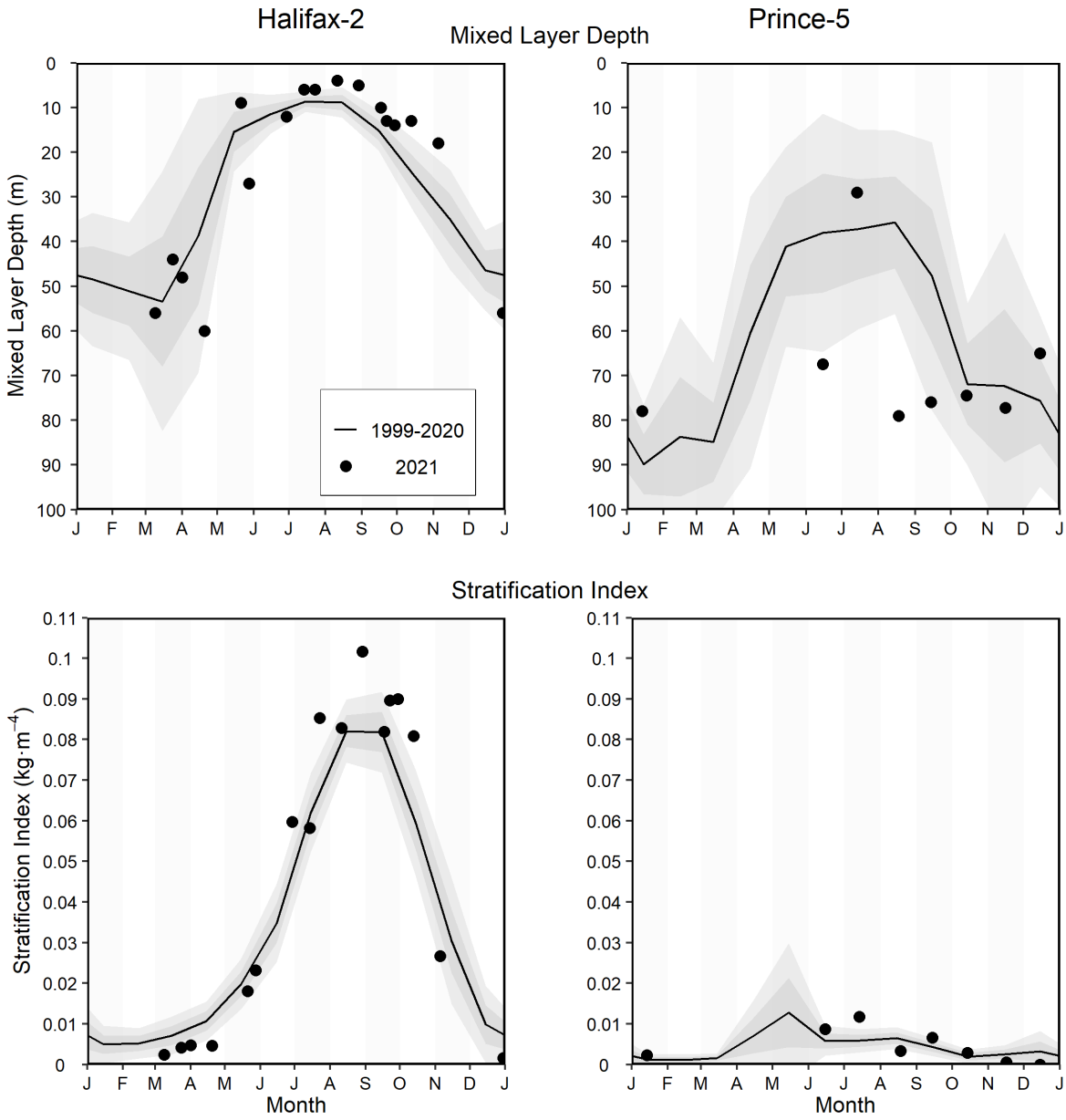

Figure 6. Mixing properties (mixed layer depth, stratification index) at the Maritimes high-frequency sampling stations comparing 2021 data (solid circle) with mean conditions from 1999–2020 (solid line). The gray shaded ribbons represent the standard deviation (±0.5 and ±1 sd) of the monthly means. Tick marks on the horizontal axes indicate the 1st day of the month.

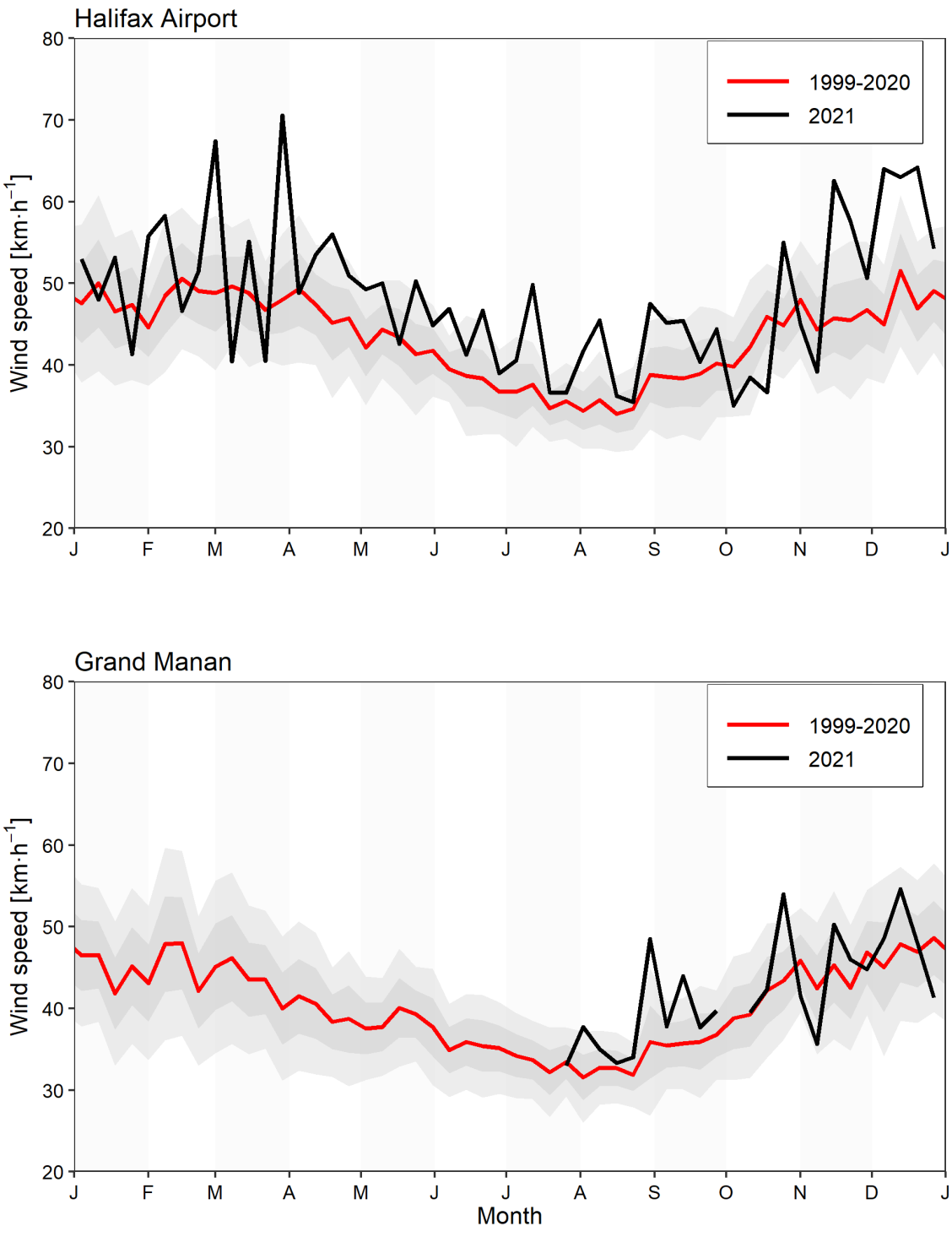

Figure 7. Weekly mean of maximum daily wind gust at Halifax Stanfield International Airport (representative of wind conditions at Halifax-2) and Grand Manan Island (representative of wind conditions at Prince-5) for the year 2021 (black line) and the 1999–2020 climatology (red line). The gray shaded ribbons represent the standard deviation (±0.5 and ±1 sd) of the weekly means. Tick marks on the horizontal axes indicate the 1st day of the month.

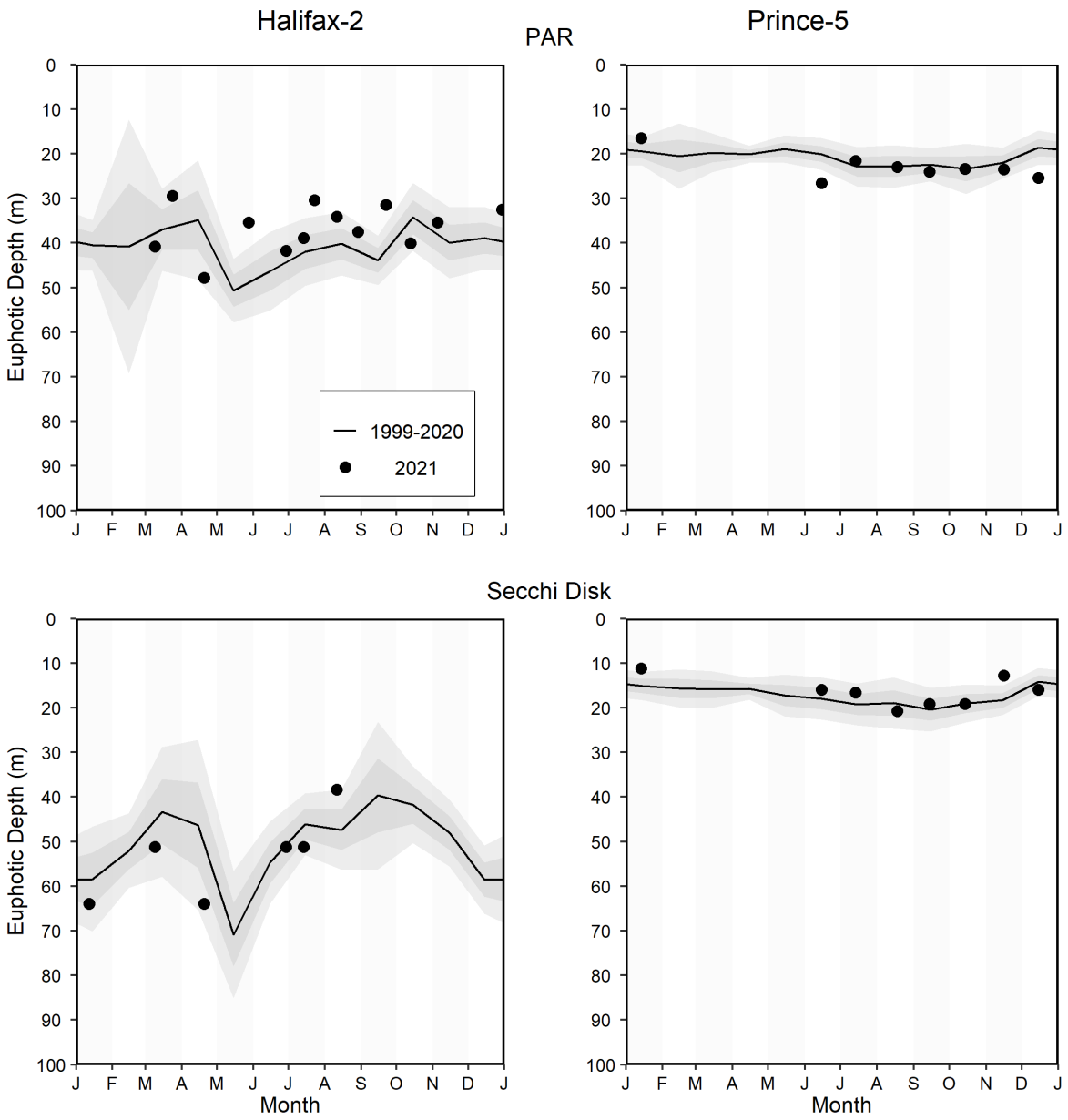

Figure 8. Optical properties (euphotic depth from PAR irradiance meter and Secchi disc) at the Maritimes high-frequency sampling stations. Year 2021 data (solid circle) compared with mean conditions from 1999–2020 (solid line), except 2001–2020 for euphotic depth from PAR at Prince-5. The gray shaded ribbons represent the standard deviation (±0.5 and ±1 sd) of the monthly means. Tick marks on the horizontal axes indicate the 1st day of the month.

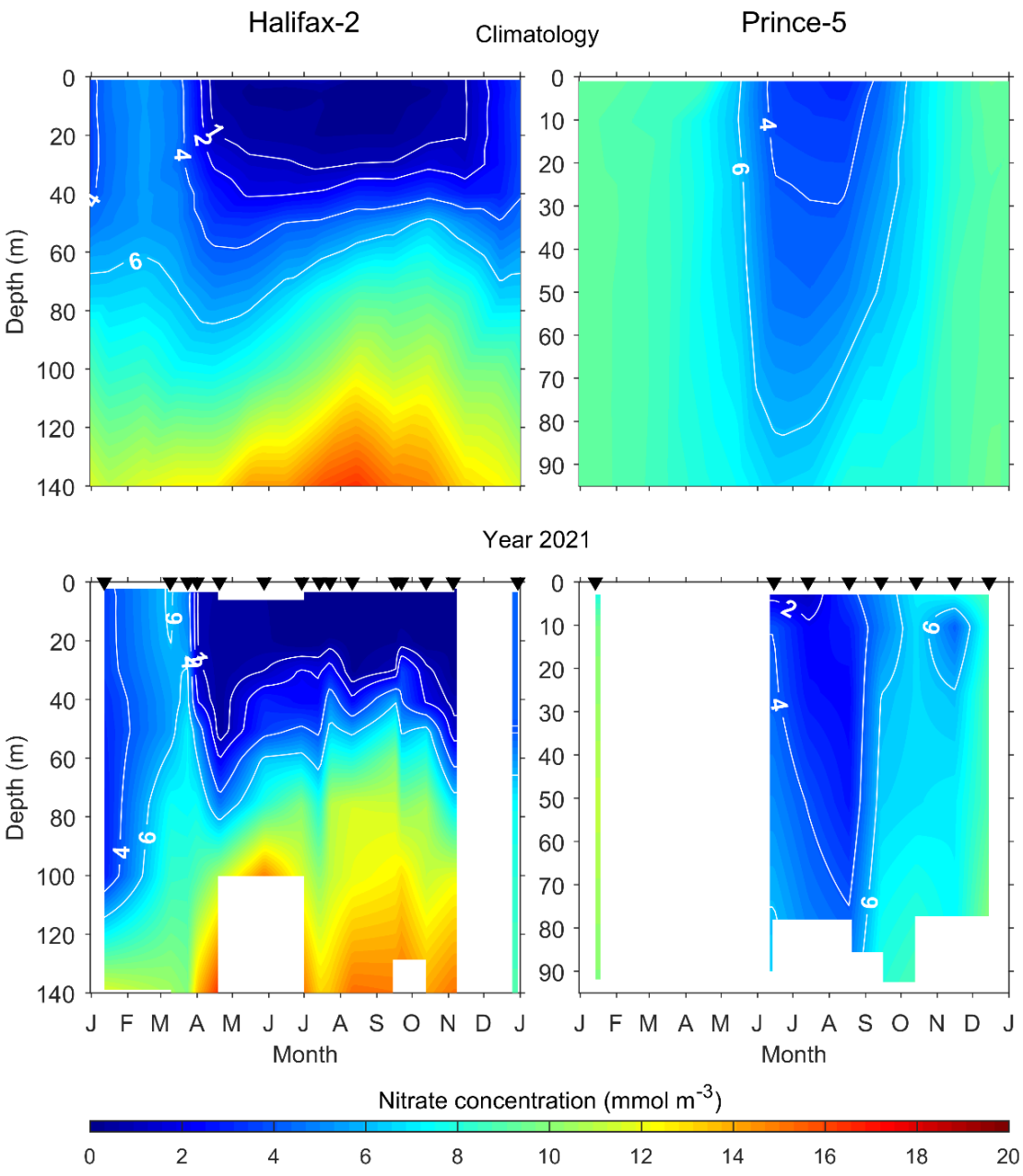

Figure 9. Comparison of the annual cycle of nitrate concentrations (mmol·m^{-3}) in 2021 (bottom panels) with climatological conditions from 1999–2020 (upper panels) at the Maritimes high-frequency sampling stations. Black triangles in the bottom panels indicate sampling dates. Tick marks on the horizontal axes indicate the 1st day of the month. White areas indicate no data.

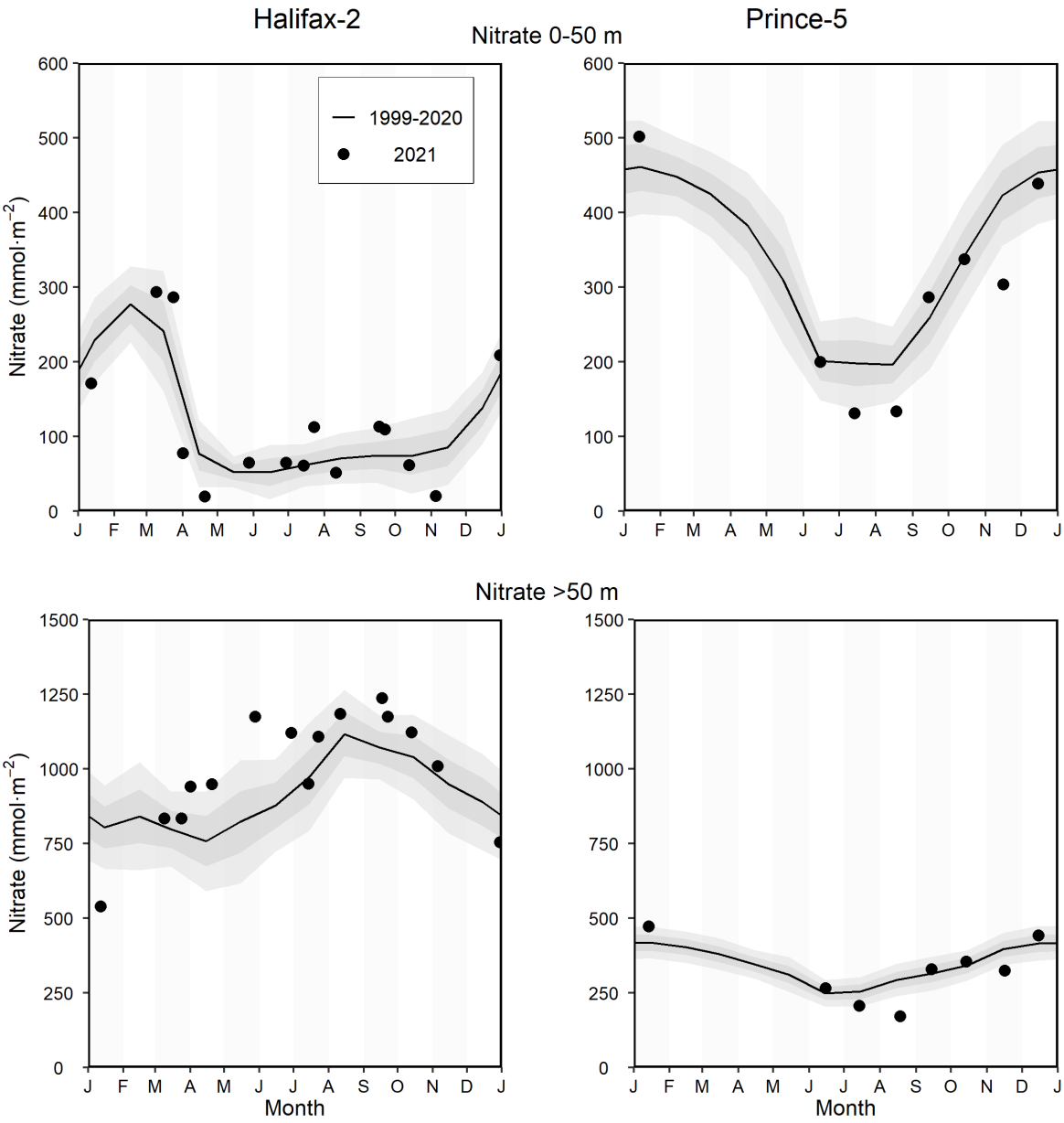

Figure 10. Comparison of the 2021 nitrate inventory (solid circle) data with mean conditions from 1999–2020 (solid line) at the Maritimes high-frequency sampling stations. Upper panels: surface (0–50 m) nitrate inventory. Lower panels: deep (50–150 m for Halifax-2 and 50–95 m for Prince-5) nitrate inventory. The gray shaded ribbons represent the standard deviation (±0.5 and ±1 sd) of the monthly means. Tick marks on the horizontal axes indicate the 1st day of the month.

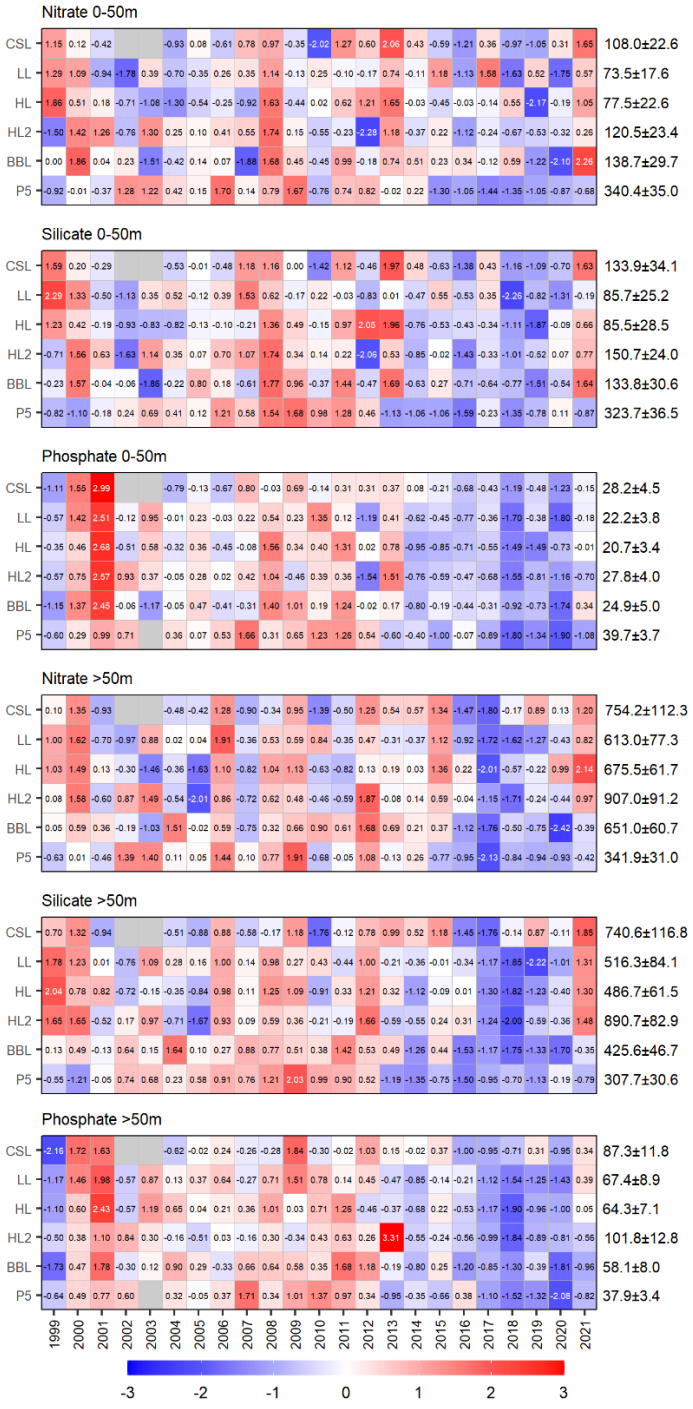

Figure 11. Annual anomaly scorecards for surface (0–50 m) and deep (50–150 m) nitrate, silicate, and phosphate inventories. Values in each cell are anomalies from the mean for the reference period, 1999–2020, in standard deviation (sd) units (mean and sd listed at right in units of mmol·m^{-2}). Red (blue) cells indicate higher- (lower-) than-normal nutrients. Gray cells indicate missing data. CSL: Cabot Strait section; LL: Louisbourg section; HL: Halifax section; HL2: Halifax-2; BBL: Browns Bank section; P5: Prince-5.

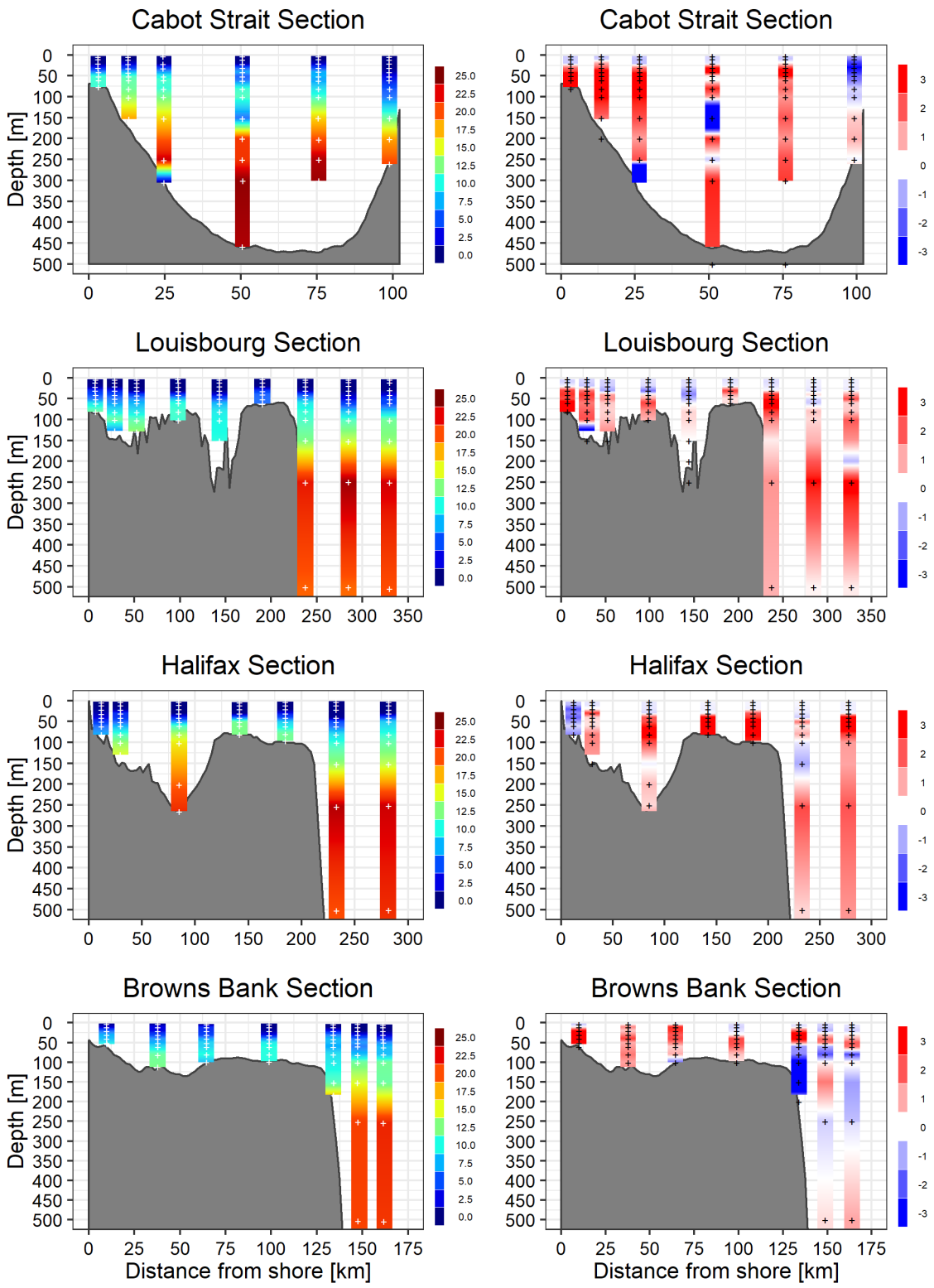

Figure 12. Vertical profiles of nitrate concentration (mmol·m^{-3}) (left panels) and their anomalies (mmol·m^{-3}) from 1999–2020 conditions (right panels) for each occupied stations along the SS sections in fall 2021. White markers on the left panels indicate the actual sampling depths for 2021. Black markers on the right panels indicate the depths at which station-specific climatological values were calculated.

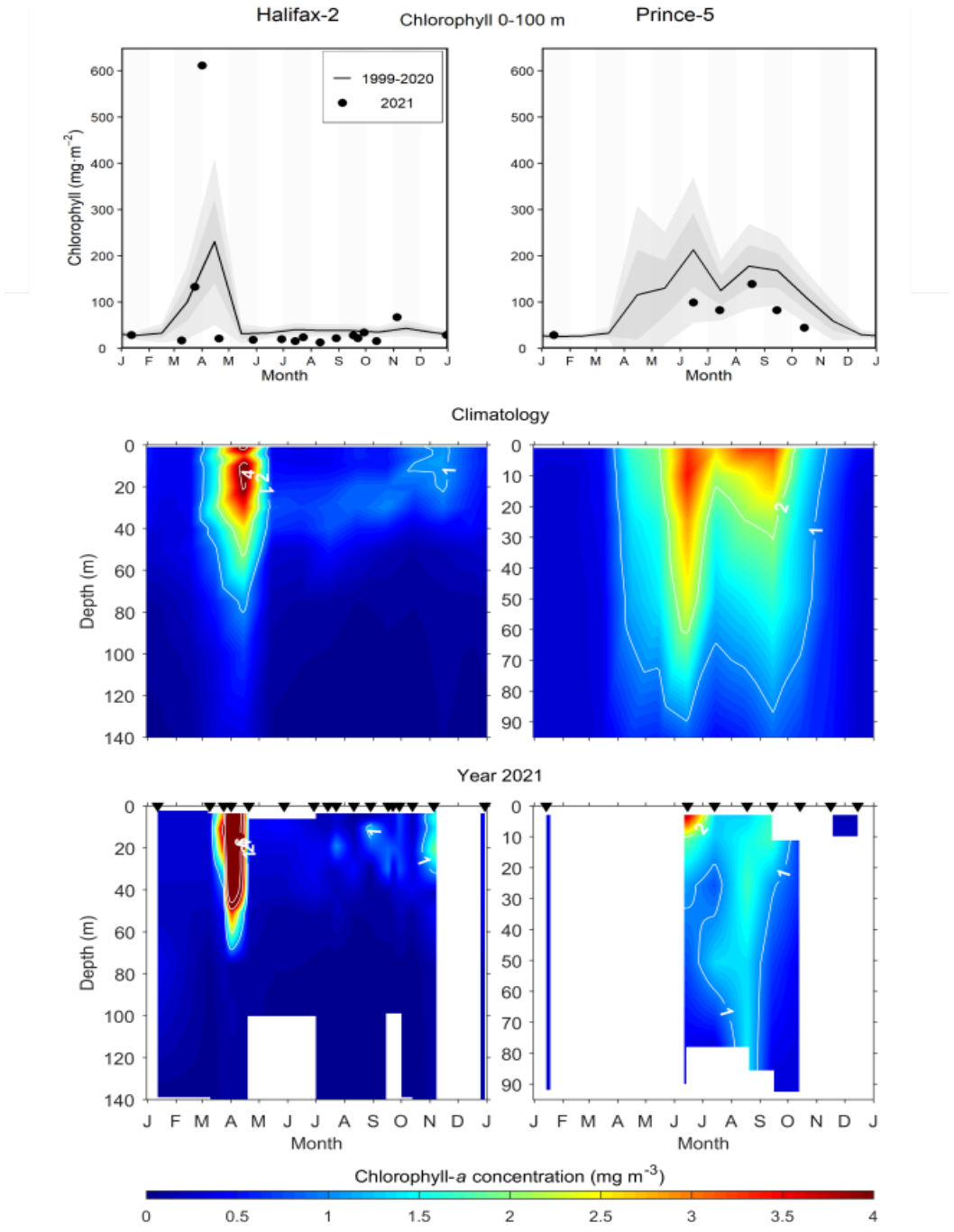

Figure 13. Annual variability in chlorophyll-a concentrations at the Maritimes time-series stations (left column: Halifax-2, right column: Prince-5). Top row: chlorophyll-a inventories (0–100 m at Halifax-2, 0–95 m at Prince-5) in 2021 (open circle) and mean values 1999–2020 (solid line). The gray shaded ribbons represent the standard deviation (±0.5 and ±1 sd) of the monthly means. Middle row: Mean (1999–2020) annual cycle of the vertical structure of chlorophyll-a concentrations (mg·m^{-3}). Bottom row: annual cycle of the vertical structure of chlorophyll-a concentrations in 2021. Black triangles in the bottom panels indicate sampling dates. Tick marks on the horizontal axes indicate the 1st day of the month. White areas indicate no data.

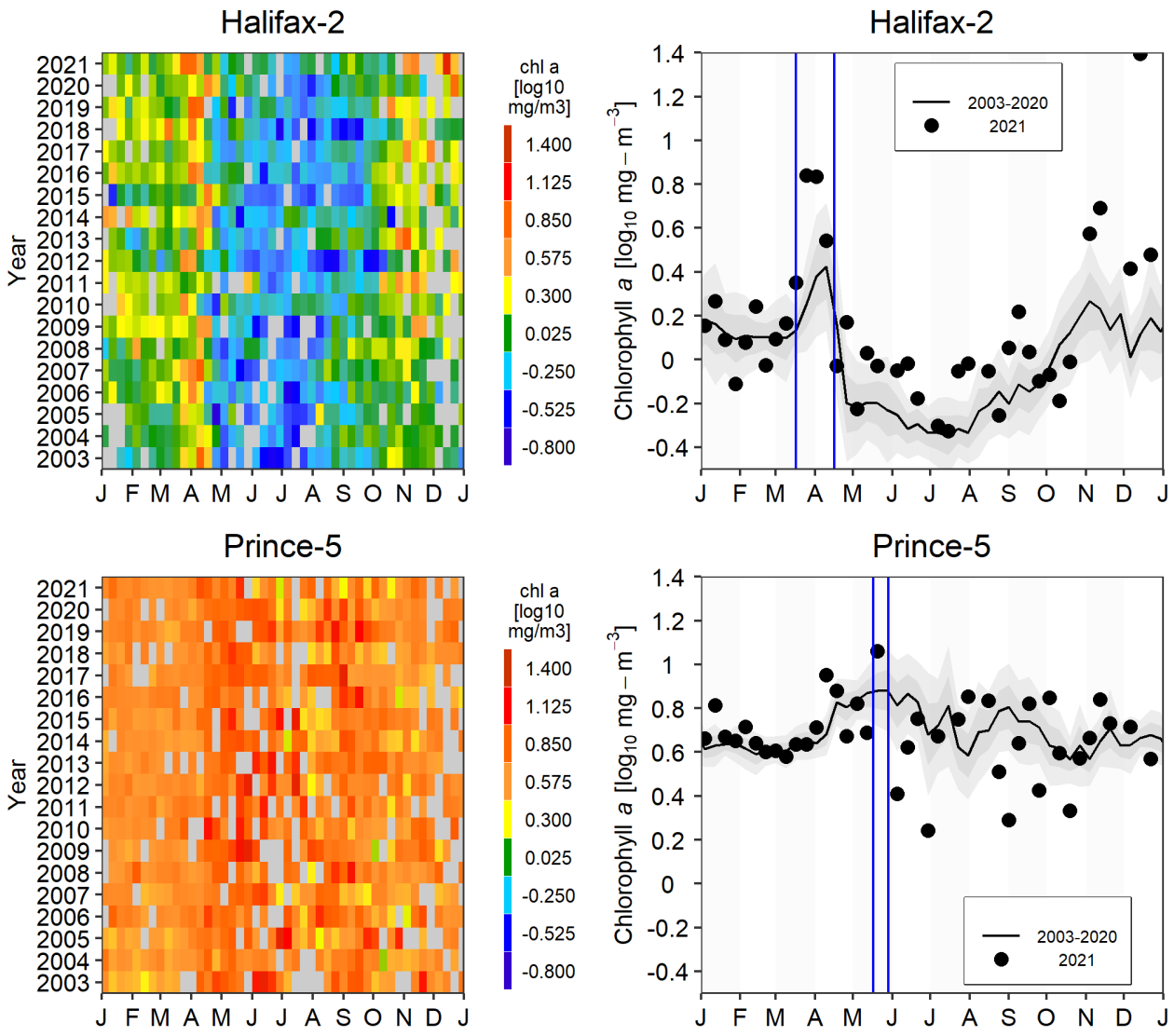

Figure 14. Weekly surface chlorophyll-a concentration from remotely sensed ocean colour data for Halifax-2 (top panels) and Prince-5 (bottom panels). Data from MODIS 2003–2021. Left panels: Time series of annual variation in chlorophyll-a concentrations. Gray pixels indicate missing data. Right panels: Comparison of 2021 (solid circle) surface chlorophyll-a concentrations with mean conditions from 2003–2020 (solid line). The gray shaded ribbons represent the standard deviation (±0.5 and ±1 sd) of the weekly means. Vertical blue lines delimit the period of the spring bloom as calculated by the PhytoFit application. Tick marks on the horizontal axes indicate the 1st day of the month.

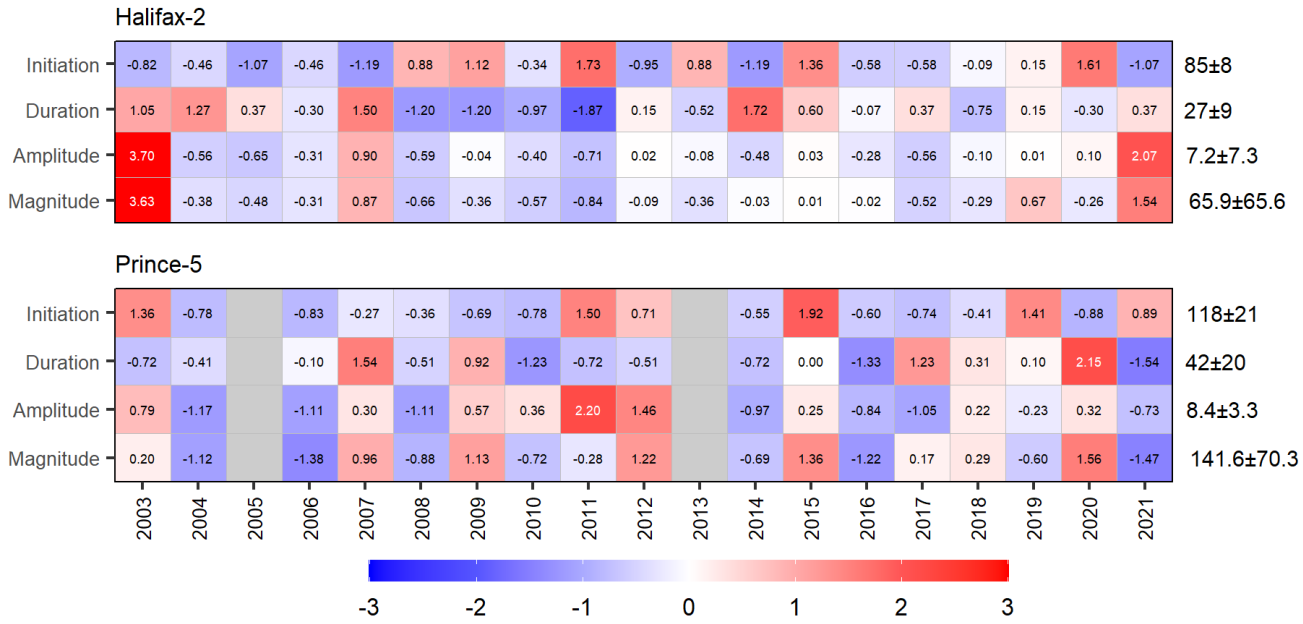

Figure 15. Annual anomaly scorecards for spring bloom parameters for Halifax-2 (top panel) and Prince-5 (bottom panel). Values in each cell are anomalies from the mean for the reference period, 2003–2020, in standard deviation (sd) units (mean and sd listed at right in units of Day-of-Year for Initiation, Days for Duration, $mg_{chl} \cdot m^{-3}$ for Amplitude, and $mg_{chl} \cdot m^{-3} \cdot d$ for Magnitude). Red (blue) cells indicate later (earlier) initiation, longer (shorter) duration or higher- (lower-) than-normal amplitude or magnitude. Gray cells indicate missing data.

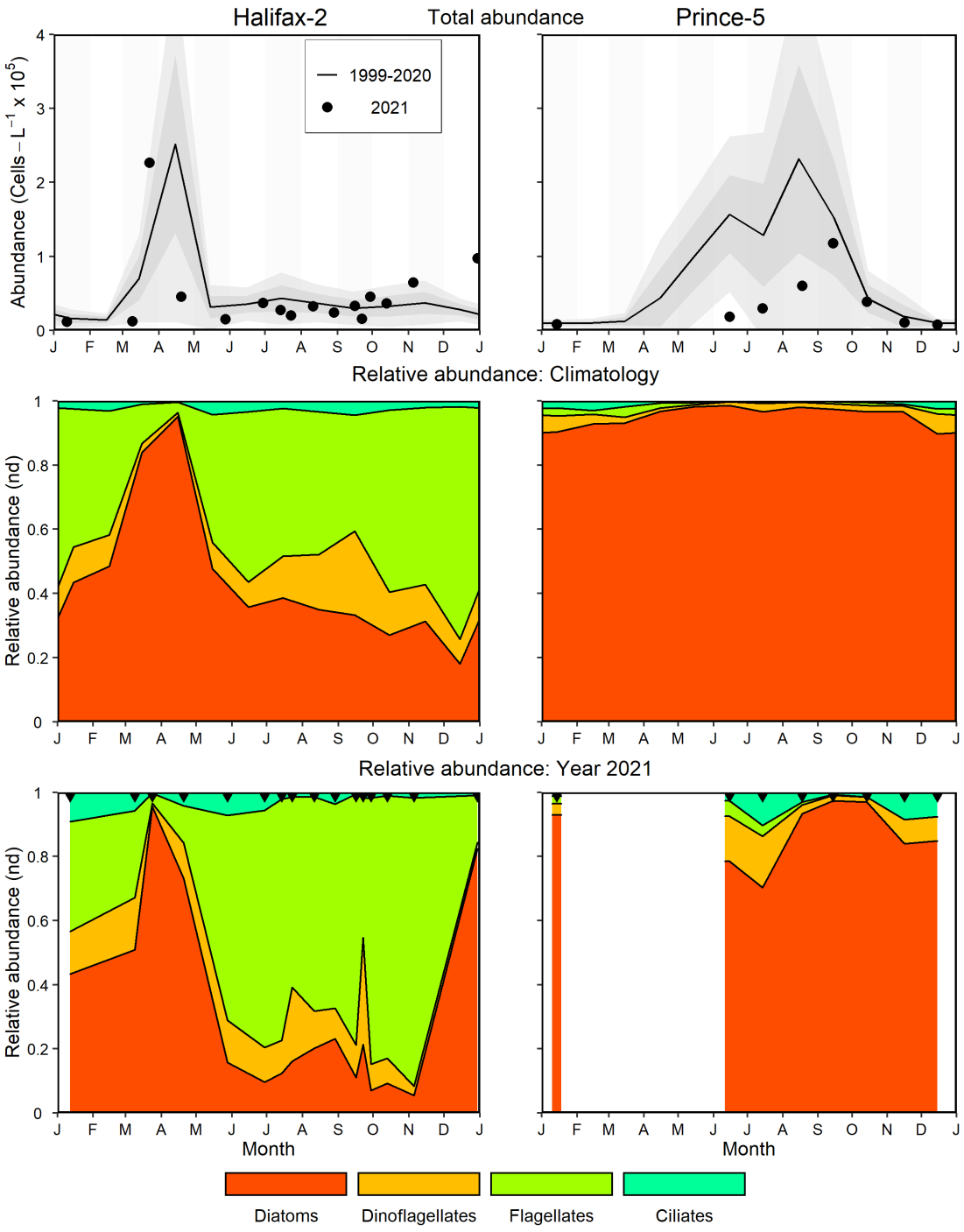

Figure 16. Comparison of 2021 phytoplankton abundance and community composition with mean conditions from 1999–2020 at the Maritimes high-frequency sampling stations (Halifax-2: left panels; Prince-5: right panels). Upper panels: 2021 phytoplankton abundance (solid circle) and mean conditions from 1999–2020 (solid line). The gray shaded ribbons represent the standard deviation (±0.5 and ±1 sd) of the monthly means. Middle panels: Phytoplankton climatological relative abundance from 1999–2020. Lower panels: 2021 phytoplankton relative abundance. nd = no dimensions. Black triangles in the bottom panels indicate sampling dates. Tick marks on the horizontal axes indicate the 1st day of the month. White areas indicate no data.

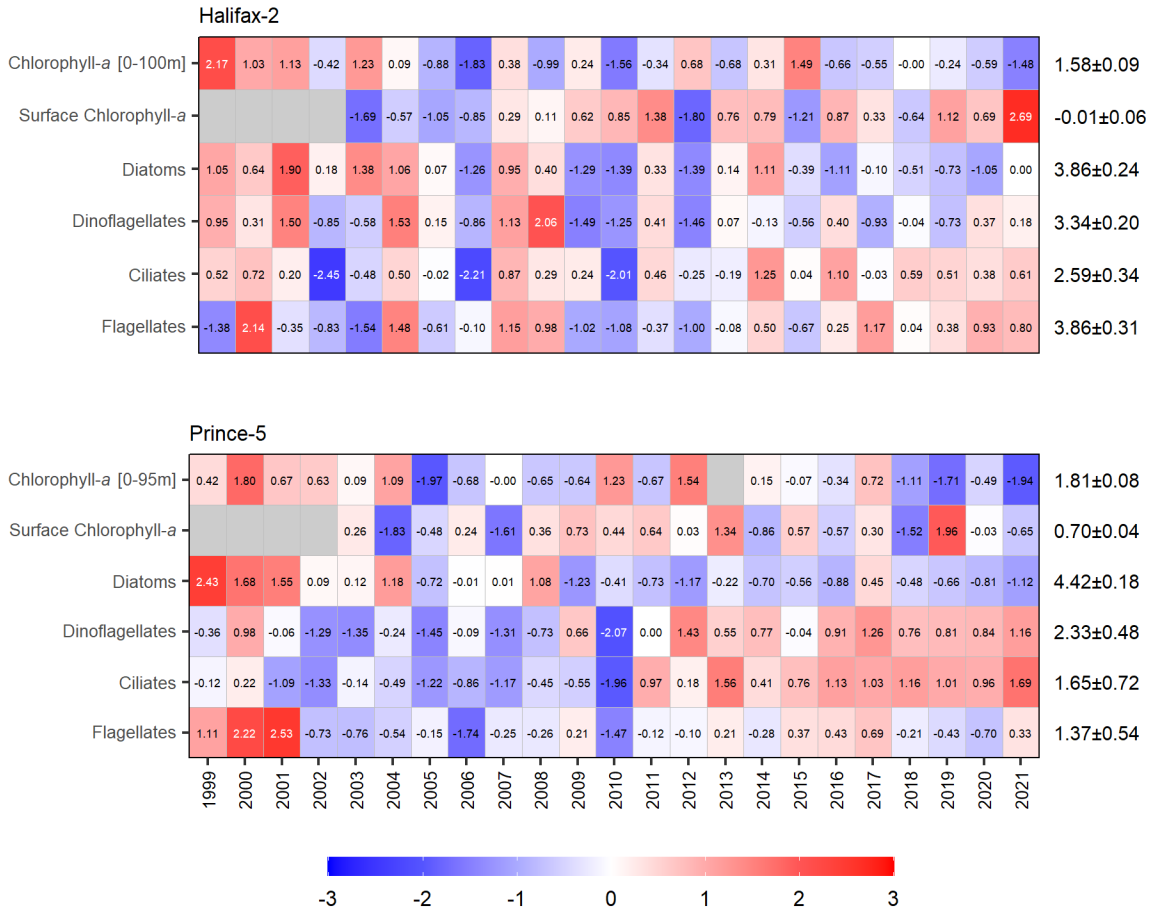

Figure 17. Annual anomaly scorecards for in situ chlorophyll-a inventory, remote sensing surface chlorophyll-a concentration, and phytoplankton abundance at the Maritimes high-frequency sampling stations. Values in each cell are anomalies from the mean for the reference period, for the reference period, 1999–2020 for in situ chlorophyll-a inventory and phytoplankton abundance, and 2003–2020 for remotely sensed surface chlorophyll-a, in standard deviation (sd) units (mean and sd listed at right in units of $log_{10}(mg \cdot m^{-2})$ for chlorophyll-a inventory, $log_{10}(mg \cdot m^{-3})$ for chlorophyll-a concentration, and $log_{10}(cells \cdot L^{-1}+1)$ for phytoplankton abundance). Red (blue) cells indicate higher- (lower-) than-normal chlorophyll-a inventories/concentrations or phytoplankton abundances. Gray cells indicate missing data.

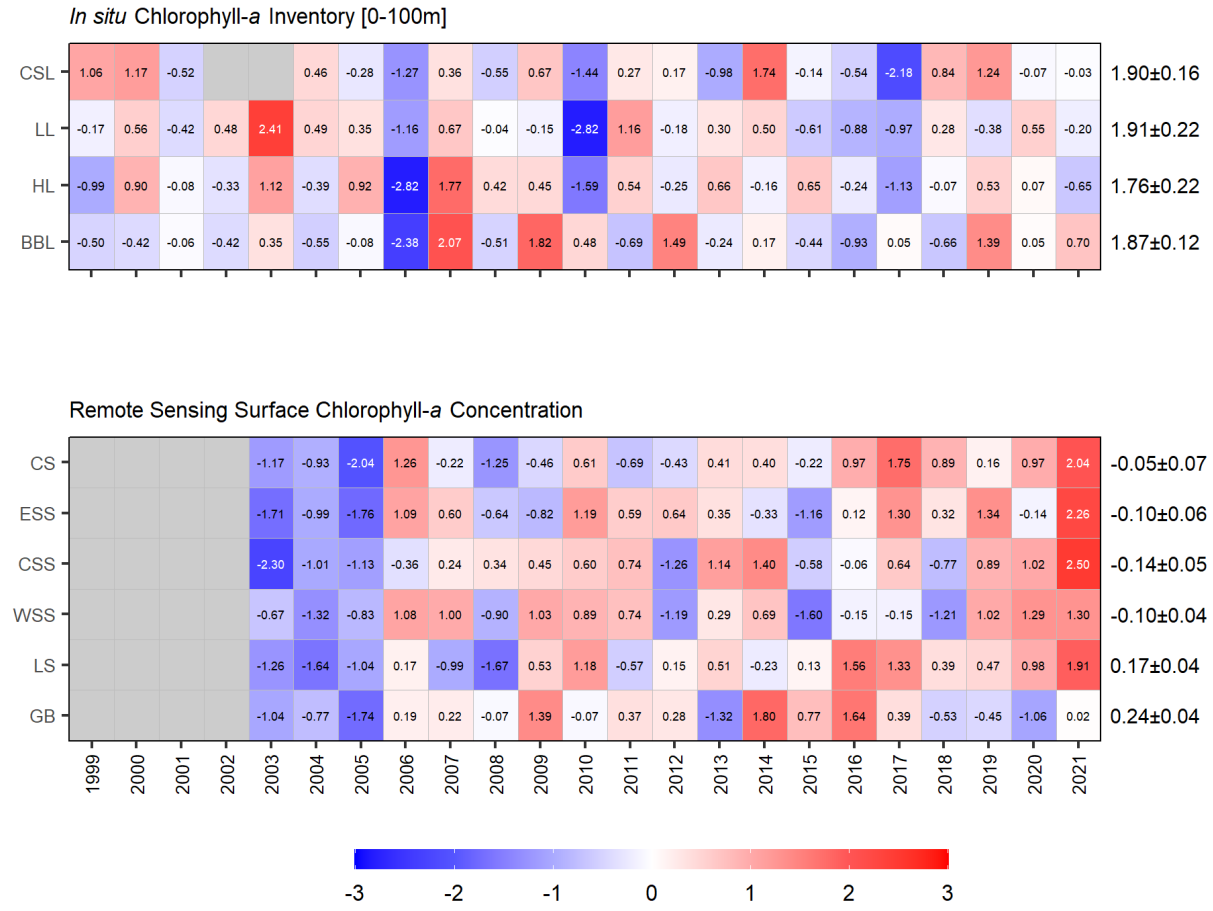

Figure 18. Annual anomaly scorecards for in situ chlorophyll-a inventory (0–100 m) on the Cabot Strait [CSL], Louisbourg [LL], Halifax [HL] and Browns Bank [BBL] sections (top panel) and for remote sensing surface chlorophyll-a concentrations on the Cabot Strait [CS], Eastern Scotian Shelf [ESS], Central Scotian Shelf [CSS], Western Scotian Shelf [WSS], Lurcher Shoal [LS], and Georges Bank [GB] sub-regions (bottom panel) from MODIS data 2003–2021. Values in each cell are anomalies from the mean for the reference period, 1999–2020 for in situ chlorophyll-a inventory and 2003–2020 for remotely sensed surface chlorophyll-a, in standard deviation (sd) units (mean and sd listed at right in units of $\log_{10}(mg \cdot m^{-2})$ *for chlorophyll-a inventory and* $\log_{10}(mg \cdot m^{-3})$ *for chlorophyll-a concentration). Red (blue) cells indicate higher- (lower-) than-normal chlorophyll-a inventories or surface chlorophyll-a concentrations. Gray cells indicate missing data.*

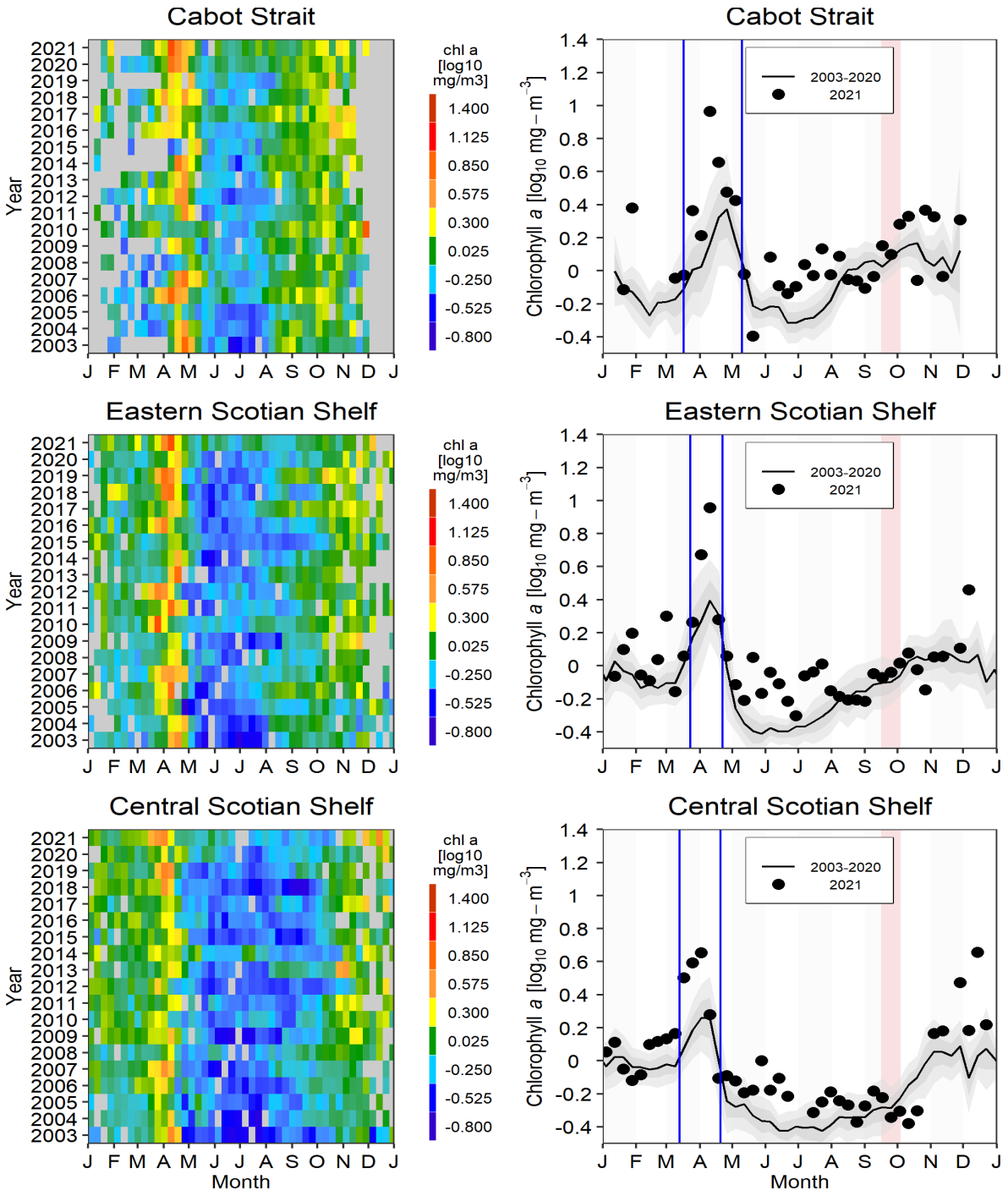

Figure 19a. Weekly surface chlorophyll-a concentrations from remotely sensed ocean colour data in the Cabot Strait (top), Eastern Scotian Shelf (middle), and Central Scotian Shelf (bottom) sub-regions. Data from MODIS 2003–2021. Left panels: Time series of annual variation in chlorophyll-a concentrations. Gray pixels indicate missing data. Right panels: Comparison of 2021 (solid circle) surface chlorophyll-a concentrations with mean conditions from 2003–2020 (solid line) in the same sub-regions. The gray shaded ribbons represent the standard deviation (±0.5 and ±1 sd) of the weekly means. Vertical blue lines delimit the period of the spring bloom as calculated by the PhytoFit application. The pink vertical stripe indicates the timing of the fall mission. Tick marks on the horizontal axes indicate the 1st day of the month.

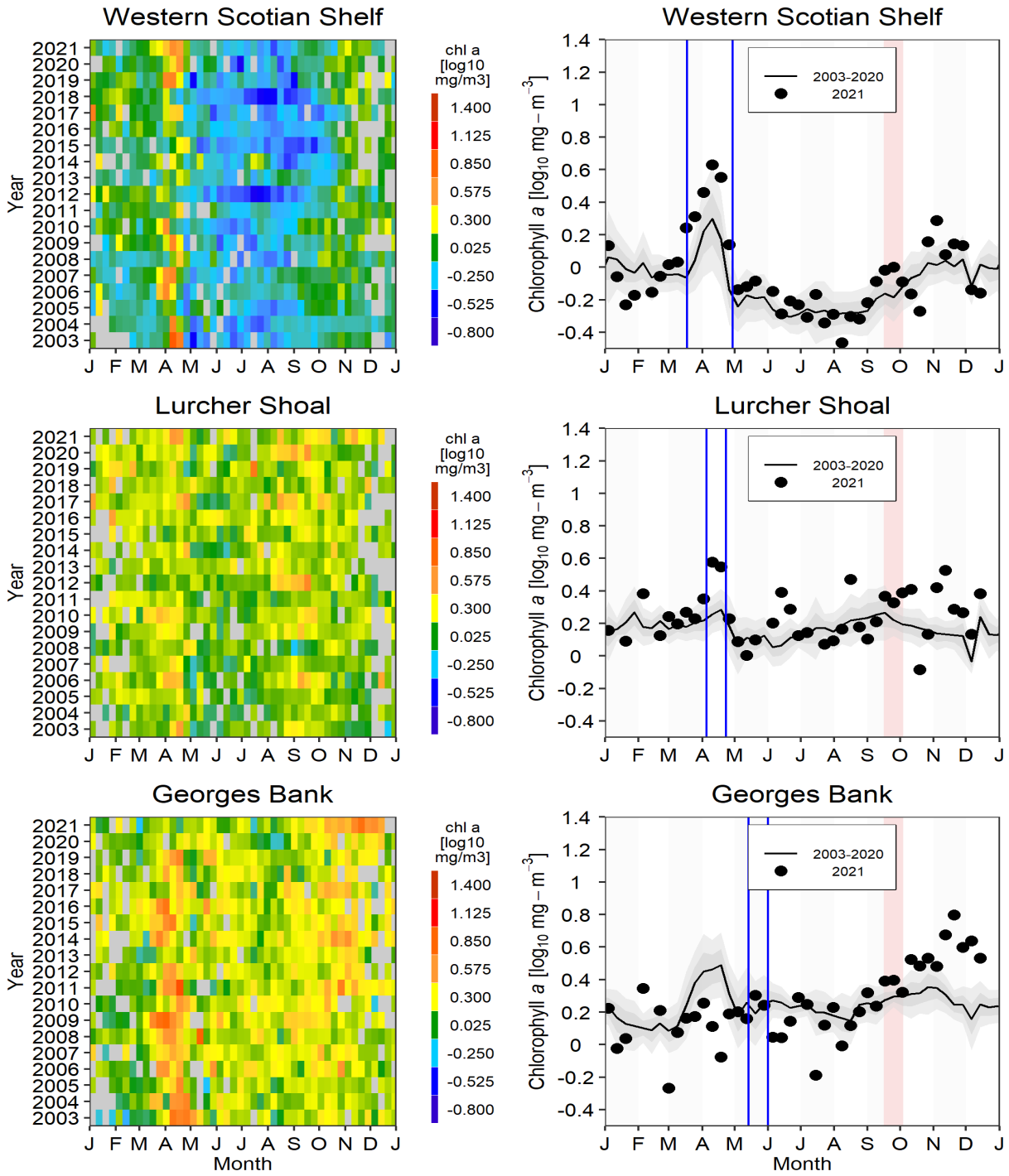

Figure 19b. Weekly surface chlorophyll-a concentrations from remotely sensed ocean colour data in the Western Scotian Shelf (top), Lurcher Shoal (middle), and Georges Bank (bottom) sub-regions. Data from MODIS 2003–2021. Left panels: Time series of annual variation in chlorophyll-a concentrations. Gray pixels indicate missing data. Right panels: Comparison of 2021 (solid circle) surface chlorophyll-a concentrations with mean conditions from 2003–2020 (solid line) in the same sub-regions. The gray shaded ribbons represent the standard deviation (±0.5 and ±1 sd) of the weekly means. Vertical blue lines delimit the period of the spring bloom as calculated by the PhytoFit application. The pink vertical stripe indicates the timing of the fall mission. Tick marks on the horizontal axes indicate the 1st day of the month.

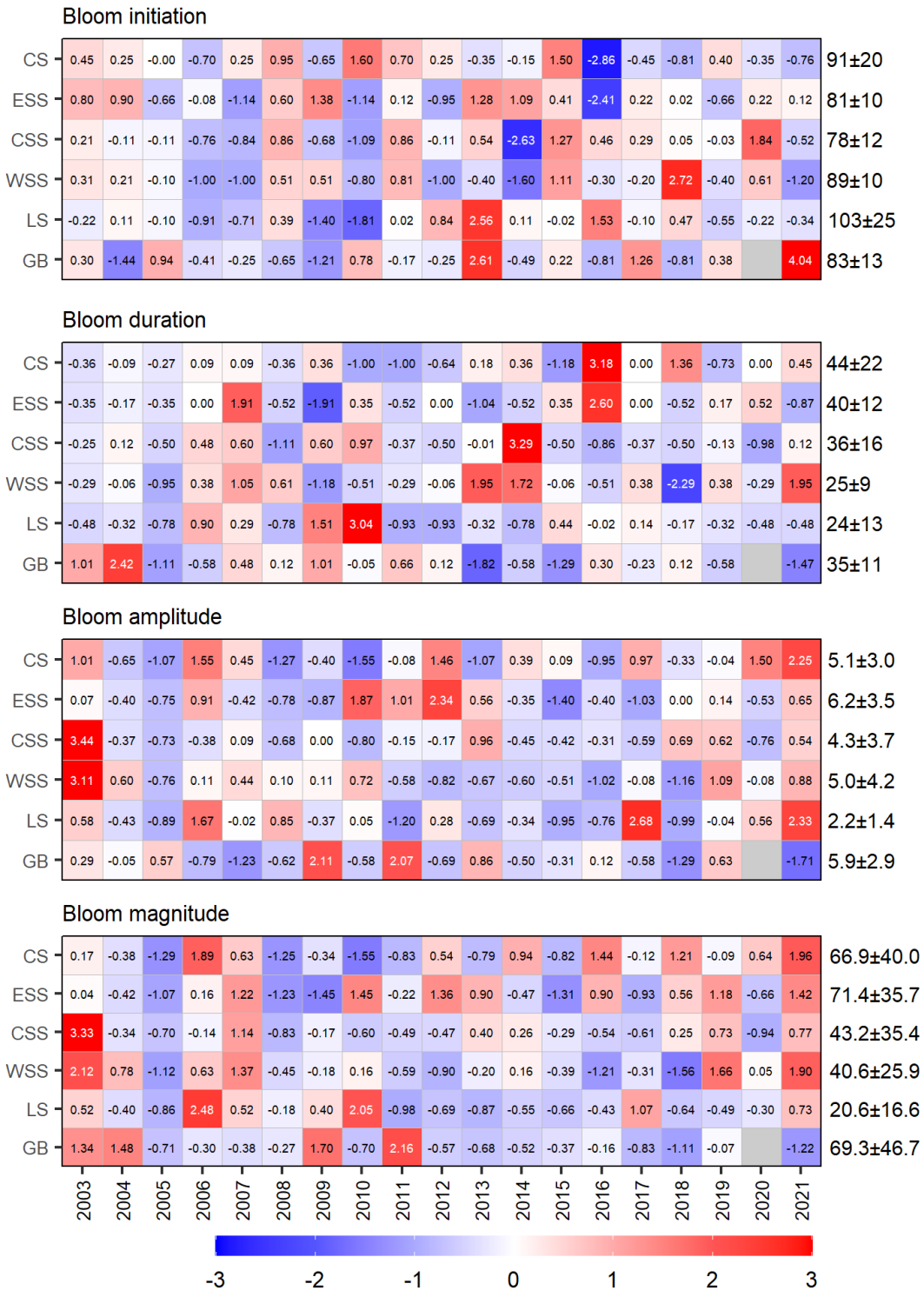

Figure 20. Annual anomaly scorecards for spring bloom parameters. Values in each cell are anomalies from the mean for the reference period, 2003–2020, in standard deviation (sd) units (mean and sd listed at right in units of Day-of-Year for Initiation, Days for Duration, $mg_{chl} \cdot m^{-3}$ for Amplitude, and $mg_{chl} \cdot m^{-3} \cdot d$ for Magnitude). Red (blue) cells indicate later (earlier) initiation, longer (shorter) duration or higher- (lower-) than-normal amplitude or magnitude. Gray cells indicate missing data.

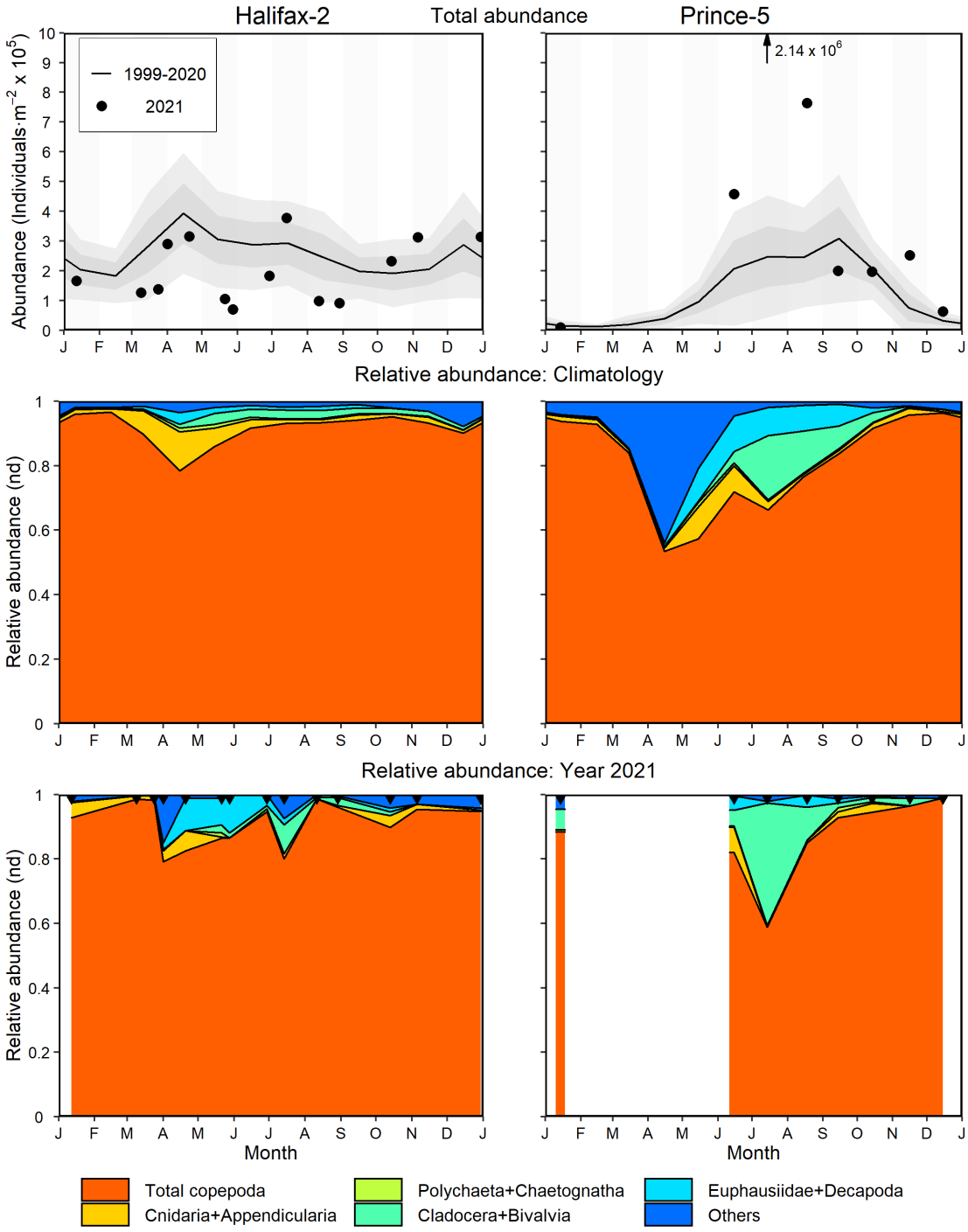

Figure 21. Zooplankton (> 200 µm) abundance and community composition in 2021 and mean conditions 1999–2020 at the Maritimes high-frequency sampling stations (Halifax-2, left panels; Prince-5, right panels). Upper panels: Zooplankton abundance in 2021 (solid circle) and mean conditions 1999–2020 (solid line). The gray shaded ribbons represent the standard deviation (±0.5 and ±1 sd) of the monthly means. Middle panels: Climatology of major groups relative abundances 1999–2020. Lower panels: major groups relative abundances in 2021. nd = no dimensions. Black triangles in the bottom panels indicate sampling dates. Tick marks on the horizontal axes indicate the 1st day of the month. White areas indicate no data.

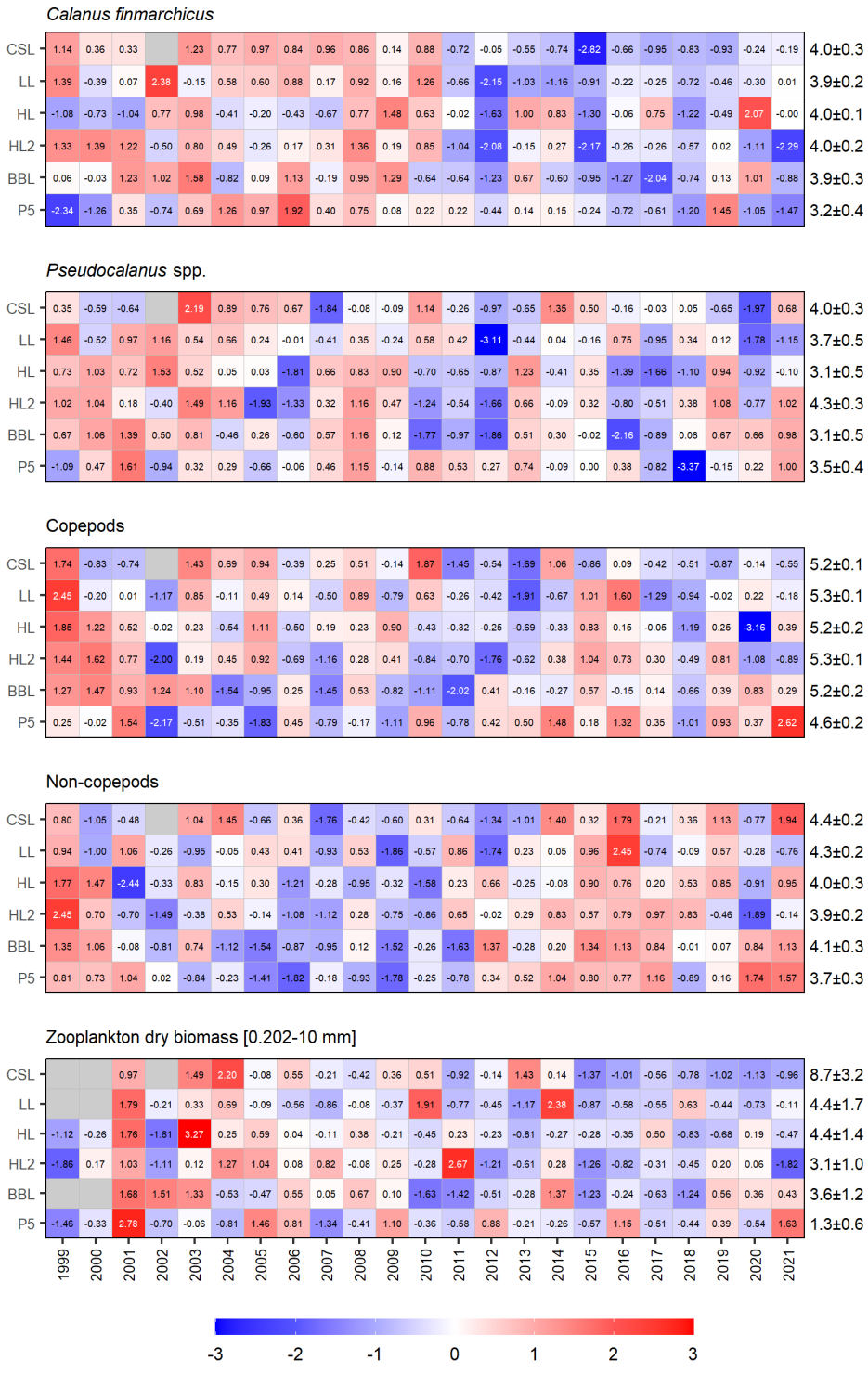

Figure 22. Annual anomaly scorecards for zooplankton abundance and biomass. Values in each cell are anomalies from the mean for the reference period, 1999–2020, in standard deviation (sd) units (mean and sd listed at right in units of log_{10}(individuals·m^{-2}+1) for abundance and g·m^{-2} for biomass). Red (blue) cells indicate higher- (lower-) than-normal abundances or biomass. Gray cells indicate missing data. CSL: Cabot Strait section; LL: Louisbourg section; HL: Halifax section; HL2: Halifax-2; BBL: Browns Bank section; P5: Prince-5.

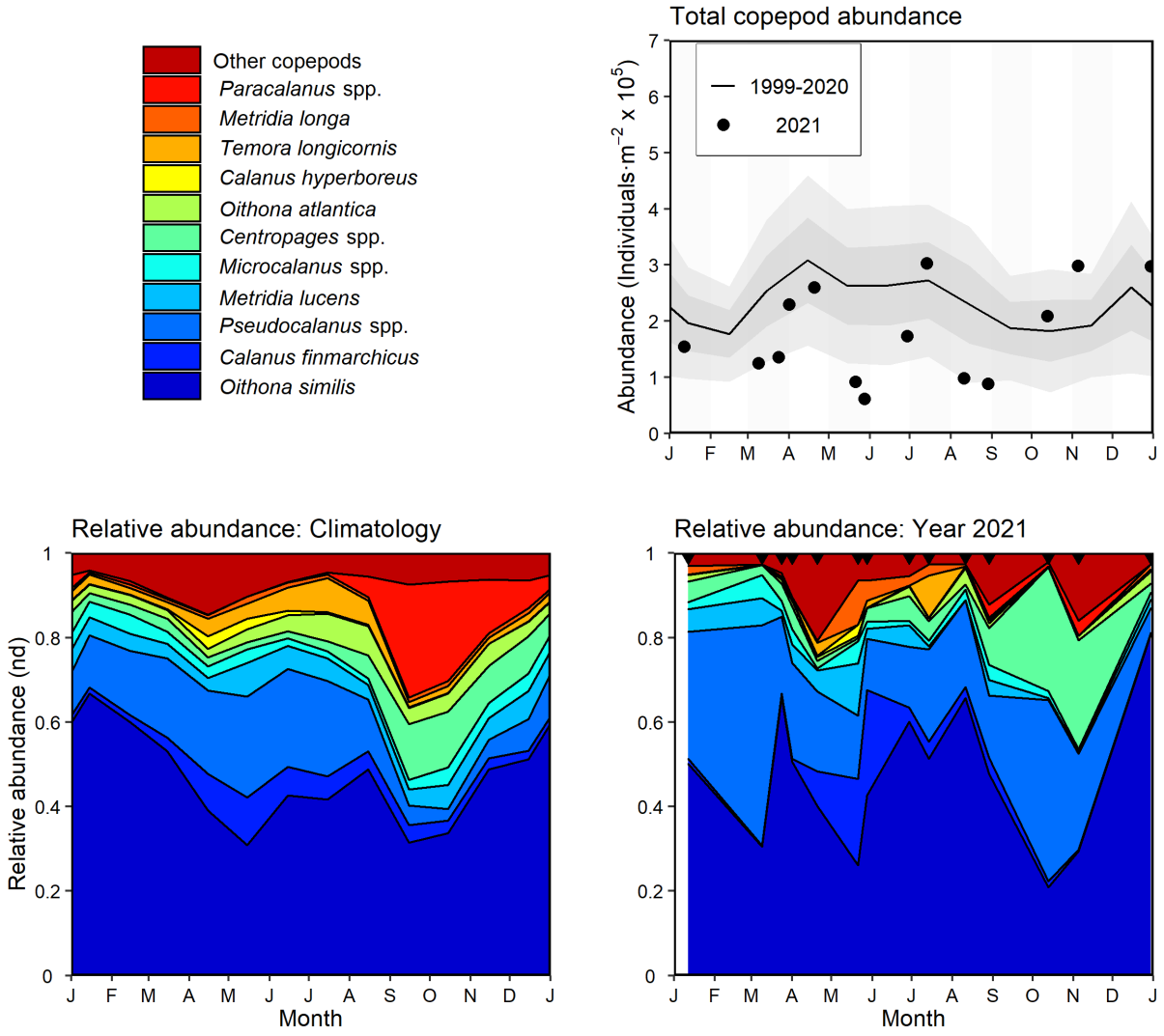

Figure 23a. Variability of dominant copepods at Halifax-2. The top 95% copepod taxa by abundance are shown individually; unidentified copepods (mostly nauplii) are grouped as "others". Upper right panel: copepod abundance in 2021 (solid circle) and mean conditions, 1999–2020 (solid line). The gray shaded ribbons represent the standard deviation (±0.5 and ±1 sd) of the monthly means. Bottom left panel: Climatology of copepod relative abundances, 1999–2020. Bottom right panel: copepod relative abundances in 2021. nd = no dimensions. Black triangles in the bottom right panel indicate sampling dates. Tick marks on the horizontal axes indicate the 1st day of the month.

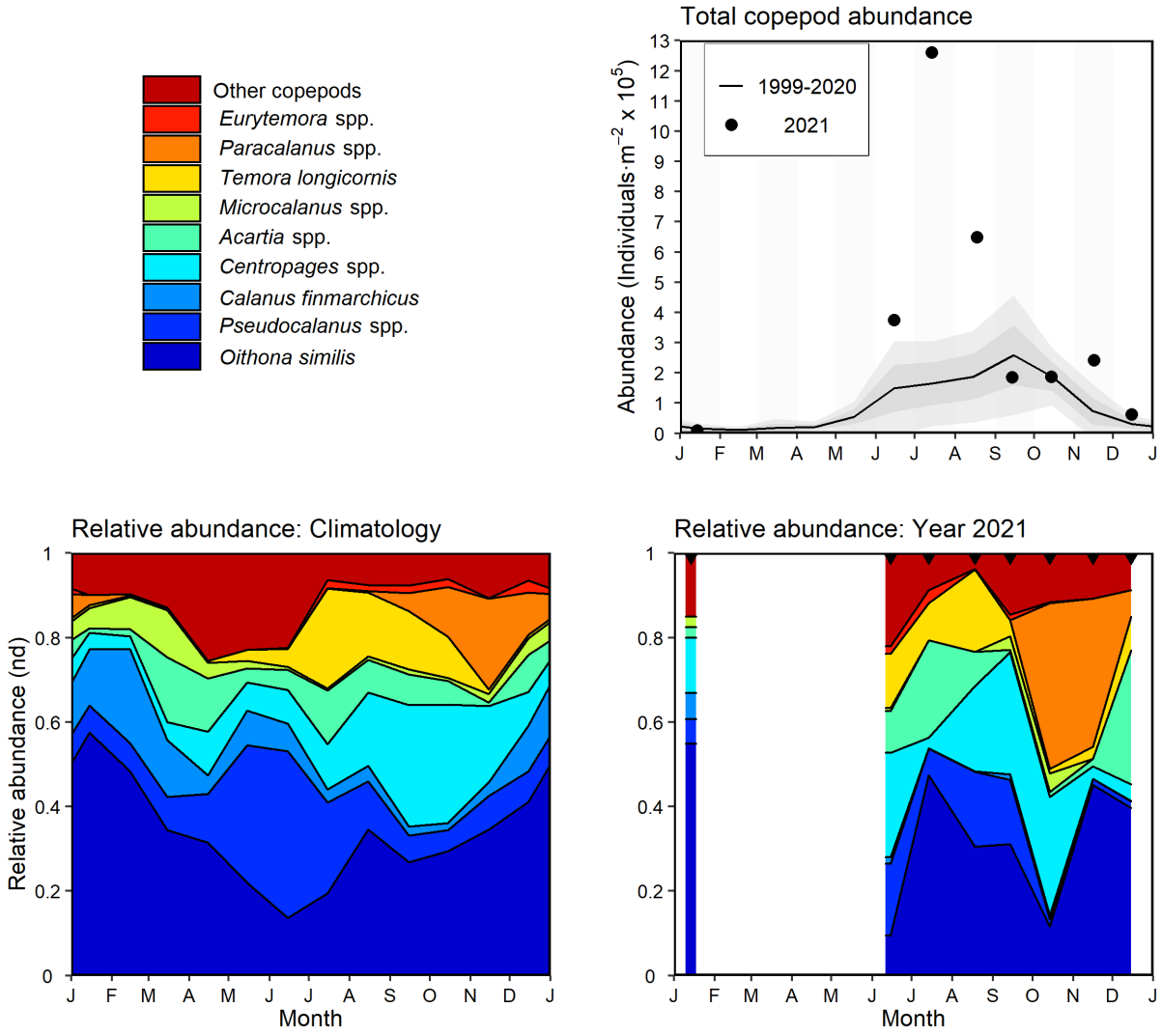

Figure 23b. Variability of dominant copepods at Prince-5. The top 95% copepod taxa by abundance are shown individually; unidentified copepods (mostly nauplii) are grouped as "others". Upper right panel: copepod abundance in 2021 (solid circle) and mean conditions, 1999–2020 (solid line). The gray shaded ribbons represent the standard deviation (±0.5 and ±1 sd) of the monthly means. Bottom left panel: Climatology of copepod relative abundances, 1999–2020. Bottom right panel: copepod relative abundances in 2021. nd = no dimensions. Black triangles in the bottom right panel indicate sampling dates. Tick marks on the horizontal axes indicate the 1st day of the month. White areas indicate no data.

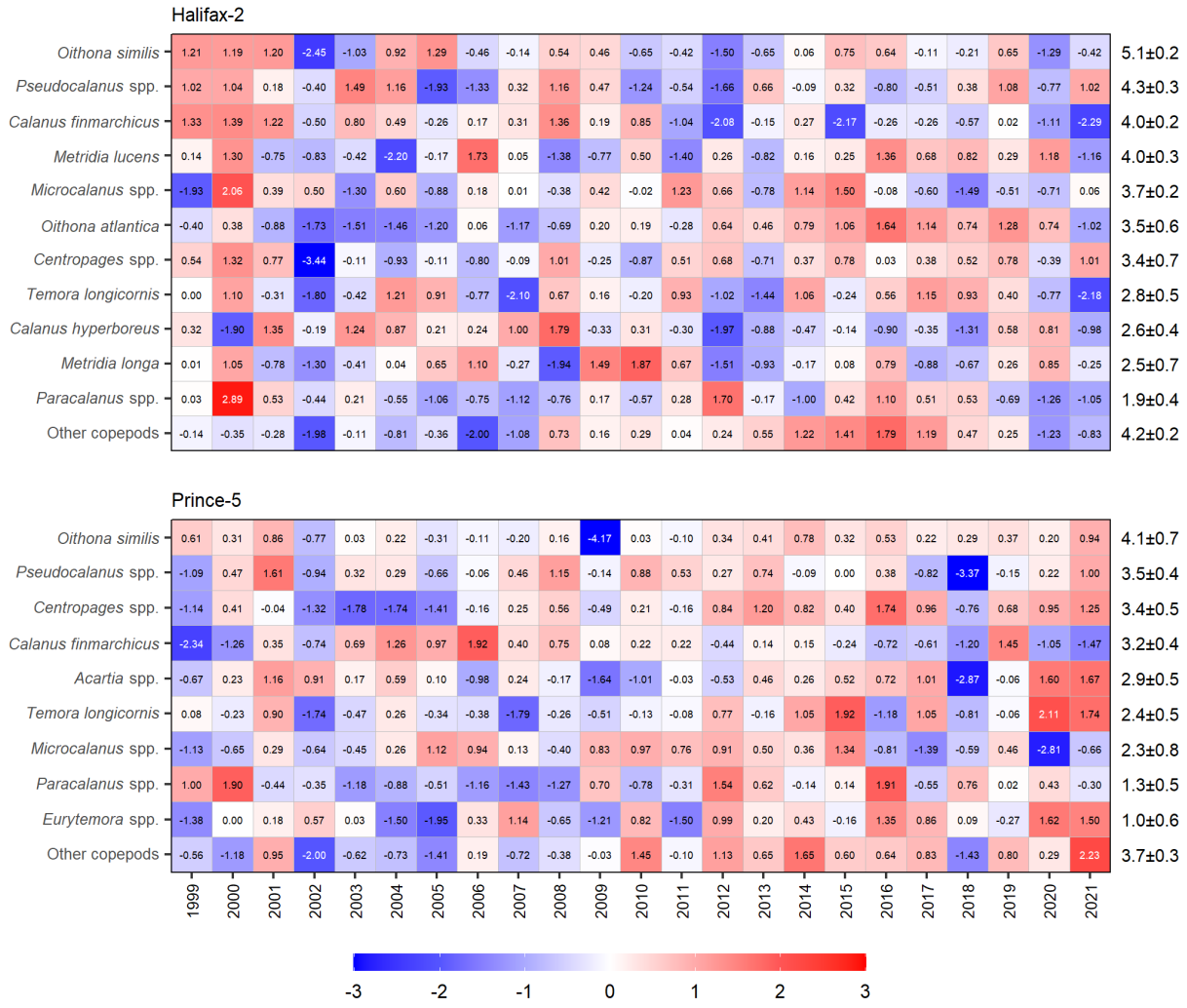

Figure 24. Annual anomaly scorecards for dominant copepods abundances at the Maritimes high-frequency sampling stations (top panel: Halifax-2; bottom panel: Prince-5). Values in each cell are anomalies from the mean for the reference period, 1999–2020, in standard deviation (sd) units (mean and sd listed at right in units of $log_{10}(individuals \cdot m^{-2}+1)$). Red (blue) cells indicate higher- (lower-) than-normal abundances. Gray cells indicate missing data.

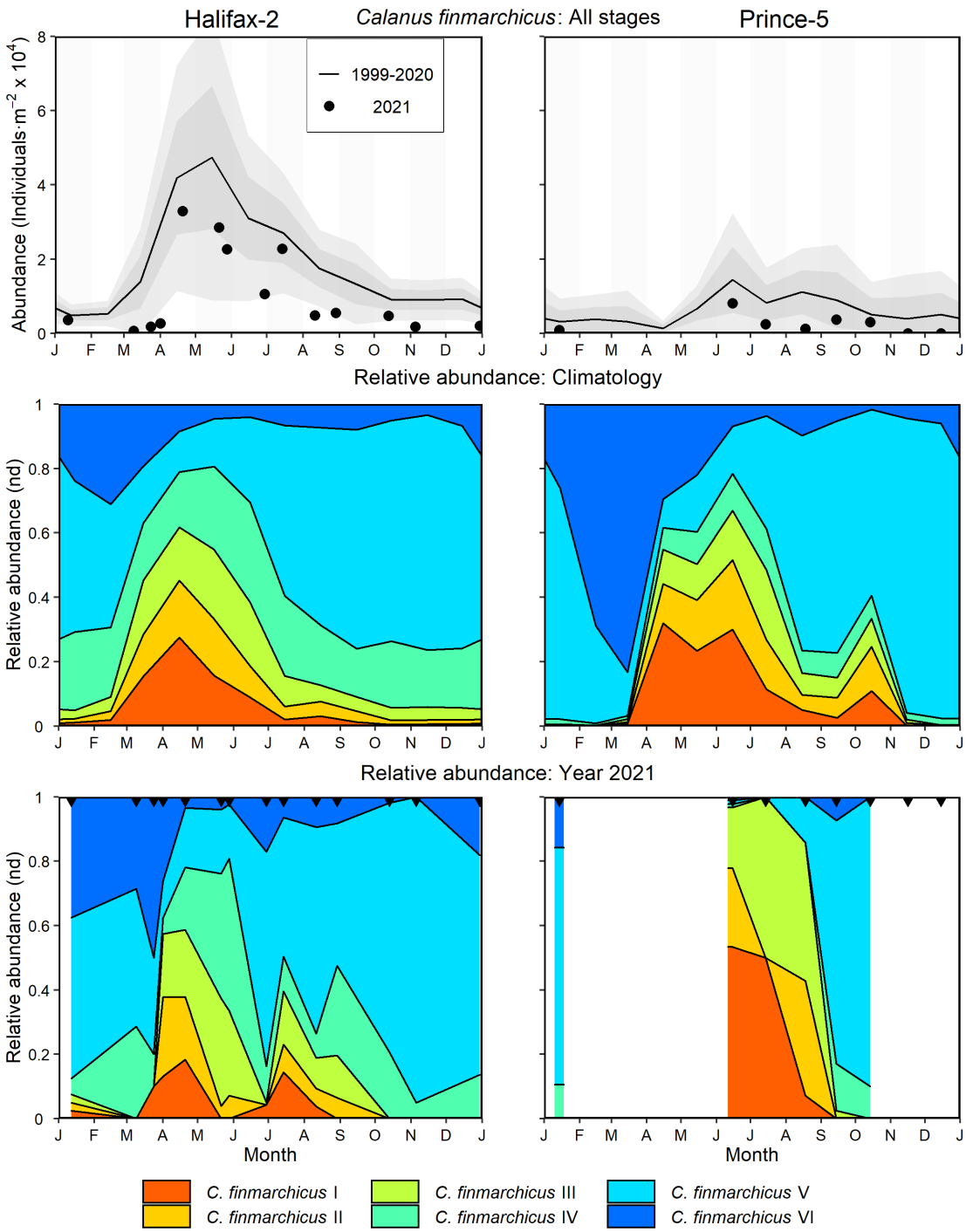

Figure 25. Calanus finmarchicus abundance and developmental stage distributions in 2021 and mean conditions 1999–2020 at the Maritimes high-frequency sampling stations (Halifax-2, left panels; Prince-5, right panels). Upper panels: C. finmarchicus abundance in 2021 (solid circle) and mean conditions 1999–2020 (solid line). The gray shaded ribbons represent the standard deviation (±0.5 and ±1 sd) of the monthly means. Middle panels: Climatological C. finmarchicus stage relative abundances, 1999–2020. Lower panels: C. finmarchicus stage relative abundances in 2021. nd = no dimensions. Black triangles in the bottom panels indicate sampling dates. Tick marks on the horizontal axes indicate the 1st day of the month. White areas indicate no data.

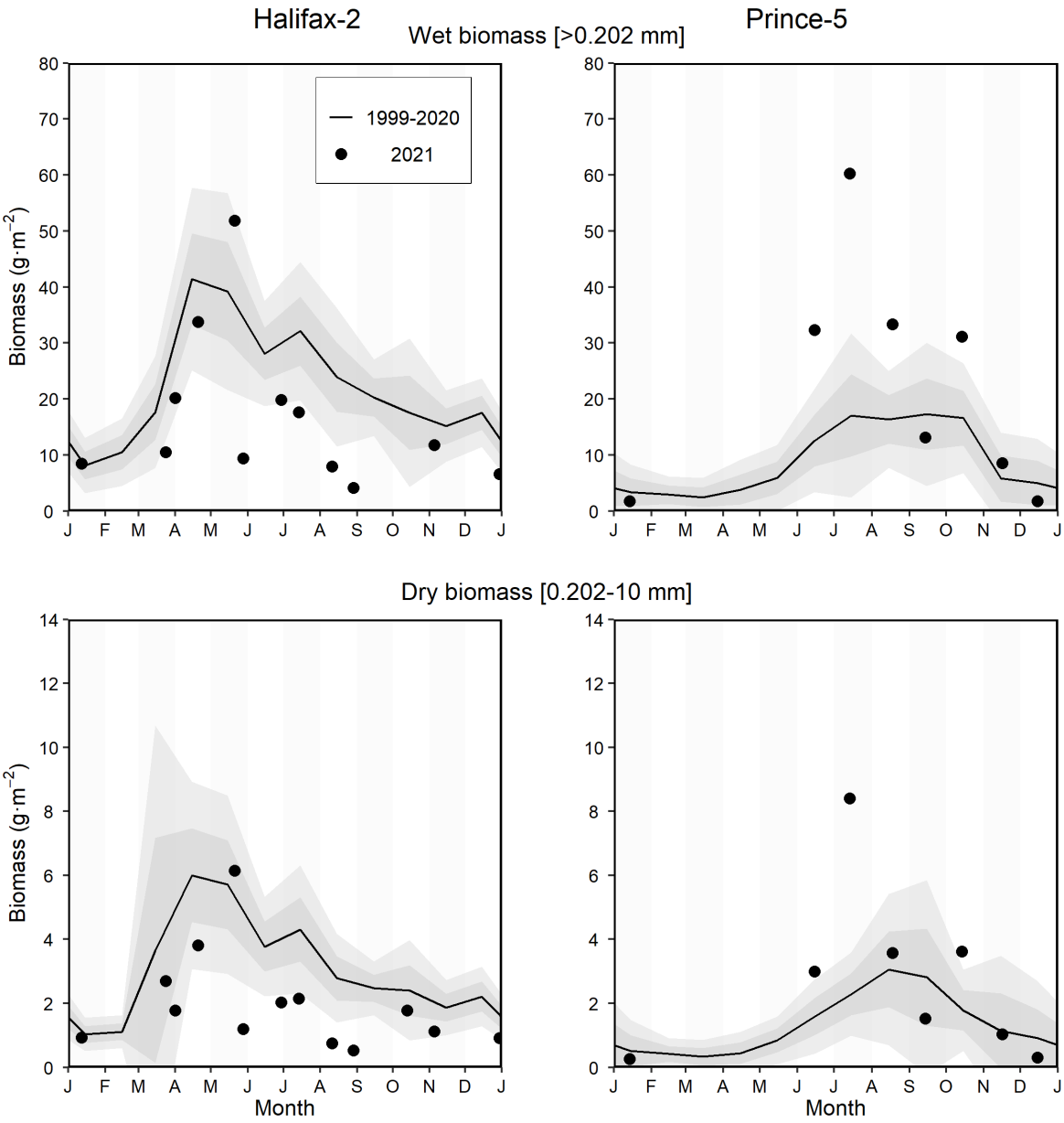

Figure 26. Zooplankton total wet biomass (upper panels) and mesozooplankton dry biomass (bottom panels) (integrated from surface to bottom) in 2021 (solid circle) and mean conditions 1999–2020 (solid line) at the Maritimes high-frequency sampling stations. The gray shaded ribbons represent the standard deviation (±0.5 and ±1 sd) of the monthly means. Left panels: Halifax-2; right panels: Prince-5. Tick marks on the horizontal axes indicate the 1st day of the month.

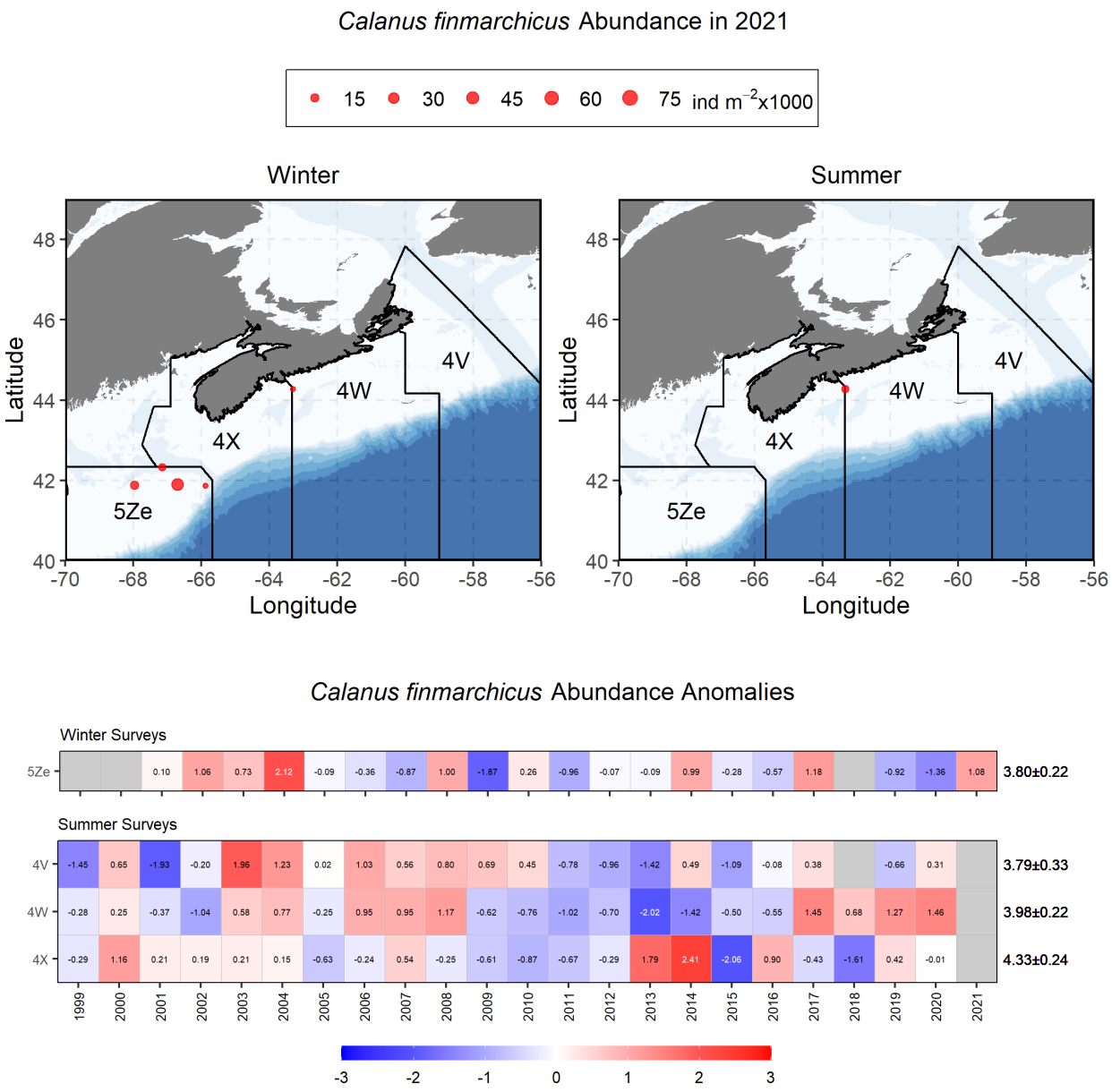

Figure 27. Spatial distribution of Calanus finmarchicus abundance in 2021 (upper panels) and seasonal anomaly scorecards of C. finmarchicus abundance (lower panels) from ecosystem trawl surveys on Georges Bank (5Ze in winter) and the Scotian Shelf and eastern Gulf of Maine (4X, 4W, and 4V in summer), 1999–2021. Values in each cell are anomalies from the mean for the reference period, 1999–2020, in standard deviation (sd) units (mean and sd listed at right in units of log_{10}[individuals·m^{-2}+1]). Red (blue) cells indicate higher- (lower-) than-normal abundances. Gray cells indicate missing data.

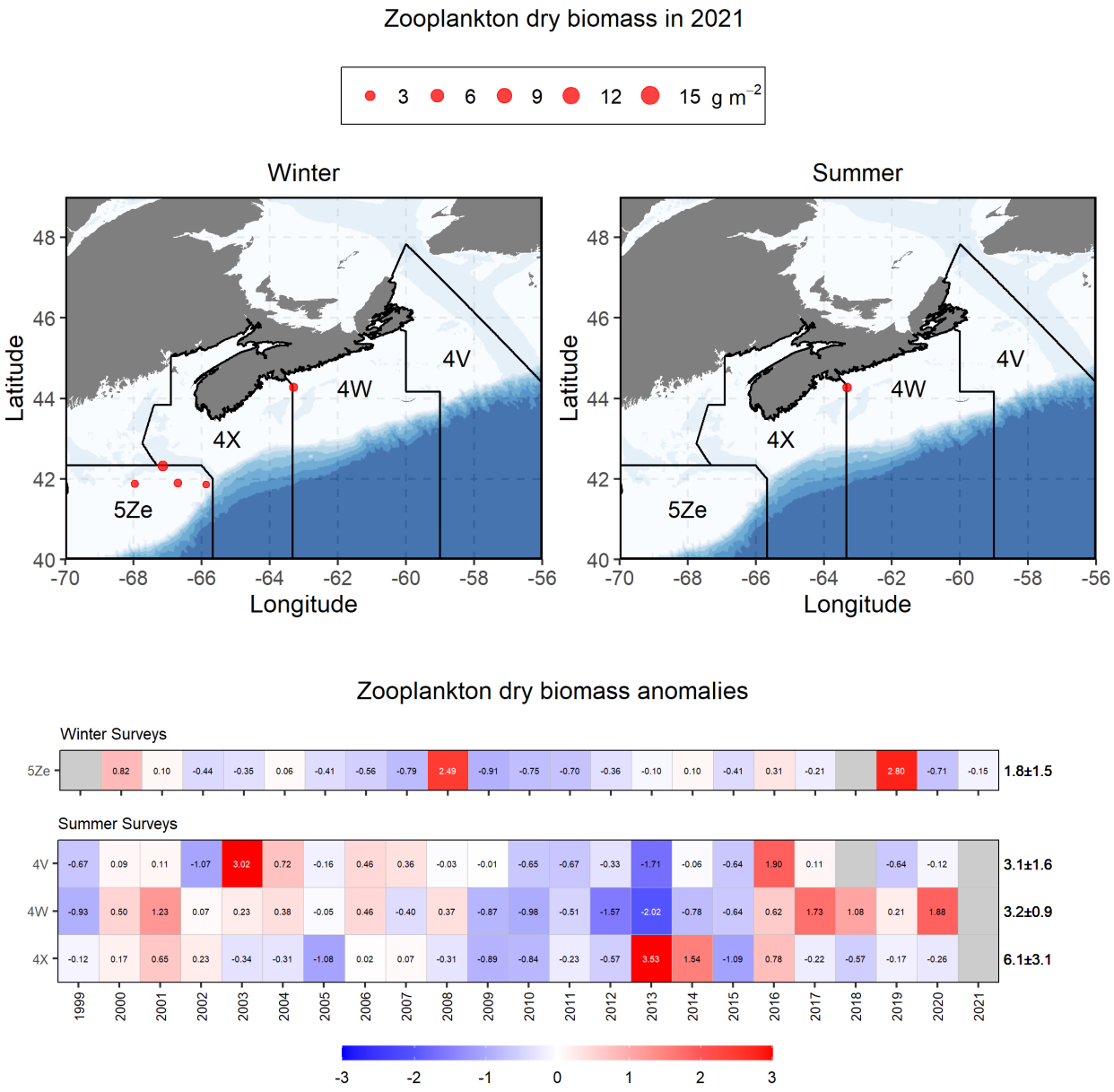

Figure 28. Spatial distribution of zooplankton dry biomass in 2021 (upper panels) and seasonal anomaly scorecards of zooplankton dry biomass (lower panels) from ecosystem trawl surveys on Georges Bank (5Ze in winter) and the Scotian Shelf and eastern Gulf of Maine (4X, 4W, and 4V in summer), 1999–2021. Values in each cell are anomalies from the mean for the reference period, 1999–2020, in standard deviation (sd) units (mean and sd listed at right in units of g·m^{-2}). Red (blue) cells indicate higher- (lower-) than-normal biomass. Gray cells indicate missing data.

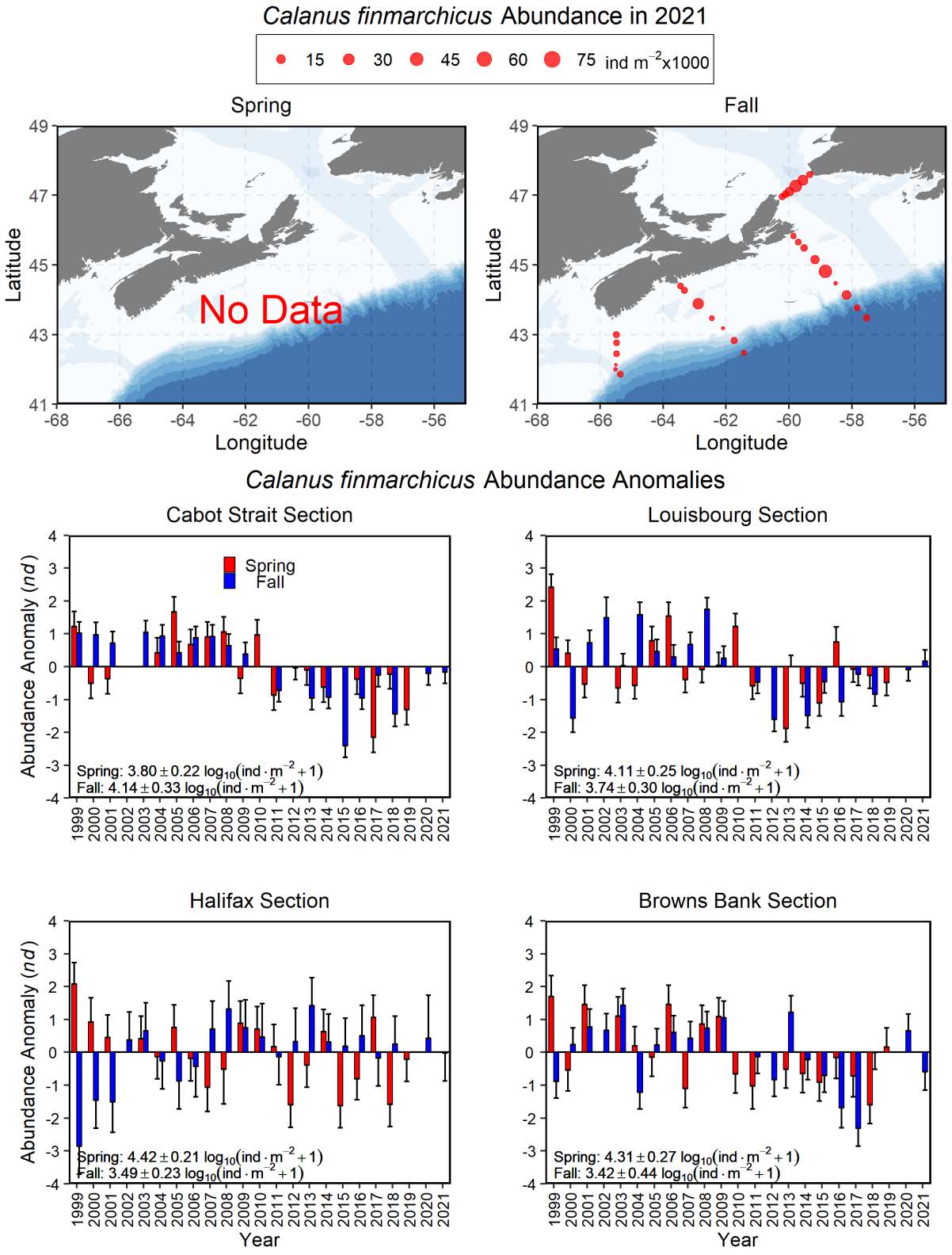

Figure 29. Spatial distribution of Calanus finmarchicus abundance in 2021 (upper panels) and time series of C. finmarchicus abundance anomalies on Scotian Shelf sections (middle and lower panels) in spring and fall, 1999–2021. Vertical lines in lower panels represent the standard error of the seasonal anomaly.

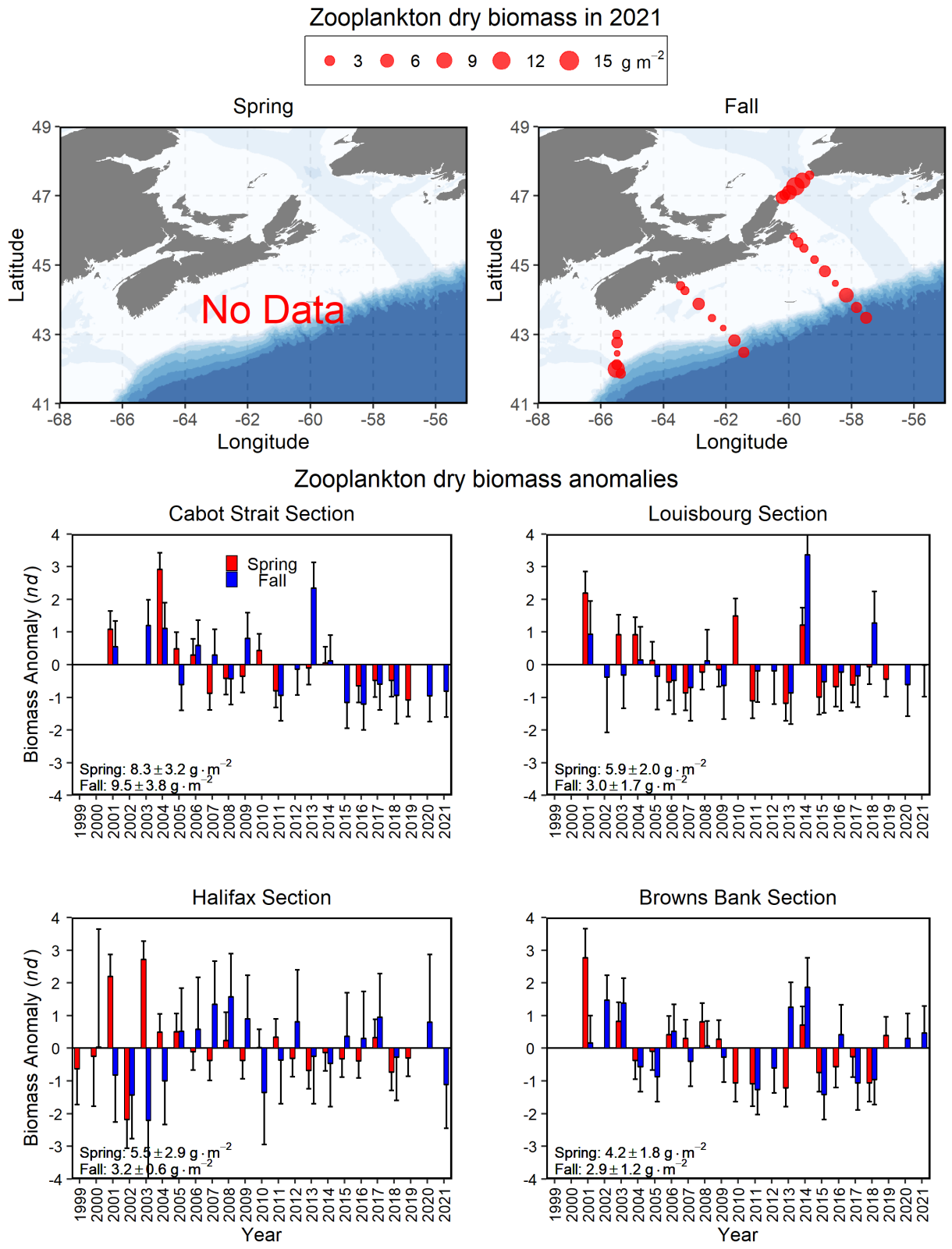

Figure 30. Spatial distribution of zooplankton dry biomass in 2021 (upper panels) and time series of zooplankton dry biomass anomalies on Scotian Shelf sections (middle and lower panels) in spring and fall, 1999–2021. Vertical lines in lower panels represent the standard error of the seasonal anomaly.

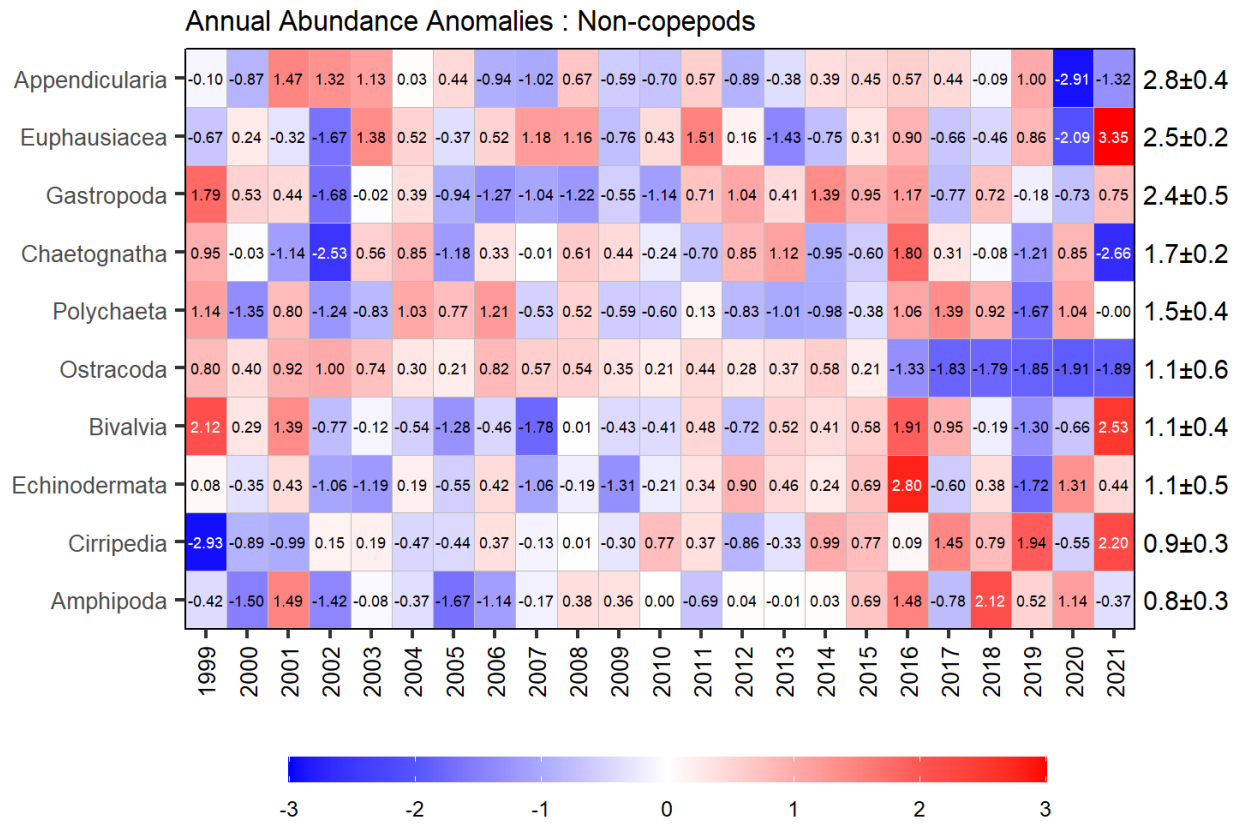

Figure 31. Annual anomaly scorecard for non-copepod groups abundances on the Scotian Shelf sections, ordered from higher- to lower-abundance. Values in each cell are anomalies from the mean for the reference period, 1999–2020, in standard deviation (sd) units (mean and sd listed at right in units of log_{10}*(individuals·m*$^{-2}$*+1)). Red (blue) cells indicate higher- (lower-) than-normal abundances.*

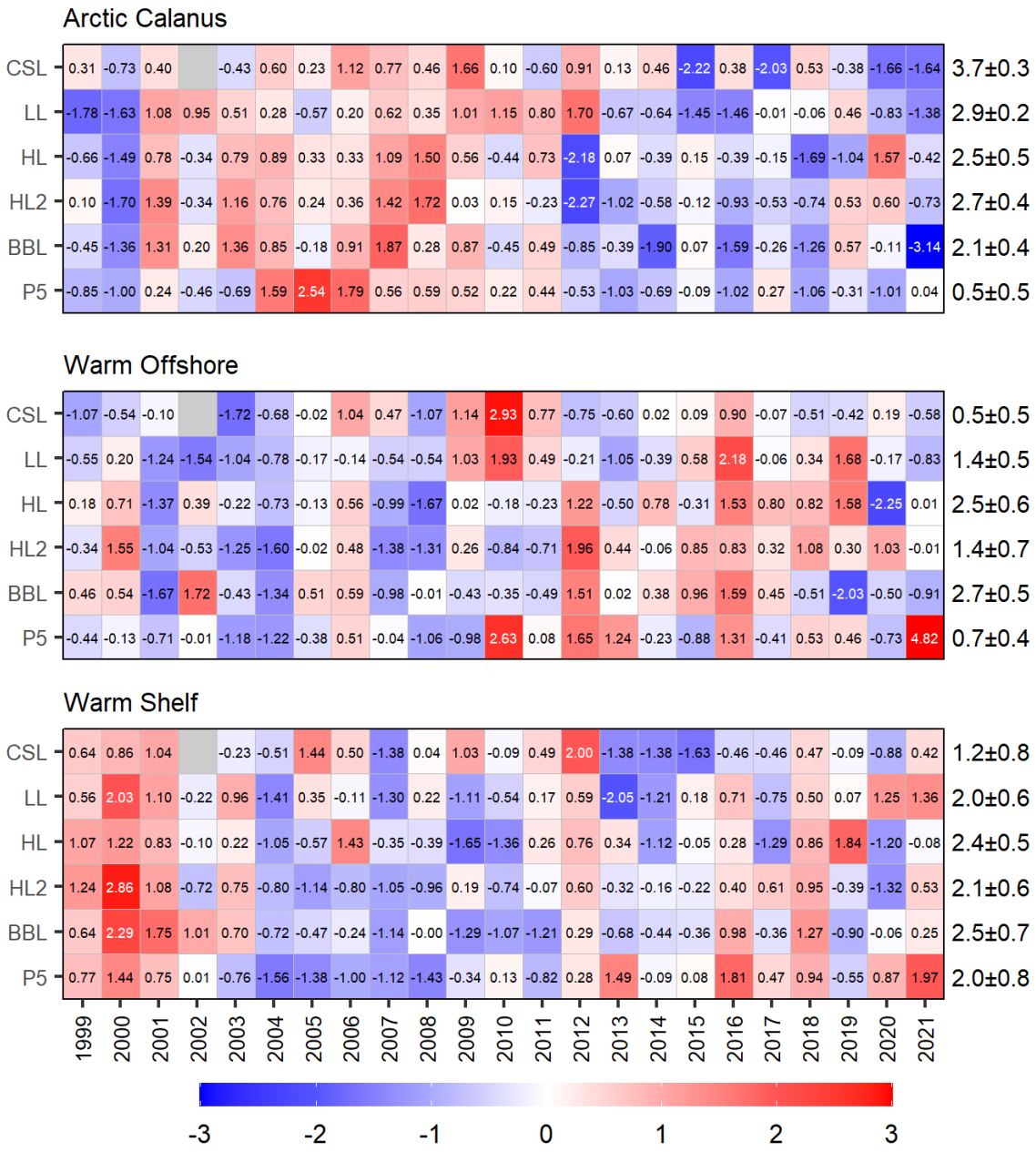

Figure 32. Annual anomaly scorecards for copepod indicator species grouped abundances. Values in each cell are anomalies from the mean for the reference period, 1999–2020, in standard deviation (sd) units (mean and sd listed at right in units of log_{10}[individuals·m^{-2}+1]). Red (blue) cells indicate higher-(lower-) than-normal abundances. Gray cells indicate missing data. CSL: Cabot Strait section; LL: Louisbourg section; HL: Halifax section; HL2: Halifax-2; BBL: Browns Bank section; P5: Prince-5.

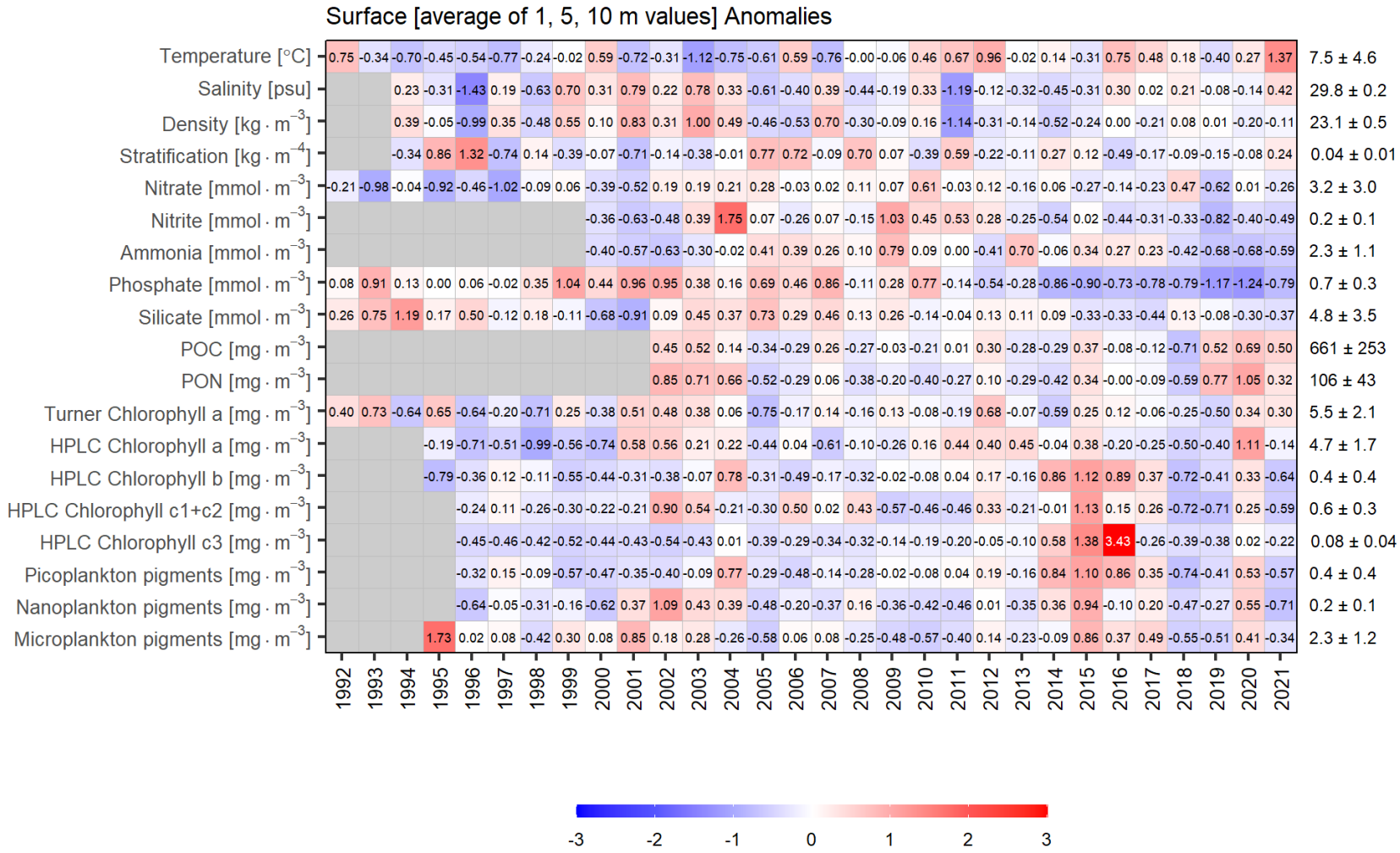

Figure 33. Annual anomaly scorecard for environmental and phytoplankton conditions in the upper water column (2 m, 5 m, and 10 m) in Bedford Basin. Values in each cell are anomalies from the mean for the reference period, 1999–2020, in standard deviation (sd) units (mean and sd listed at right). Red (blue) cells indicate higher- (lower-) than-normal levels for a given variable. Gray cells indicate missing data. POC and PON represent particulate organic carbon and nitrogen, respectively.

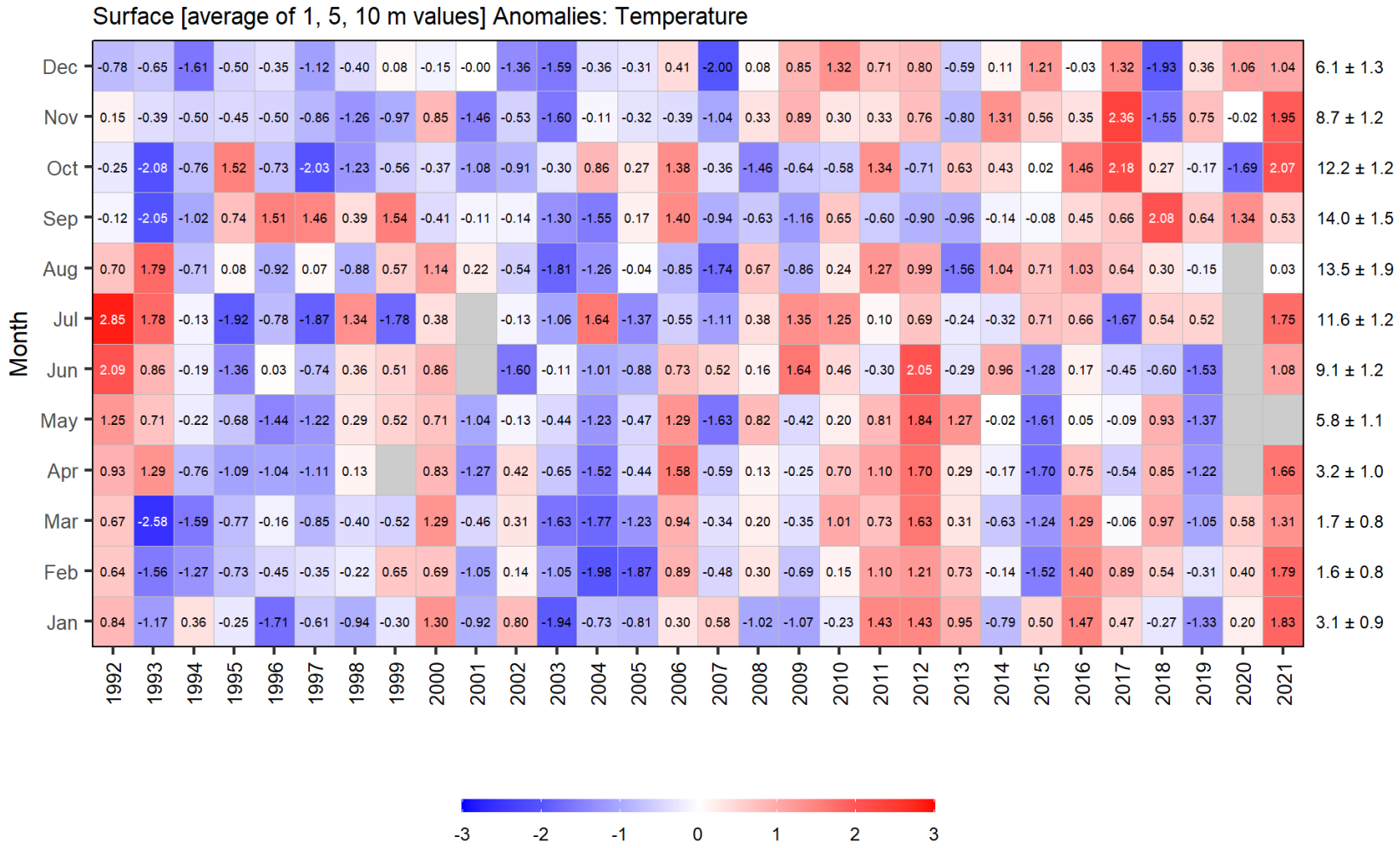

Figure 34. Monthly anomaly scorecard for temperature in the upper water column (2 m, 5 m, and 10 m) in Bedford Basin. Values in each cell are anomalies from the monthly means for the reference period, 1999–2020, in standard deviation (sd) units (mean and sd listed at right in units of °C). Red (blue) cells indicate higher- (lower-) than-normal temperature. Gray cells indicate missing data.

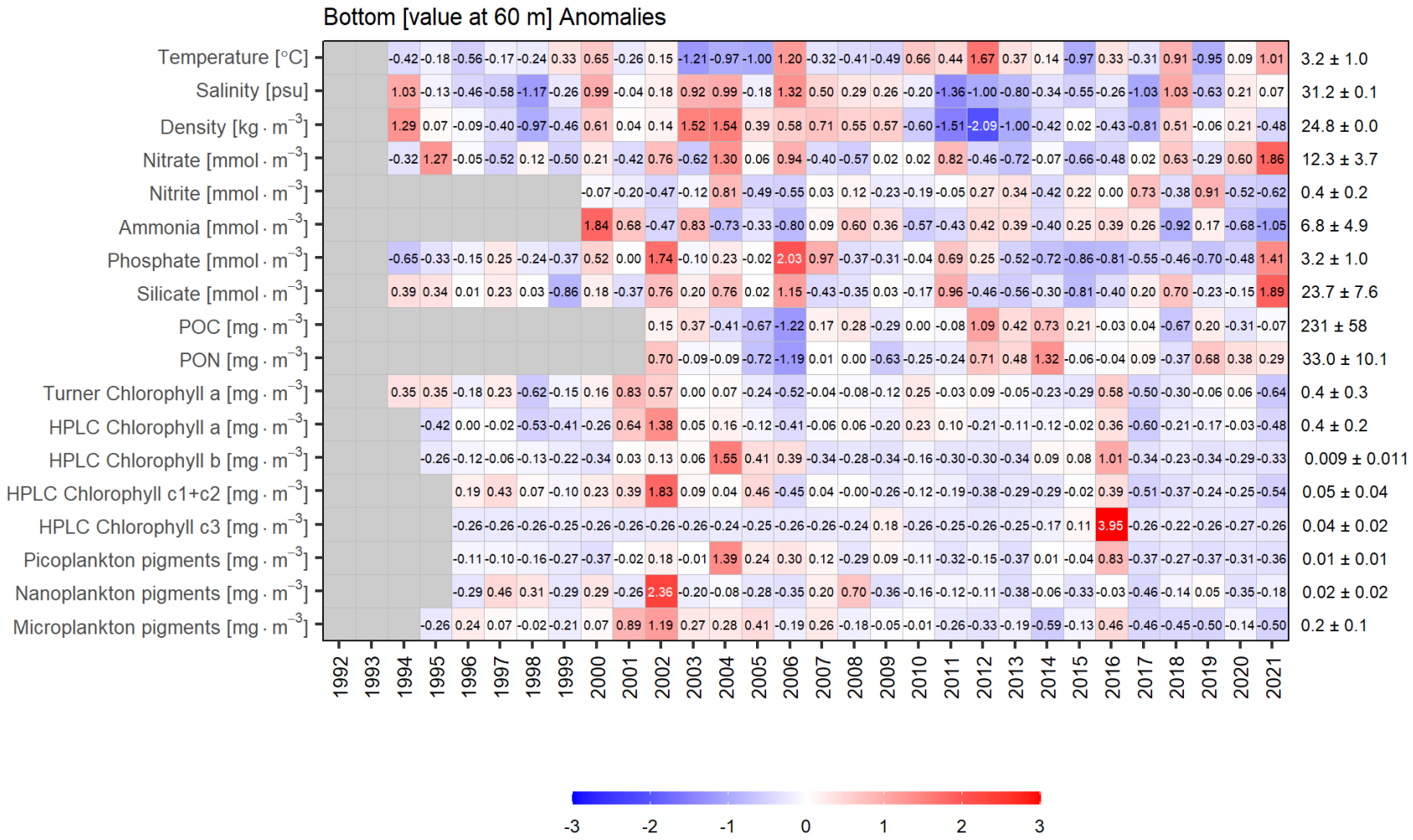

Figure 35. Annual anomaly scorecard for environmental and phytoplankton conditions at 60 m in Bedford Basin. Values in each cell are anomalies from the mean for the reference period, 1999–2020, in standard deviation (sd) units (mean and sd listed at right). Red (blue) cells indicate higher- (lower-) than-normal levels for a given variable. Gray cells indicate missing data. POC and PON represent particulate organic carbon and nitrogen, respectively.

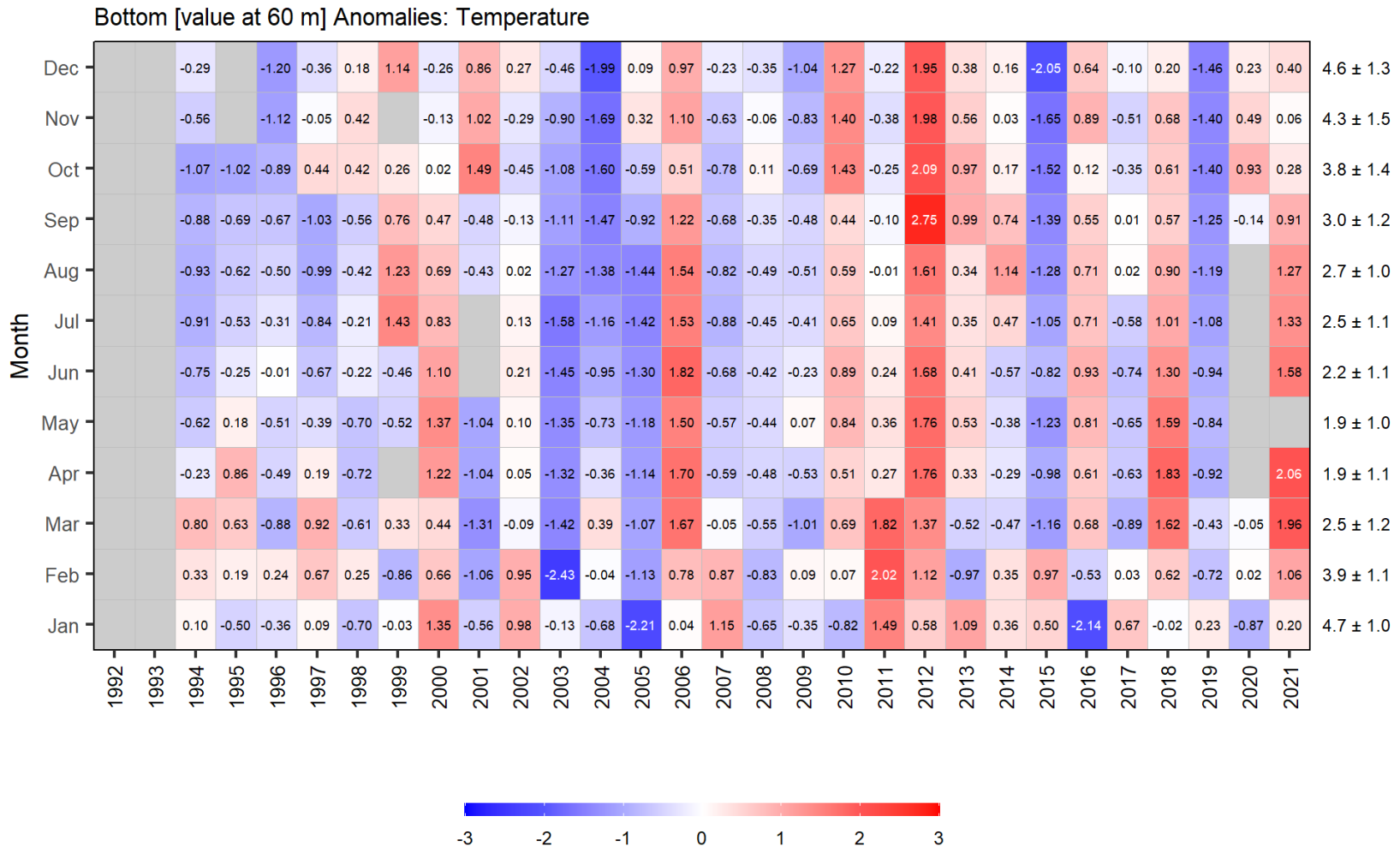

Figure 36. Monthly anomaly scorecard for temperature at 60 m in Bedford Basin. Values in each cell are anomalies from the monthly means for the reference period, 1999–2020, in standard deviation (sd) units (mean and sd listed at right in units of °C). Red (blue) cells indicate higher- (lower-) than-normal temperatures. Gray cells indicate missing data.

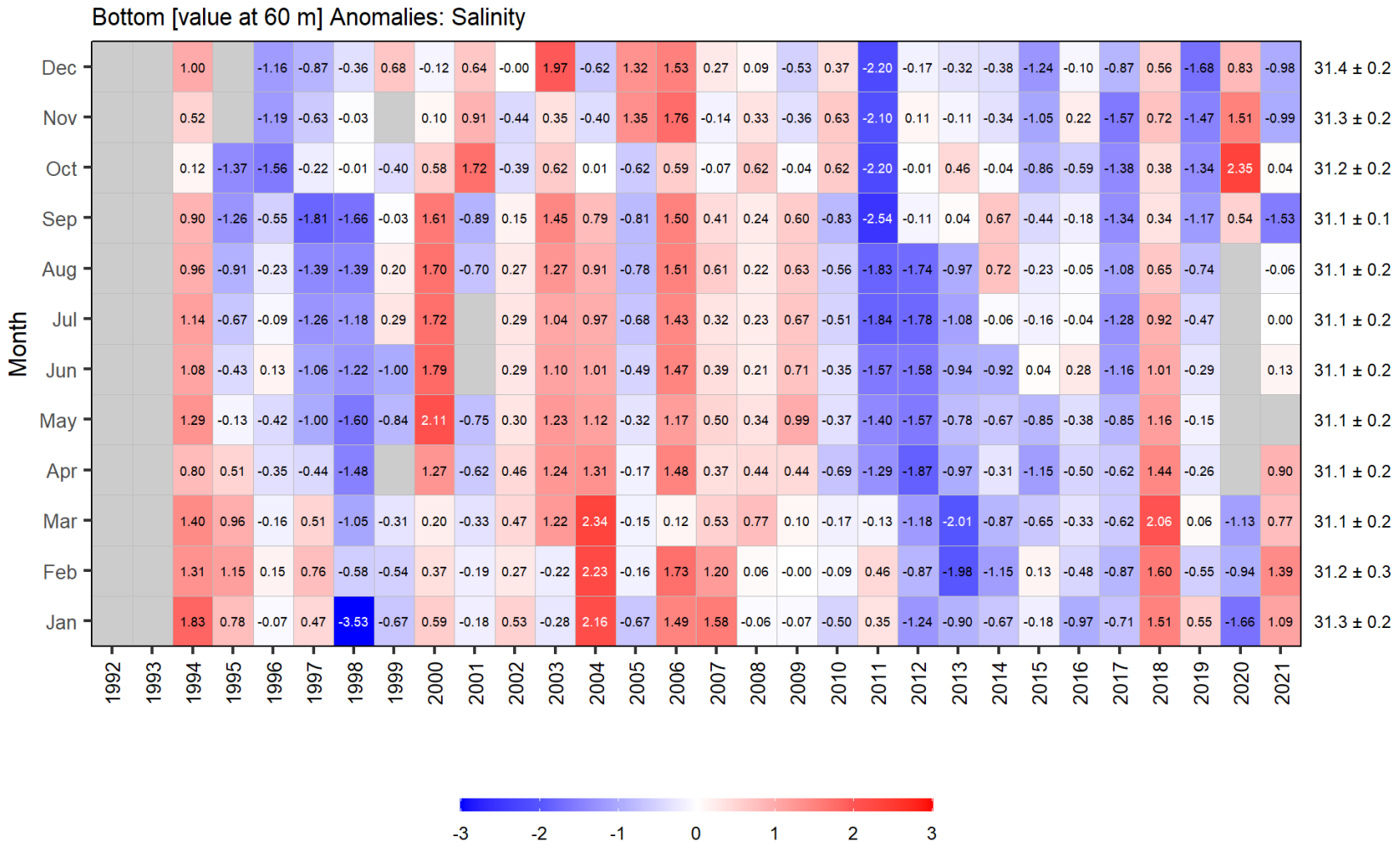

Figure 37. Monthly anomaly scorecard for salinity at 60 m in Bedford Basin. Values in each cell are anomalies from the monthly means for the reference period, 1999–2020, in standard deviation (sd) units (mean and sd listed at right in units of psu). Red (blue) cells indicate higher- (lower-) than-normal salinities. Gray cells indicate missing data.

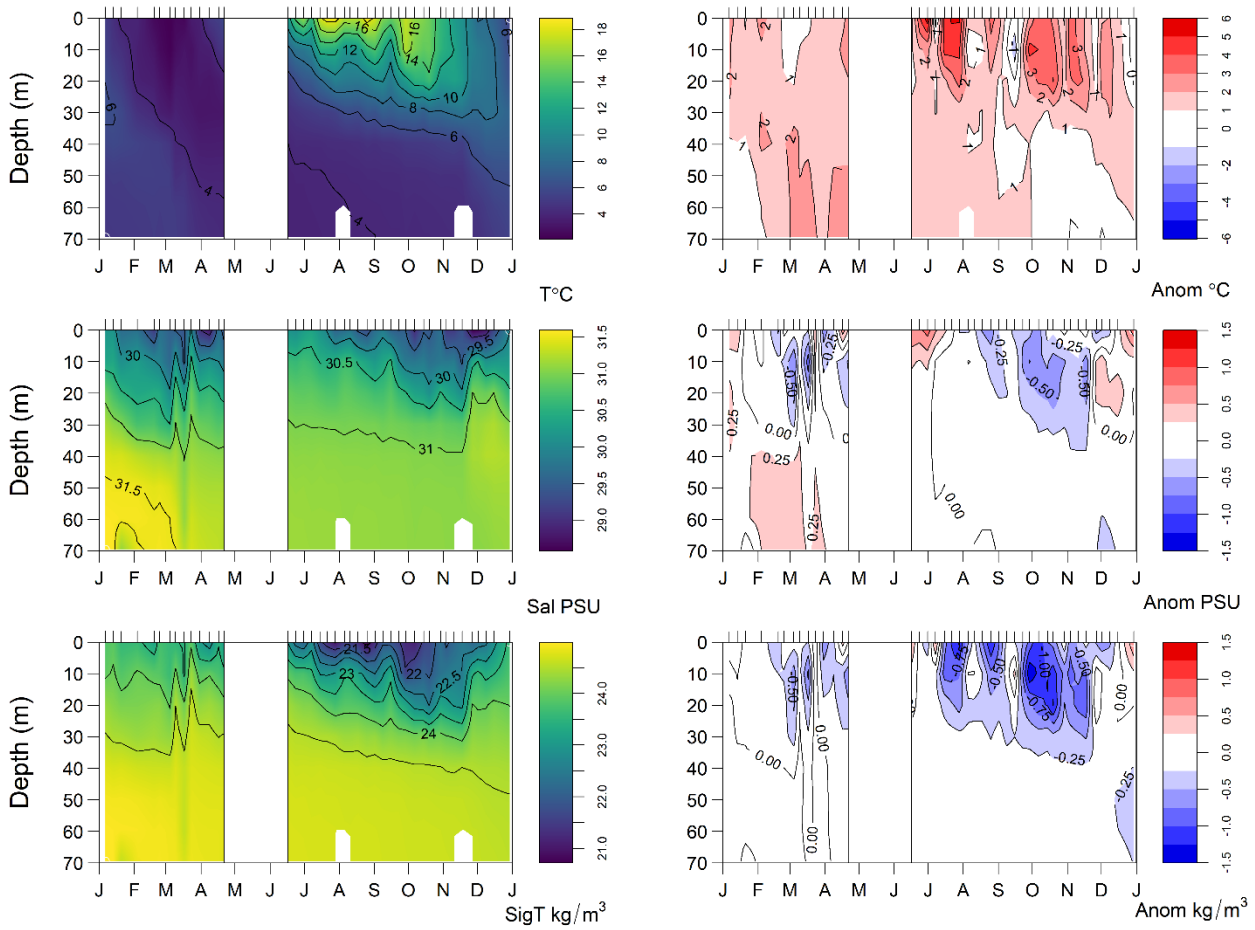

Figure 38. Annual cycle of temperature (top left sub-panel), salinity (middle left sub-panel), and density (lower left sub-panel) in Bedford Basin in 2021 and their anomalies with respect to 1999–2020 monthly means (right sub-panels). Tick marks on the top horizontal axes indicate sampling dates. Tick marks on the bottom horizontal axes indicate the 1st day of the month. No information is shown for the period without sampling from mid-April to mid-June.

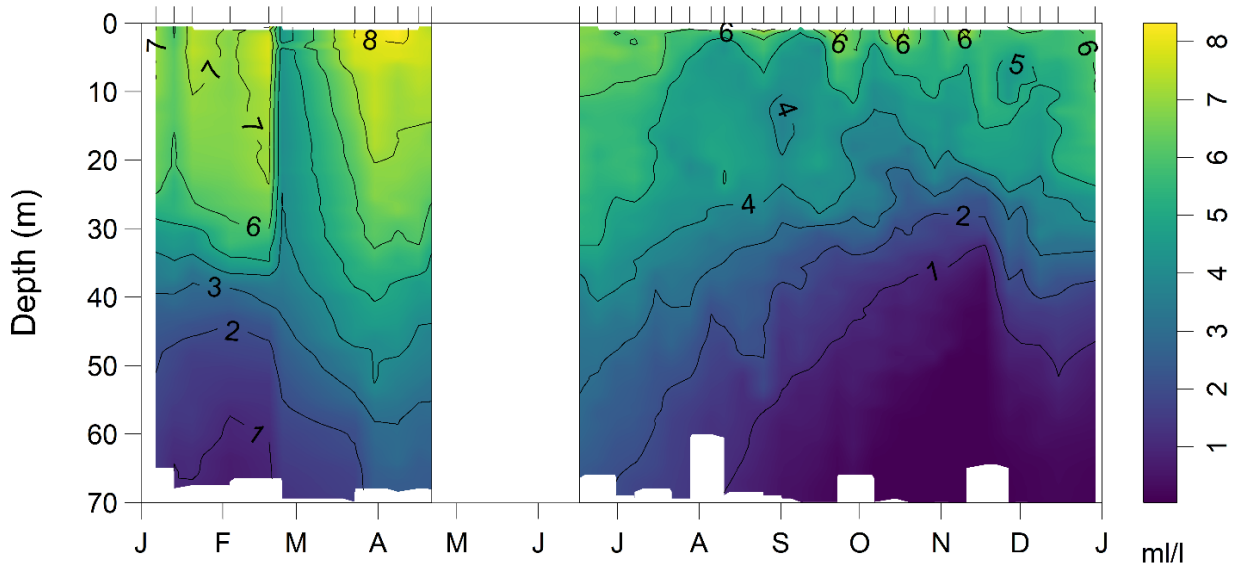

Figure 39. Annual cycle of dissolved oxygen concentration (in ml/l) in Bedford Basin during 2021. Tick marks on the top horizontal axes indicate sampling dates. Tick marks on the bottom horizontal axes indicate the 1st day of the month. No information is shown for the period without sampling from mid-April to mid-June, and 3 sampling events in March are not included in the interpolation.

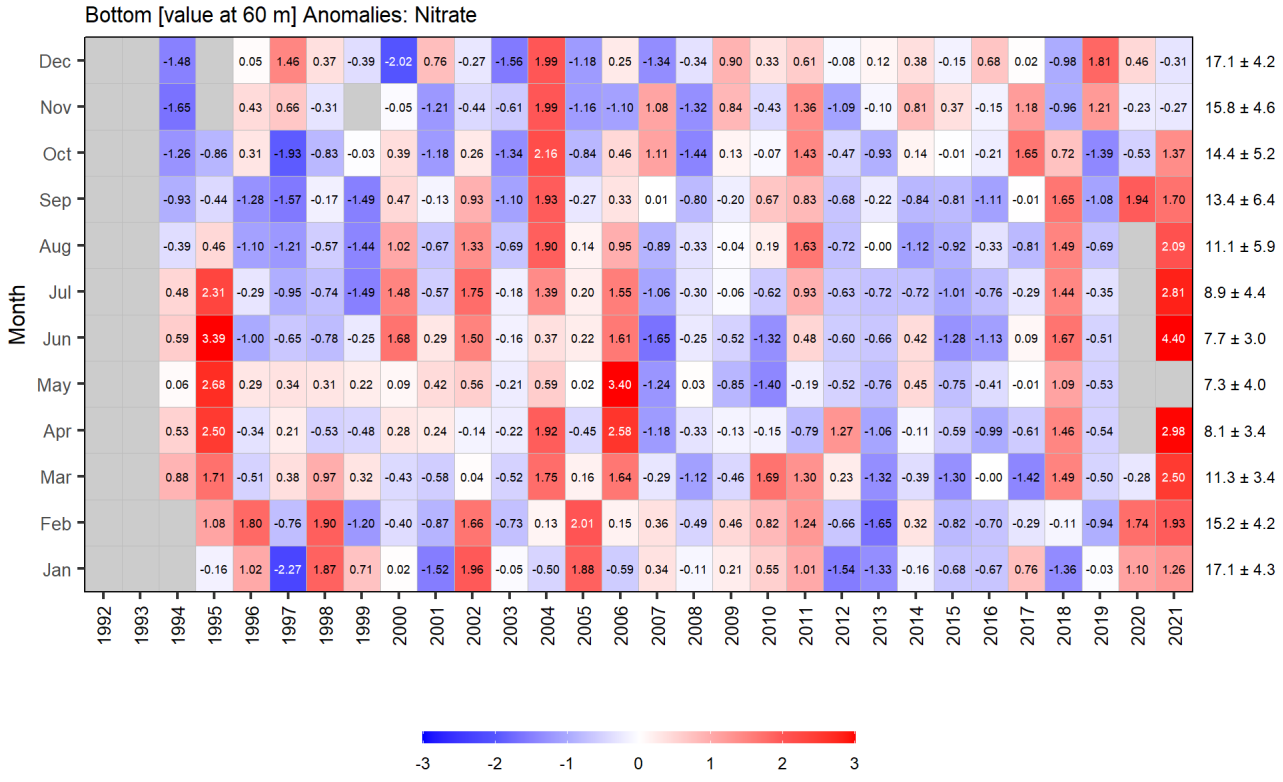

Figure 40. Monthly anomaly scorecard for nitrate at 60 m in Bedford Basin. Values in each cell are anomalies from the monthly means for the reference period, 1999–2020, in standard deviation (sd) units (mean and sd listed at right in units of mmol·m^{-3}). Red (blue) cells indicate higher- (lower-) than-normal nitrate concentrations. Gray cells indicate missing data.

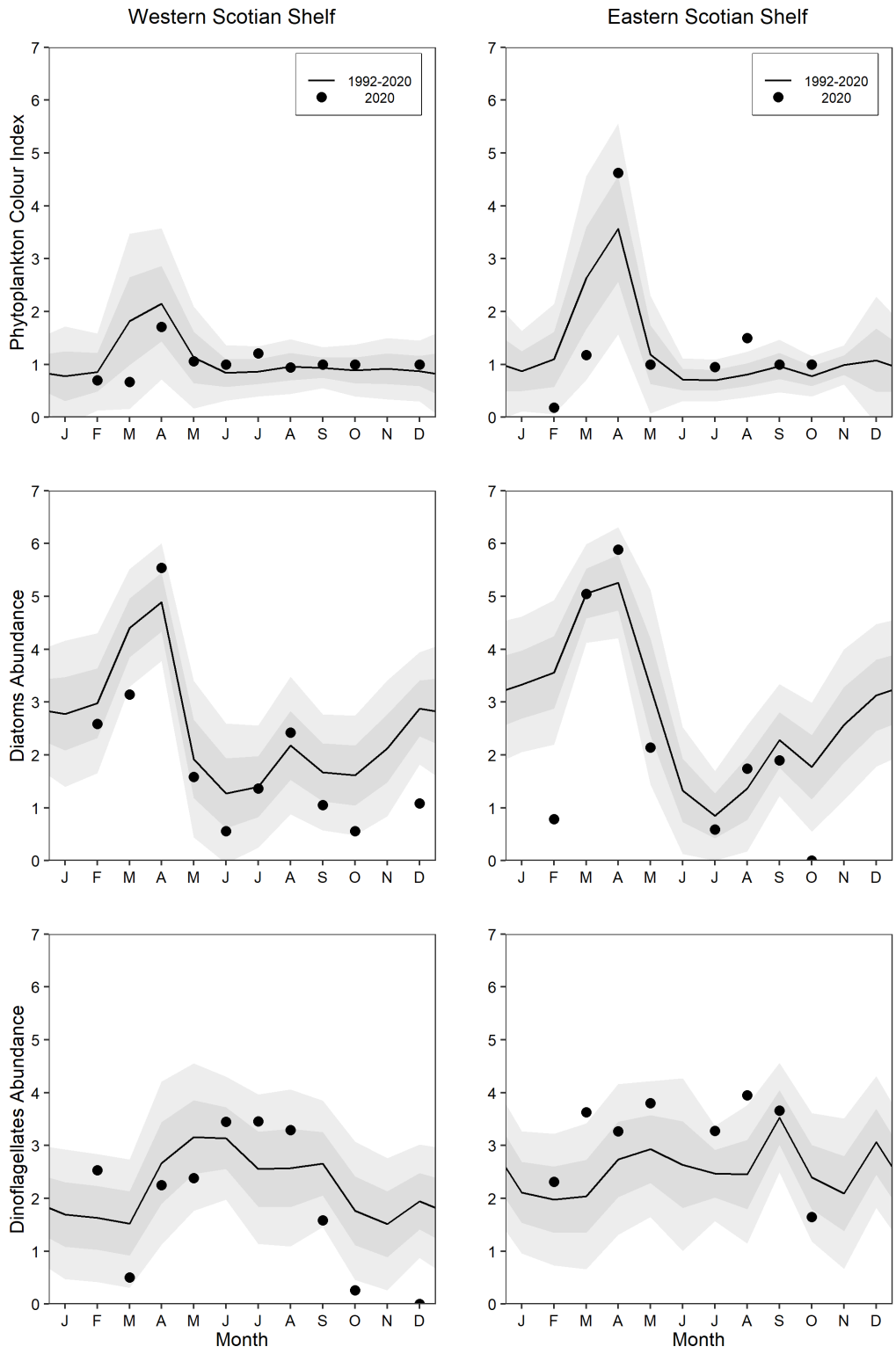

Figure 41. CPR phytoplankton abundance indices in 2020 and mean conditions, 1992–2020 (solid line) on the Western Scotian Shelf (left panels) and Eastern Scotian Shelf (right panels). The gray shaded ribbons represent the standard deviation (±0.5 and ±1 sd) of the monthly means.

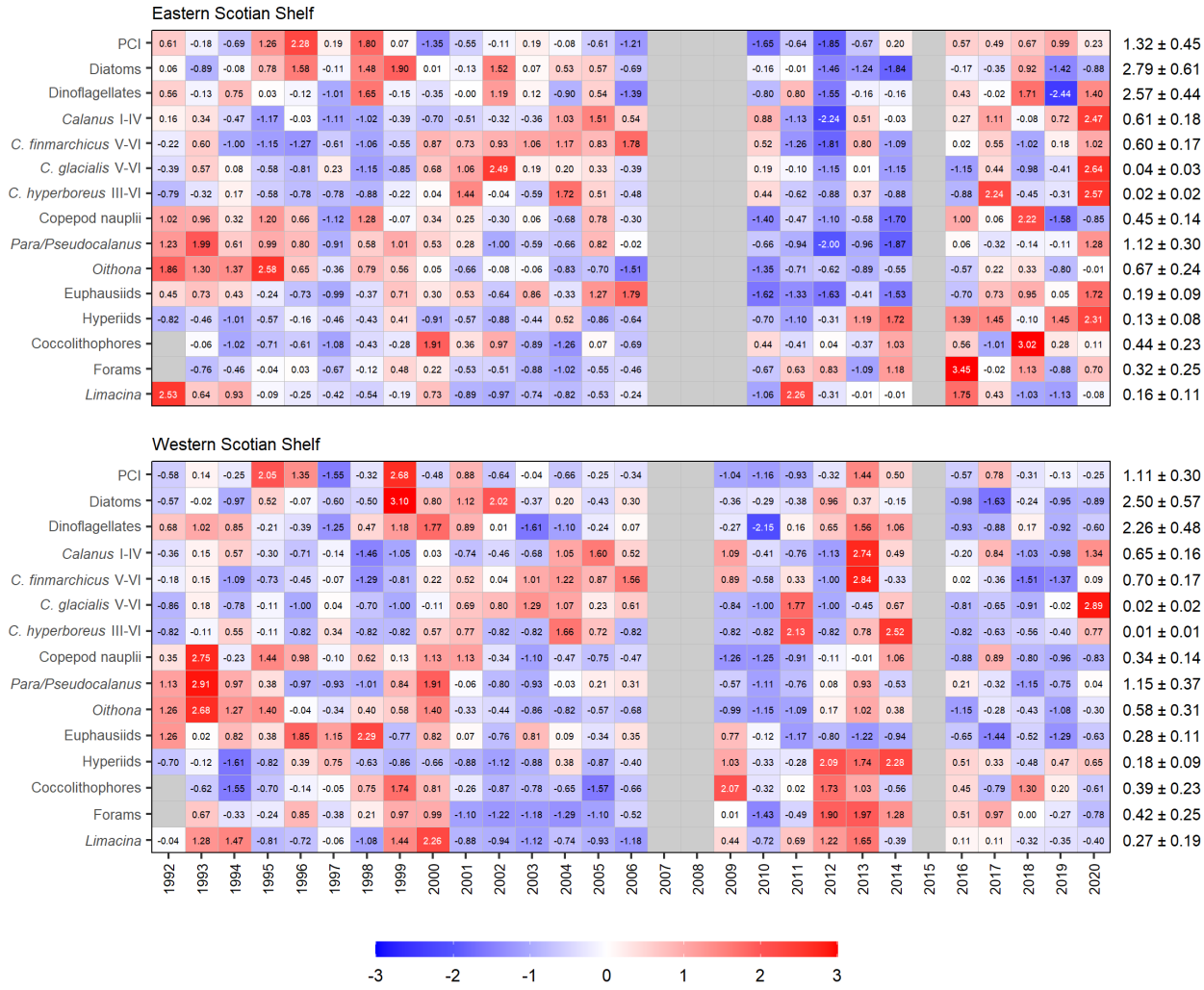

Figure 42. Annual anomaly scorecard for the abundances of phytoplankton and zooplankton taxa observed with the CPR on the Eastern Scotian Shelf (upper panel) and Western Scotian Shelf (lower panel). Values in each cell are anomalies from the annual means for the reference period, 1992–2020, in standard deviation (sd) units (mean and sd listed at right as dimensionless number for PCI and in units of log_{10}(cells·sample^{-1}+1) for phytoplankton abundance and log_{10}(individuals·sample^{-1}+1) for zooplankton abundance). Red (blue) cells indicate higher- (lower-) than-normal abundances. Gray cells correspond to years where either there was sampling in 8 or fewer months, or years where there was a gap in sampling of 3 or more consecutive months. PCI represents the phytoplankton color index.

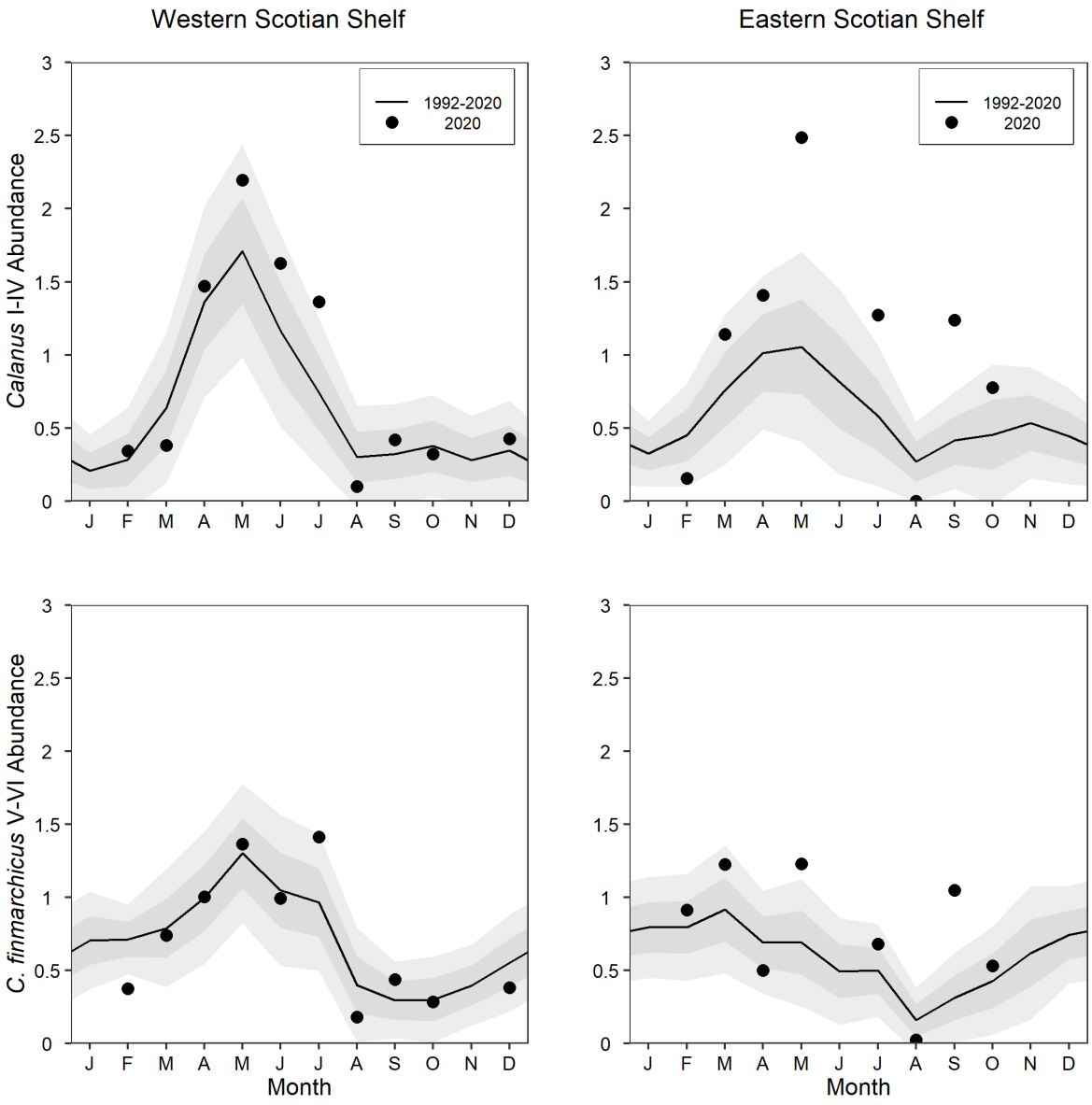

Figure 43. CPR abundance indices for Calanus I–IV (mostly Calanus finmarchicus, upper row) and C. finmarchicus V–VI (lower row) in 2020 and mean conditions, 1992–2020 (solid line) on the Western Scotian Shelf (left panels) and Eastern Scotian Shelf (right panels). The gray shaded ribbons represent the standard deviation (±0.5 and ±1 sd) of the monthly means.

APPENDIX A

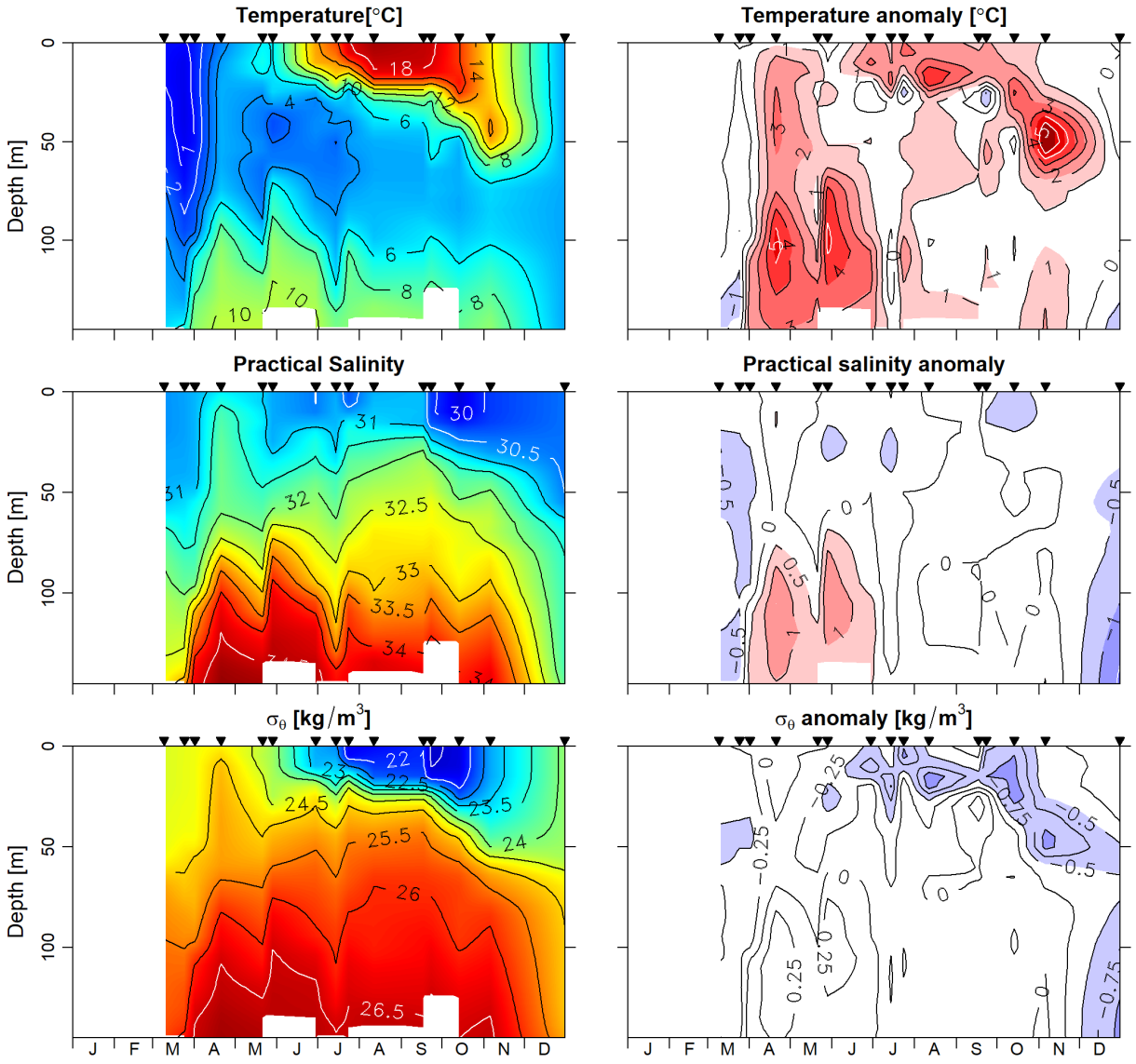

Figure A.1. The 2021 annual cycles of temperature (top panel), salinity (middle panel), and density (lower panel) and their anomalies with respect to 1981–2010 monthly means (right panels) for Halifax station 2. Triangles indicate times of sampling. (Courtesy of Hebert et al. In preparation[1]; Figure 14 from original document).

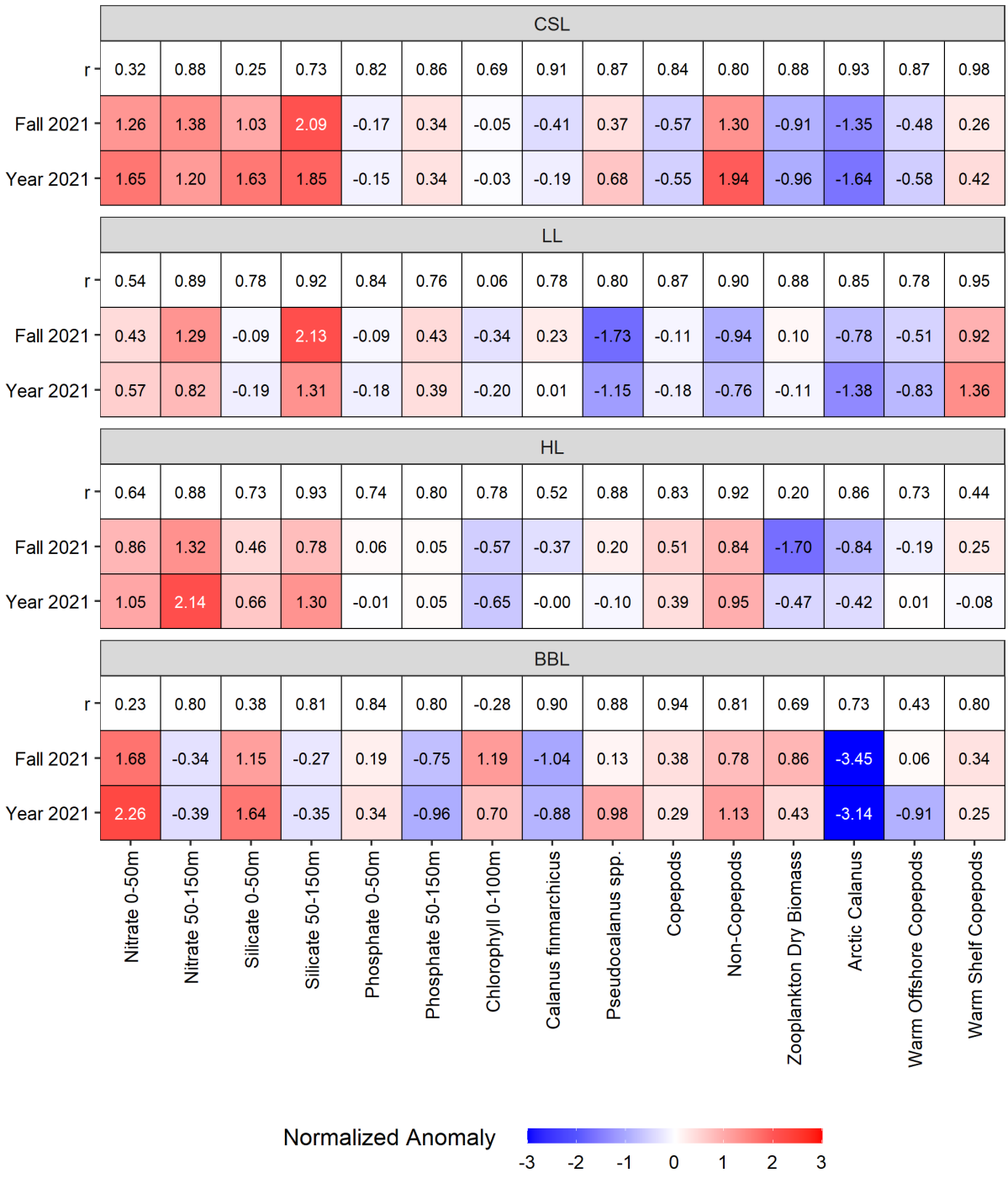

Figure A.2. Comparison of 2021 annual and fall normalized anomalies. For each section, the first row indicates the correlation coefficient (r) between the annual and the fall anomalies calculated from data for the years with full occupation for each index. The second row indicates 2021 normalized fall anomalies for each index. The third row indicates 2021 annual normalized anomalies for each index, estimated from the general linear model. CSL: Cabot Strait section; LL: Louisbourg section; HL: Halifax section; BBL: Browns Bank section.